The Initiation of Base Excision Repair in Nucleosome Core Particles

By
Erin Elizabeth Kennedy
B.S. Lehigh University, 2013

A dissertation submitted in partial fulfillment of the requirements for the degree of Doctor of Philosophy in the Division of Biology and Medicine at Brown University

Providence, Rhode Island
May 2019

This dissertation by Erin Elizabeth Kennedy is accepted in its present form by the Department of Molecular Biology, Cell Biology, and Biochemistry as satisfying the dissertation requirement for the degree of Doctor of Philosophy.

Date: _____ _____
Dr. Sarah Delaney, Advisor

Recommended to the Graduate Council

Date: _____ _____
Dr. Richard Freiman, Reader

Date: _____ _____
Dr. Alexandra Deaconescu, Reader

Date: _____ _____
Dr. Eric Morrow, Reader

Date: _____ _____
Dr. Penny Beuning, Reader

Approved by the Graduate Council

Date: _____ _____
Dr. Andrew Campbell,
Dean of the Graduate School

Curriculum Vitae
ERIN E. KENNEDY

EDUCATION

Doctor of Philosophy in Molecular Biology, Cell Biology, and Biochemistry
September 2013 – May 2019
Brown University in Providence, RI

Bachelor of Science in Molecular Biology
September 2009 – May 2013
Lehigh University in Bethlehem, PA
Honors in Molecular Biology, Minor in General Psychology

RESEARCH EXPERIENCE

Graduate Research Assistant, Department of Chemistry, Brown University
Advisor: Dr. Sarah Delaney
June 2014 – May 2019

- Conducted research focused on DNA damage repair, using kinetic assays to examine the activity of glycosylase enzymes in the context of packaged DNA.
- Represented the group by presenting research at a regional meeting, department-wide seminars, and poster sessions at conferences.
- Trained and mentored several undergraduate and graduate students through development and execution of independent research projects in the laboratory.
- Responsible for equipment maintenance and laboratory management.
- Skills: design and execution of enzymatic assays, protein expression and purification, HPLC purification of DNA, UV-Vis for DNA and protein quantitation, DNA footprinting techniques.

Undergraduate Student Researcher, Department of Biological Sciences, Lehigh University
Advisor: Dr. Linda Lowe-Krentz
September 2011 – May 2013

- Introduced a fluorescently tagged cGMP-dependent protein kinase protocol to study the role of heparin signaling in the mitogen-activated protein kinase pathway.
- Completed a senior thesis to earn Departmental Honors.
- Skills: fluorescent microscopy, primary cell culture, gel electrophoreses, western blotting.

SUPERS Intern, Department of Radiology and Oncology, University of Pennsylvania
Advisor: Dr. Theresa Busch
Summers 2011 and 2012

- 1 of 15 accepted to the Summer Undergraduate Program for Educating Research Scientists (SUPERS) program from competitive applicant pool. Invited back for a second summer.
- Project 1: studied comparisons between macroscopic and microscopic measurements of oxygen and photosensitizer in tumors to predict Photodynamic Therapy response.
- Project 2: explored epidermal growth factor inhibitor effects on tumor necrosis.
- Skills: cryosectioning, immunohistochemistry, fluorescent microscopy, ImageJ analysis.

SEA-PHAGES Participant, Department of Biological Sciences, Lehigh University
Advisor: Dr. Vassie Ware
September 2010 – May 2011

- Part of the HHMI Science Education Alliance Phage Hunters Advancing Genomics and Evolutionary Science (SEA-PHAGES) to study the molecular genetics of bacteriophages.
- 1 of 15 students chosen to participate from a competitive application process.
- Isolated and purified a novel phage and contributed observations to the actinobacteriophage database at http://phagesdb.org/phages/Mooch/.

PUBLICATIONS

- **Kennedy EE**, Li C, Delaney S. "The architectural nuances of nucleosomes revealed by global repair profiling of human alkyladenine DNA glycosylase." *Manuscript submitted.*
- **Kennedy EE**, Caffrey PJ, Delaney S. "Initiating Base Excision Repair in Nucleosome Core Particles." Invited Review. *DNA Repair* (2018). doi: 10.1016/j.dnarep.2018.08.011
- Bilotti K, **Kennedy EE**, Li C, and Delaney S. "Human OGG1 activity in nucleosomes is facilitated by transient unwrapping of DNA and is influenced by the local histone environment." *DNA Repair* (2017) 59: 1-8. doi: 10.1016/j.dnarep.2017.08.010
- Pope WH, Bowman CA, Russell DA, Jacobs-Sera D, Asai DJ, Cresawn SG, Jacobs Jr. WR, Hendrix RW, Lawrence JG, Hatfull GF, **Science Education Alliance Phage Hunters Advancing Genomics and Evolutionary Science**, Phage Hunters Integrating Research and Education, Mycobacterial Genetics Course. "Whole genome comparison of a large collection of mycobacteriophages reveals a continuum of phage genetic diversity." *eLife* (2015) 4: 06416.

INVITED SEMINAR

Providence Area Research Forum (PAARF) Meeting
November 2017
Title: *The Initiation of Base Excision Repair in Nucleosome Core Particles*

CONFERENCES AND POSTER PRESENTATIONS

- February 2019: Gordon Research Conference on Mammalian DNA Repair (Ventura, CA)
- August 2018: The 256th American Chemical Society National Meeting (Boston, MA)
- March 2016: Gordon Research Seminar and Conference on DNA Damage, Mutation, and Cancer (Ventura, CA)
- June 2015: The 19th Conversation of the Journal of Biomolecular Structure and Dynamics (Albany, NY)
- June 2014: International Workshop on Radiation Damage to DNA (Boston, MA)

AWARDS AND HONORS

Graduate Center Bar/Naragansett Brewing Company Conference Travel Award, Providence, RI
February 2019

Trainee on NIH Pre-Doctoral Training Grant T32GM007601
Academic Years 2015 and 2016

- 1 of 8 trainees, appointed based on excellent academic and laboratory performance.

SKILLS AND TRAINING

Sheridan Center Teaching Certificate in Reflective Teaching, Brown University
September 2015 – March 2016

- Participated in workshops and small discussion sections focused on teaching and communication strategies.
- Focus on critical reflection of teaching and learning, learning goals as a communicator, and design of courses and assignments.

New Enzymology Kinetic Workshop
January 2016

- Participated in a week-long workshop hosted by Dr. Kenneth Johnson at UT Austin.
- Trained in designing enzyme kinetics experiments and in use of KinTek Explorer software.

Writing Experiences

- Provided scientific and editorial feedback in > 5 manuscript editing sessions to rigorously prepare laboratory manuscripts for journal submission.
- Contributed literature surveys, preliminary data, and writing for group grant proposals.
- Detailed laboratory protocols for experimental procedures and equipment maintenance.
- Applied for the NIH F31 Ruth L. Kirschtein National Research Service Award for Individual Pre-doctoral Fellowship in December 2015.
- Applied for the National Defense Science and Engineering Graduate Fellowship in 2015.
- Applied for the NSF Graduate Research Fellowship Program (GRFP) in 2015.

TEACHING AND MENTORING EXPERIENCE

Undergraduate Mentoring in the Delaney Laboratory, Brown University
October 2015 – May 2019

Responsible Conduct in Research Course TA, Brown University
September 2017 – October 2017

- Facilitated discussions revolving around ethical practices in the biosciences, kept organized records of student participation, and graded the final examination.
- Recruited by Dean Elizabeth Harrington

Co-Chair of First-year mentor program for MCBGP, Brown University
September 2016 – May 2017

- Organized events for first-year and senior MCB graduate student mentors during first-year transition into graduate school and milestones.

Senior Student Mentor of MCBGP First-Year Student, Brown University
September 2015 – May 2018

Developmental Biology Course TA, Brown University
Professor Kristi Wharton
September 2014 – December 2014

Biochemistry Laboratory Course Preparatory TA, Lehigh University
September 2012 – December 2012

- Recruited by members of the Department of Biological Sciences.

SERVICE AND LEADERSHIP

First Annual Craig Yennie STEM Outreach Day, Hartford, Connecticut
April 2019

- Helped facilitate a chemistry demonstration for middle-school students to spark their interest in the sciences.

Graduate Student Council Representative for the MCB Graduate Program, Brown University
September 2014 – May 2018

- Attended monthly meetings to advocate for MCB student interests and distribute information between groups.

MCBGP Recruitment Co-Chair, Brown University
December 2015 – February 2016

- Planned and facilitated visitation program for 15 prospective students for three different visitation weekends, including planning the itinerary, interviewing prospective students, and organizing current graduate student participation.

Habitat for Humanity, South County, Rhode Island
September 2013 – September 2014

- Participated in four days of all-women builds.

Preface and Acknowledgements

To my advisor, Dr. Sarah Delaney, who pushed me to become a better scientist and communicator. Thank you for taking a chance on a molecular biologist who was fascinated by DNA damage repair.

To my labmates who became my friends. Thank you for creating an environment that made me want to go to lab, even when my experiments were not working.

To my friends who supported me from near and far. Thank you for the laughs and great times.

To my family, for being my biggest cheerleaders and for encouraging me in all I do. Thank you for everything.

To Charlie, for making sure that I left the lab occasionally. Thank you for the love and support. We did it.

I dedicate this dissertation to Dr. Stephen Tuttle, the best SUPERS dad the program will ever know.

Table of Contents

List of Tables and Schemes

List of Figures

Thesis Abstract

Despite being essential for organismal survival, genomic DNA is chemically reactive and susceptible to modification to generate mutagenic and/or cytotoxic lesions. These lesions include oxidation, alkylation, and deamination of the nucleobases. The removal of modified nucleobase lesions is the responsibility of the base excision repair (BER) pathway. BER is initiated by glycosylases that search for and remove the lesions. Previous characterizations of glycosylase activity have used DNA oligonucleotides, but a majority of eukaryotic DNA exists in a packaged environment. The basic unit of DNA packaging is the nucleosome core particle (NCP). This thesis focuses on characterizing the activity of three representative glycosylase-lesion pairs in NCPs: (1) human oxoguanine DNA glycosylase (hOGG1) on 8-oxo-7,8-dihydroguanine, (2) uracil DNA glycosylase (UDG) on uracil (U), and (3) human alkyladenine DNA glycosylase (AAG) on 1,N^6-ethenoadenine (εA). hOGG1 and UDG activity was evaluated using kinetic studies of lesions positioned in various rotational positions near the DNA ends of the NCP. Lesion repair was enhanced relative to analogous rotational positions located on the dyad, suggesting that transient unwrapping of DNA ends facilitated repair. Additionally, histone tails were shown to suppress hOGG1 activity, but not UDG, emphasizing that local NCP architectural features can differentially influence glycosylase activity. UDG searching for lesions was also characterized in NCPs, specifically its processivity, or ability to remove multiple U in a single DNA binding event. Preliminary results show UDG processivity is greatly reduced in NCPs relative to duplex. The small amount of processivity observed is due to dissociative transfer (“hopping”) with no contribution of associative transfer (“sliding”). Lastly, AAG activity was characterized across a variety of translational and rotational positions simultaneously utilizing a global εA-containing NCP population to determine kinetic parameters at 49 distinct sites. Overall, the amount of excision by AAG correlated with solution accessibility characterized by hydroxyl radical footprinting and

exhibited monophasic kinetics. Exceptions to this repair-accessibility correlation are likely due to local NCP architectures, such as differences in DNA dynamics, DNA wrapping, and interaction with histone tails. These *in vitro* NCP experiments provide powerful molecular understanding for biological relationships between DNA damage and repair seen in eukaryotic genomes. These comparable observations between *in vivo* and *in vitro* systems allows for a more complete understanding of BER-specific contributions to mutational spectra in human cancers and may provide insight into the resolution of these disease-inducing mutations.

Chapter 1. Introduction †

† Adapted from:

Kennedy E.E.*, Caffrey P.J.*, Delaney, S. (2018)

Initiating base excision repair in chromatin.

DNA Repair 71, 87-92

*These authors contributed equally to this work

1.1. Introduction to DNA

The genetic information essential for the survival of all organisms is stored in the crucial biomolecule called deoxyribonucleic acid (DNA). The double helical structure of DNA, as first described by James Watson and Francis Crick in 1953, contains two complementary polynucleotide strands arranged in an antiparallel orientation to create what is known as a DNA duplex.[1] Each strand of the duplex is made up of monomeric units called nucleotides, connected in a linear manner by phosphodiester bonds. Each nucleotide is composed of a deoxyribose sugar, a phosphate group, and a nitrogenous nucleobase. There are four canonical nucleobases: adenine (A), thymine (T), cytosine (C), and guanine (G). The nucleobases are derivatives of either pyrimidines (T and C) or purines (A and G). Complementary DNA strands are paired via hydrogen bonding of nucleobases on opposite strands, A with T and C with G (**Figure 1.1.**)

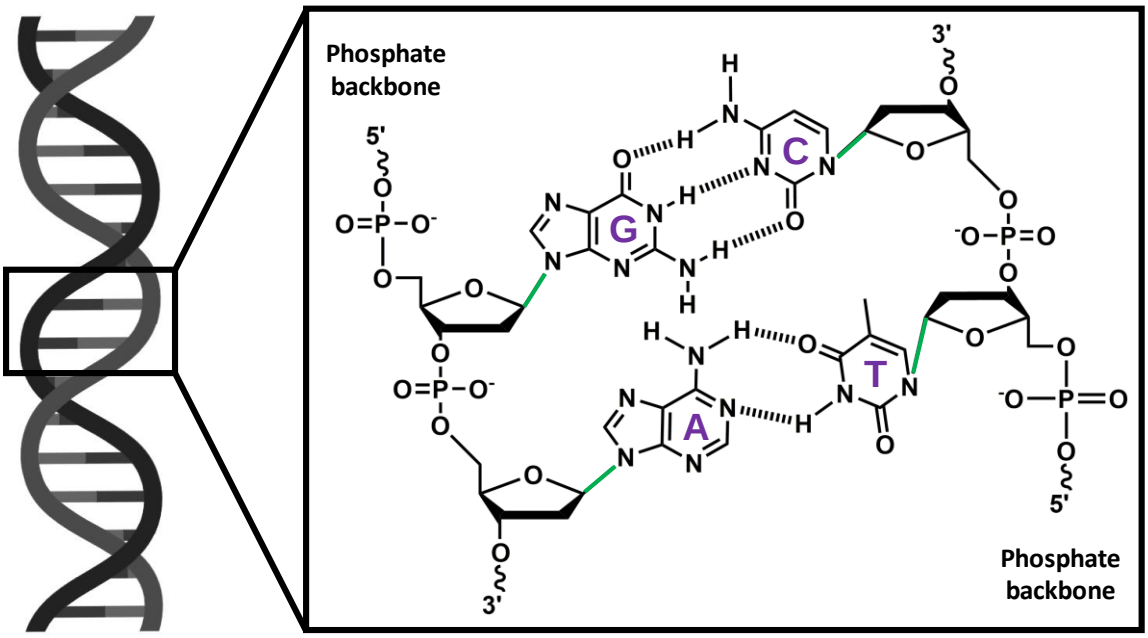

Figure 1.1. DNA double helix structure and canonical base pairing. Duplex formation occurs when G pairs with C, and A pairs with T on complementary strands. The sugar phosphate backbone connects the nucleotides together on a single strand. Dashed bonds represent hydrogen bonding between pairs. The *N*-glycosidic bonds are highlighted in green.

1.2. DNA is chemically reactive

Despite containing crucial genetic instructions, genomic DNA has a physiochemical composition that renders it susceptible to modification and decomposition.[2,3] The reactive environment of the cell and the presence of environmental factors threaten the integrity of the DNA and the genetic information it contains.[4,5] Not only are the sources of damage wide-ranging, but also there is high diversity in the types of damage including single- and double-strand breaks, inter- and intra-strand crosslinks, abasic sites, and modification of the nucleobases.[6]

The basis of this thesis will focus on the modification of nucleobases to generate lesions. Examples of nucleobase lesions deriving from oxidation, alkylation, deamination, and hydrolysis are shown in **Figure 1.2.**[7] Normal cellular processes can lead to all types of events: reactive oxygen species generated from cellular metabolism and inflammatory responses can generate oxidized nucleobases,[8] lipid peroxidation metabolism intermediates cause alkylation modifications to nucleobases,[9] and spontaneous deamination of exocyclic amines found in A, G, and C simply happen under physiological conditions.[10] Representative lesions that will be discussed further in this thesis include 8-oxo-7,8-dihydroguanine (8-oxoG) resulting from the oxidation of G, 1,N^6-ethenoadenine (εA) from the alkylation of A, and uracil (U) from the deamination of C.

When formed in DNA, nucleobase modifications may modulate or eliminate base-pairing properties. For example, the alkylation of A to εA causes the complete loss of hydrogen bonding to T and causes A to G mutations upon replication (**Figure 1.3.A**).[11] The deamination of C to U loses one hydrogen bond to create a wobble pair with G (**Figure 1.3.B**). The persistence of the U:G mispair during replication can allow for an A to be inserted opposite U, resulting in a C to T mutation. In the case of 8-oxoG, its base pairing with C remains the same. However, the 8-oxoG can rotate 180 degrees about the

glycosidic bond to base pair with A, which can result in a G to T mutation after replication (**Figure 1.3.C**).

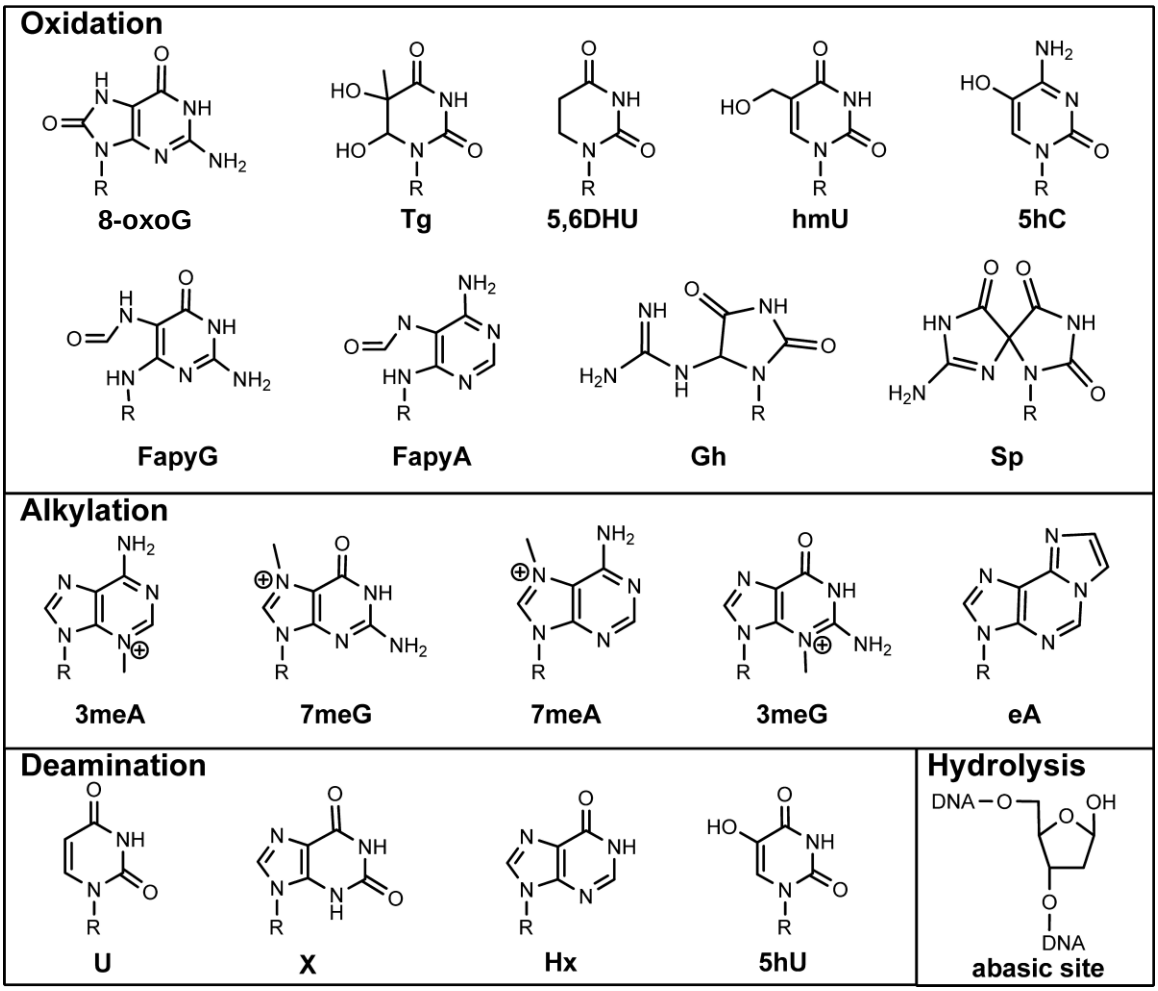

Figure 1.2. Nucleobase lesions result from oxidation, alkylation, deamination, and hydrolysis events. The above structures show examples of DNA lesions that form due to chemical modification of the nucleobase: 8-oxo-7,8-dihydroguanine (8oxoG); thymine glycol (Tg); 5,6-dihydrouracil (5,6DHU); hydroxymethyluracil (hmU); 5-hydroxycytosine (5hC); 4,6-diamino-5-formamidopyrimidine G (FapyG); 4,6-diamino-5-formamidopyrimidine A (FapyA); guanidinohydantoin (Gh); spiroiminodihydantoin (Sp); 3-methyladenine (3meA); 7-methylguanine (7meG); 7-methyladenine (7meA); 3-methylguanine (3meG); 1,N^6-ethenoadenine (εA); uracil (U); xanthine (X); hypoxanthine (Hx); 5-hydroxyuracil (5hU). Hydrolysis of the glycosidic bond produces an abasic site. *Figure adapted from reference 7*.

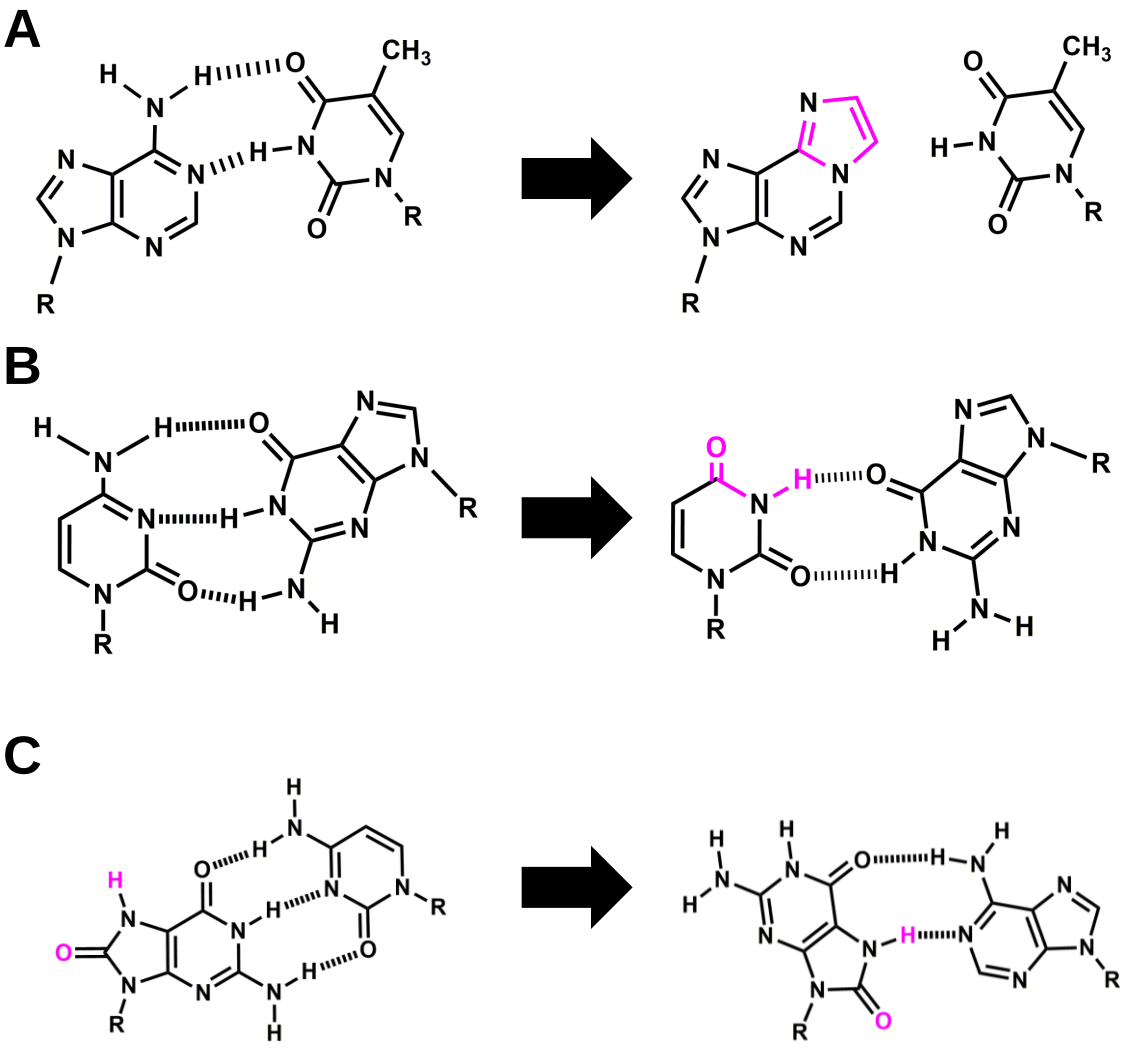

Figure 1.3. Examples of mutagenic mispairing due to chemical modifications to nucleobases. (A) The alkylation of A results in the formation of εA and the complete loss of hydrogen bonding to T. **(B)** The deamination of C to U results in a loss of a hydrogen bond that causes a wobble U:G bp. **(C)** The oxidation of G results in 8-oxoG which can either remain paired with C (*anti* conformation), or may rotate 180 degrees about the glycosidic bond to hydrogen bond in the *syn* conformation with A. Structural features that differ from the canonical base are highlighted in pink.

1.3. Base excision repair

The preservation of the genome is crucial for cell and organismal survival, as well as for the faithful transfer of genetic information to the next generation for species' survival. Under normal physiological conditions, the typical cell is estimated to acquire between

10,000 – 20,000 lesions per day.[2] Fortunately, our cells have multiple repair processes to rectify a majority of the damage that can form in DNA.[6] These pathways, including single-strand break repair, double-strand break repair (either non-homologous end joining or homologous recombination), mismatch repair, nucleotide excision repair, and base excision repair, are each responsible for the resolution of different types of damage that may occur.[12–14] Repair of DNA is possible due to the redundancy of genetic information stored in the form of duplex DNA; repair of damage located on one strand is directed by the information contained on the undamaged strand.

Specifically, the repair of single nucleobase lesions is the task of the base excision repair (BER) pathway, which is initiated when a lesion is recognized and removed by a damage-specific glycosylase (**Figure 1.4.**).[7] Glycosylases remove the nucleobase by cleaving the *N*-glycosidic bond to result in an abasic site. The resulting abasic site is recognized by AP Endonuclease-1 (APE1), which cleaves the phosphate backbone to create a nick site containing a 3'-OH and 5'-deoxyribose phosphate group (5'-dRP). Polymerase beta (polβ) processes this intermediate by

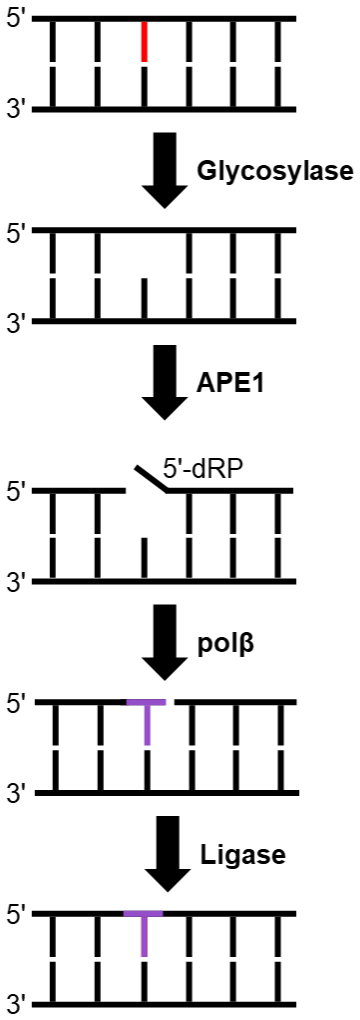

Figure 1.4. Base excision repair. BER is initiated with the recognition and removal of a nucleobase lesion (red) by a damage-specific glycosylase. The resulting abasic site is recognized by APE1, which cleaves 5' to the abasic site to create a nick with 3'-OH and 5'-deoxyribose phosphate (5'-dRP) ends. Polβ first removes the 5'-dRP and then inserts the correct nucleotide (purple). Lastly, a ligase seals the nick between the 3'-OH of the new nucleotide and the 5'-phosphate to rejoin the phosphate backbone and complete repair.

first removing the 5'-dRP and then inserting the correct nucleotide on the 3' side of the nick.[15] A DNA ligase seals the nick to rejoin the phosphate backbone and completes the repair.

1.4. DNA glycosylases

There are eleven glycosylases that have been identified in humans and they are categorized based on their structural architecture, falling into one of six superfamilies.[16] The advent of synthetic organic chemistry methods to produce DNA oligonucleotides with a single and site-specifically incorporated lesion made it possible for substrate specificity identifications and mechanistic studies of glycosylases to understand how BER is initiated.

1.4.1. Searching for lesion substrates by glycosylases

The first task of the DNA glycosylase is to find its rare lesion substrate among the entirety of the genomic DNA. Given the average formation of ~10,000 lesions per cell per day, this searching task of DNA glycosylases is a formidable challenge analogous to finding a needle in a haystack, due to the presence of ~12,000,000,000 undamaged nucleobases to search through as well.[2,17] Fast, efficient lesion searching by glycosylases to initiate BER is critical to removing damage before replication to prevent mutagenic events. Unlike other repair pathways, BER substrates are typically non-bulky and are therefore not as disruptive to the local DNA environment as bulkier lesions, like thymine dimers repaired by nucleotide excision repair. Our understanding of how lesions are found in a vast excess of undamaged DNA is incomplete despite many studies trying to address this question.[17]

The current working model in the field proposes a combination of both long-range, three-dimensional diffusion as well as shorter-range one-dimensional diffusion for the most efficient means of finding lesions. The majority of studies have focused on the one-

dimensional method, specifically how the glycosylase travels from one lesion site to another in a single binding event, or its processivity.[18] Processivity is believed to be most efficient by utilizing two modes of travel between lesion sites: associative transfer, or "sliding" along the phosphate backbone; and dissociative transfer, or small "hops" of micro-dissociations. A portion of the proceeding work will focus on processivity in the context of the human genome and will be discussed in more depth in Chapter 4.

1.4.2. Substrate specificity of glycosylases

Each glycosylase has specificity for removal of a small number of lesions (**Table 1.1.**). Some glycosylases are very specific for the removal of one type of lesion. For example, uracil DNA glycosylase (UDG) is most specifically responsible for the removal of U lesions.[19,20] Conversely, AAG has a relatively broad specificity in lesion removal, having the ability to remove at least five lesions due to alkylation or deamination of

Table 1.1. Human DNA glycosylases and their preferred substrates and bend angles.

Human Glycosylase	*E. coli* homolog	Substrate(s)[a]	Also works on ssDNA	Bend angle
AAG	AlkA	3meA, 7meA, εA, Hx, X	(not well)	22°[22]
UNG1/2	UDG	U	yes	45°[23,24]
SMUG1	MUG	U; hmU	yes	> 45°[25]
TDG		**T**:G; **U**:G; **T**:C; **T**:T	no	43°[26]
MBD4		**T**:G; **U**:G; **hmU**:G	no	57°[27]
MUTYH	MutY	**A**:8-oxoG	no	55°[28]
hOGG1	Fpg	8-oxoG; FapyG	no	70°[29]
NTH1	Nth	FapyG; Tg; 5,6DHU; 5hC; 5hU	no	55°[30]
NEIL1	Nei	Sp; Gh; FapyG; FapyA; 5,6DHT; 5,6DHU	yes	42°[31]
NEIL2		Sp; Gh; 5hU; 5,6DHT; 5,6DHU; 5hC	prefers ssDNA	
NEIL3		Sp; Gh; FapyG; FapyA	prefers ssDNA	

[a] **N**:N represents a mispair where the bolded nucleobase is the one that is removed by the glycosylase

purines.[21] It is also important to note that sometimes a canonical base must be removed by glycosylases based on the duplex context. For example, the human MUTY glycosylase recognizes and removes the A that was incorporated across from an 8-oxoG lesion after replication to prevent a G to T point mutation.[32] Additionally, thymine DNA glycosylase (TDG) removes T from T:G mispairs, resulting from the deamination of 5-methyl C.[33,34] Interestingly, not all nucleobase lesions must be removed from a duplex context. Some glycosylases have the ability to remove lesions in both single- and double-strand contexts, while others only have activity on double-strand DNA.[35–38]

1.4.3. General mechanism of glycosylases

Despite the difference in their structures and target lesions, the eleven human glycosylases share the same mechanism for removing lesions from duplex.[16] Briefly, this mechanism is referred to as the "pinch, push, plug, pull" mechanism.[39,40] Once the lesion is found, the glycosylase binds to the lesion and results in a "pinch", or bend in the surrounding DNA that causes a 22-70° kink depending on the glycosylase observed (**Table 1.1.**). This distortion of the DNA structure allows for the glycosylase to "push" the lesion out of the double helix via base flipping, into the active site of the glycosylase (**Figure 1.5.**). The glycosylase "plugs" the void left behind by the extruded lesion with an amino acid residue to stabilize the duplex structure. The "pull" refers to the stability of the lesion within the active site, where chemistry of cleaving the glycosidic bond takes place.[41]

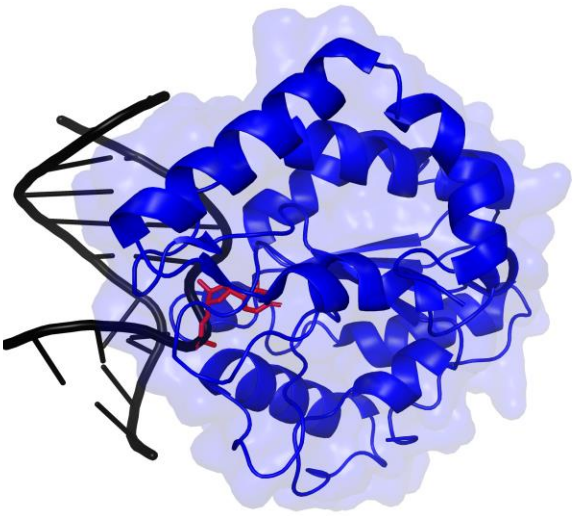

Figure 1.5. Structure of UDG bound to duplex DNA. The UDG enzyme (blue) is bound to the duplex (black) such that the lesion (red) is flipped into the active site and primed for hydrolysis of the *N*-glycosidic bond.

1.4.4. Kinetics of glycosylases

A minimal kinetic scheme for DNA glycosylases (**Figure 1.6.**) begins once the nucleobase lesion has been found, and includes the three steps of the enzymatic cycle: (1) specific binding to the DNA lesion substrate; (2) the chemistry step (k_{chem}), which is cleavage of the glycosidic bond to excise the lesion; and (3) release of the DNA product (k_{rel}). For most glycosylases, product release is rate limiting and is defined by k_{cat}, which is measured under multiple turnover (MTO) conditions ([glycosylase]<<[DNA]). For glycosylases, k_{cat} reflects product release rather than chemistry. By carrying out experiments under single-turnover (STO) conditions ([glycosylase]>>[DNA]), each enzyme has only one chance to perform chemistry before the substrate is consumed and k_{rel} does not factor into the kinetic model. The k_{obs} value is therefore reflective of the slowest step up to or including chemistry. When performing STO experiments using duplex substrates, searching and binding to the DNA substrate by glycosylases is known to be fast and $k_{obs} = k_{chem}$.

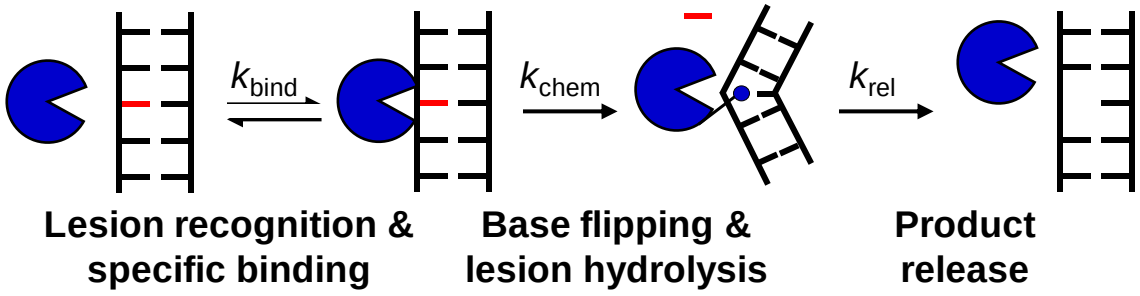

Figure 1.6. Minimal kinetic scheme for base-flipping glycosylases. Once the lesion (red rectangle) is found, the glycosylase (blue crescent) binds specifically to the DNA to flip the damaged base into the enzyme active site, while plugging the void left in the duplex with an amino acid. From here, the glycosylase performs the chemistry of cleaving the *N*-glycosidic bond (k_{chem}). After chemistry, the DNA product is released (k_{rel}).

1.5. Deficiency in BER

Failure for proper and complete repair of modified nucleobases due to insufficient activity from any of the BER enzymes can have major consequences, including decreased cell viability, accelerated aging, and cancer.[42,43] Indeed, homozygous deletions of TDG,[44] APE1,[45] and polβ,[46] are embryonic lethal in mouse models and therefore implicated in early embryonic development. Gene mutations that inactivate oxoguanine DNA glycosylase (hOGG1), the glycosylase responsible for removing 8-oxoG lesions, have been associated with esophageal, lung squamous cell carcinomas, kidney, and gastric cancers.[42] Specifically, mutations that influence the glycosylase's ability to perform chemistry efficiently have been shown to be detrimental to cell viability. For example, mutations in amino acids that are used in lesion searching in alkyladenine DNA glycosylase (AAG) have shown sensitivity to alkylating damage.[47] Additionally, mutations in polβ have been observed in ~30% of tumors in humans.[48] The importance of BER to cell viability has been studied in the context of organismal well-being, but has also emerged as a therapeutic target to specifically combat cancer cells.[49,50]

1.6. Eukaryotic DNA is packaged into NCPs

Most of the mechanistic studies and substrate specificity characterizations of glycosylases were identified using duplex substrates. However, eukaryotic genomic DNA is highly compacted and packaged into chromatin to fit about 2 m of DNA into the cell nucleus. The primary repeating unit of chromatin is the nucleosome core particle (NCP) and therefore the lowest-order element of DNA accessibility. NCPs consist of 145-147 bp of DNA wrapped ~1.7 left-handed superhelical turns around a core of histone proteins (**Figure 1.7.**), with a 2-fold axis of pseudosymmetry known as the dyad axis.[51] The octameric histone core is made up of two copies of each of the canonical histone proteins

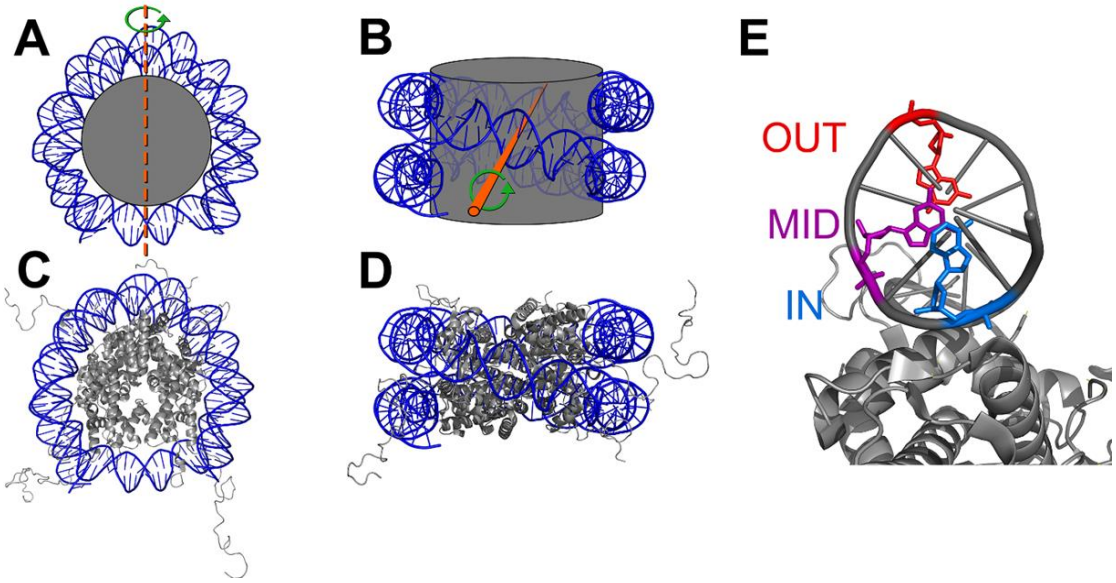

Figure 1.7. Representations of the NCP. (A) Top view and **(B)** side view of the NCP represented as a spool-and-thread cartoon. The DNA is colored blue and the histone octamer is gray. The dyad axis is indicated by a dashed orange line in **(A)** and an orange rod coming out of the plane in **(B)**. The pseudosymmetry of the histone octamer about the dyad axis is indicated by the green arrow. In **(C)** and **(D)** the histone proteins are shown as ribbon diagrams. NCP representations are merged crystal structures of an NCP containing the Widom 601 DNA, with a histone octamer containing N-terminal tail regions (PDB entries 3lz0 and 1kx5, respectively). **(E)** Rotational positions of nucleobases relative to the histone octamer core (only one DNA strand is shown for simplicity). Outward (red), midway (purple), and inward (blue) bases are indicated.

H2A, H2B, H3, and H4.[52] Each histone protein contains a globular domain and an unstructured tail region that protrudes from the center of the core.[51] As a result of the DNA's wrapping around the histone core, the DNA structure becomes slightly distorted and stretched compared with duplex.[53,54]

The position of each nucleobase in an NCP can be described with respect to the histone core, which can be varied in two ways: (1) rotational position, referring to the helical orientation, i.e. if the nucleobase is facing out towards solution or in towards the histone octamer core; and (2) translational position, referring to the location of the nucleobase relative to the dyad axis. Ensemble[55] and single molecule[56–58] FRET measurements have shown that spontaneous unwrapping of nucleosomal DNA transiently

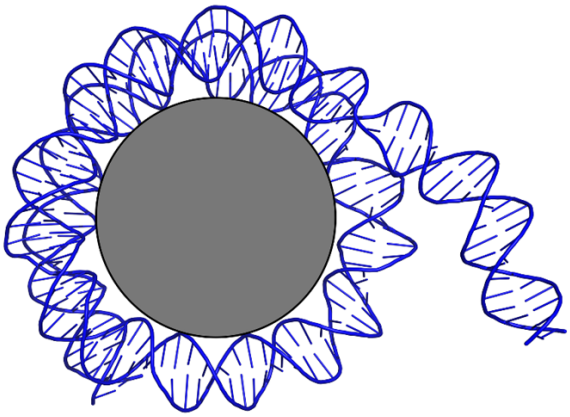

Figure 1.8. DNA unwrapping in an NCP. Spool-and-thread representation of an NCP showing an unwrapped state of one end of the DNA from the histone octamer core.

exposes nucleobases that face in towards the histone octamer core (**Figure 1.8.**). Specifically, the rate of increasing the distance between the DNA ends and the histone octamer (unwrapping) were determined to be ~0.28 ms^{-1}. Conversely, the rate of re-wrapping was ~0.49 ms^{-1}.[58] This dynamic motion ultimately results in increased solution accessibility of nucleobases closer to the ends of DNA compared with bases at the dyad axis. Indeed, restriction enzymes showed increased accessibility to recognition sites closer to ends of nucleosomal DNA compared with sites on the dyad axis.[59,60] Interestingly, NCPs have been shown to preferentially unwrap one end over the other, referred to as asymmetric unwrapping.[61–63]

Beyond the four canonical histone proteins, there are a variety of histone variants that differ from the canonical structures,[64] and are involved in the facilitation of cellular processes, including double-strand break repair.[65] In addition to swapping out canonical histone proteins, the canonical histones can be modified with post-translational modifications (PTMs) such as methylation and acetylation. An less-understood histone modification of recent interest is histone tail clipping, in which endopeptidases completely remove the histone tails to either prevent further modification or remove all previous modifications.[66] Previous studies have shown that changing the histone octamer composition in one of the above-mentioned ways may influence BER in the NCP.[67–70]

1.7. Experimental parameters and considerations for studying glycosylase activity in NCPs

There are multiple experimental factors to consider when constructing an NCP model system to examine BER *in vitro*. Some of these factors include: the histone proteins, the DNA sequence and length, and the location and geometric position of the lesion of interest. It has become increasingly clear that each of these factors can modulate the efficiency of each enzymatic player in the BER pathway. Due to this variety of experimental parameters, one must choose the best option to address the desired question(s). Below are descriptions for some of the most commonly-used systems to assemble NCPs in the laboratory.

1.7.1. Source of histone proteins

Isolation of histone octamer cores from a biological source. Many of the first studies on reconstituted NCPs used a biological source of histone octamer cores isolated from chicken erythrocytes.[71] In this procedure, chromatin is isolated and digested with micrococcal nuclease to obtain NCPs containing chicken DNA. The original chicken DNA is then exchanged for the experimental DNA of interest by incremental dialysis from high to low concentrations of salt.[71,72] Similar experiments have been performed using HeLa cells as a biological source of histone octamer cores.[73,74] An important consideration of these NCPs assembled using isolated histones is that they are subject to a diverse array of PTMs and represent a heterogeneous population.

Recombinantly expressed histone proteins. Luger and Richmond reported the first high-resolution crystal structure of an NCP.[51] Crystallization of the NCP required a homogeneous population of NCPs and led to the recombinant expression and purification of individual *Xenopus laevis* histone proteins in *E. coli.*[51,75] These individual histone proteins are then combined to form the histone octamer core. The high conservation of

the histone proteins H2A, H2B, H3, and H4 across evolution makes studies using *X. laevis* histone proteins generalizable to all eukaryotes.[76] Creating NCPs using recombinant histone proteins is an important step if a homogeneous substrate population is required. This homogeneity, however, comes at the expense of histone PTMs which are known to be biologically relevant.

1.7.2. DNA sequence

While most DNA sequences have affinity for the histone proteins, a small subset (< 5%) have a stronger, sequence-derived affinity that dictates NCP positioning.[77] These DNA are called nucleosome positioning sequences and bind histones in a predictable and reproducible manner with a defined translational and rotational position. The most commonly-used positioning sequences are the 5S rDNA and the Widom 601 sequences.

5S rDNA sequence. The first demonstration that a DNA duplex could create predictable, positioned nucleosomes used the 5S sequence from the sea urchin *L. variegatus*.[78] The 5S sequence is appealing to use for *in vitro* experiments because it is a naturally-occurring sequence that is highly conserved in other organisms.[79] Periodicity of the 5S DNA sequence in an NCP changes relative to the unwrapped version, as revealed by hydroxyl radical footprinting (HRF). It is also known that the periodicity changes within the NCP depending on the translational position relative to the dyad axis.[54] These changes in periodicity based on translational location have also been observed for other DNA sequences.[80,81] Additionally, the 5S sequence adopts multiple translational positions that are offset by multiples of 10 bp, especially when the length of the DNA surpasses the minimal 145-147 bp required to form an NCP.[82–84] However, incubating the NCPs at elevated temperatures allows the DNA to “heat shift” to a single, thermodynamically favored translational position.[85]

Widom 601 sequence. The Widom group recognized the potential benefits of using a positioning sequence and sought to identify the characteristics that define such DNA.[86] Using a SELEX approach, they selected from a library of randomized DNA sequences those that had the highest affinity for the histone octamer core. These experiments identified the 601 sequence, a synthetic positioning sequence that binds the histone octamer core in a single orientation. Crystal structures of NCPs containing 601 DNA and *X. laevis* histones serve as useful references for designing experiments to address BER in NCPs.[53,81,87] In comparison with the naturally-occurring 5S sequence, the 601 NCP has been shown to be less dynamic and less accessible to digestion by restriction enzymes.[59]

1.7.3. Incorporation of DNA lesion

Single, site-specific lesions. A common experimental set-up utilizes one lesion in a well-defined rotational and translational position. A site of interest for the lesion can be identified, in some cases with reference to a crystal structure, and DNA can be prepared in which the canonical nucleobase is replaced with a lesion. Each NCP in the population has the same lesion located in the same rotational and translational position. HRF and digestion by exonuclease III can be used to confirm the rotational and translational position of the lesion. A substantial body of literature exists that used site-specific incorporation of a lesion and serves as a major source of our current understanding of BER in NCPs.

Global incorporation of lesions. Another method of studying BER in NCPs is one that uses global incorporation of lesions. Using either PCR or chemical synthesis techniques, a population of DNA sequences can be prepared in which a lesion is globally incorporated across a variety of rotational and translational positions in NCPs. This technique has been used to create populations of NCPs in which, on a single strand, all the T sites have been replaced by U,[88–90] and the G sites have been replaced by 8-oxo-7,8-dihydroguanine (8-oxoG).[91] While T and G have been globally substituted, each NCP

contains only one lesion. By using the entire population of NCPs as a substrate in BER, the global profile of repair in packaged DNA can be identified.

1.8. Gap in knowledge and concluding remarks

The repair of DNA damage is essential for the survival of an organism. Nucleobase lesions can result from oxidation, alkylation, and/or deamination events that originate from endogenous or exogenous sources. The persistence of these nucleobase lesions leads to mutagenesis and genomic instability. Fortunately, the BER pathway is responsible for the recognition, removal, and repair of single-base lesions to protect the genetic information. However, the ubiquitous sequestration of eukaryotic DNA into chromatin presents a conundrum for BER enzymes, which interact intimately with DNA. This thesis work specifically focuses on efforts to address the initiation of BER by glycosylases in packaged DNA.

The proceeding work utilizes three different lesion-containing NCP substrate set-ups to explore the relationship between glycosylase activity in a packaged DNA environment. First, Chapter 2 examines the activities of hOGG1 and UDG in site-specific NCPs located in three rotational positions near the DNA end to determine how DNA-histone dynamics influence glycosylase activity. Chapter 3 surveys the repair profile of εA excision by AAG in 49 distinct translational and rotational positions using a population of global εA-containing NCPs to study the relationship between repair and NCP architecture. Lastly, Chapter 4 explores the processivity of UDG in NCPs containing two U lesions to investigate searching capabilities in the context of the packaged eukaryotic genome. With these studies, we aim to elucidate how BER initiation is influenced by DNA packaging. A more complete understanding of BER in the context of eukaryotic DNA will provide valuable insight into the balance between DNA damage, repair, and mutation.

1.9. References

(1) Watson, J. D., and Crick, F. H. (1953) Molecular structure of nucleic acids; a structure for deoxyribose nucleic acid. *Nature 171*, 737–8.

(2) Lindahl, T. (1993) Instability and decay of the primary structure of DNA. *Nature 362*, 709–715.

(3) Gates, K. S. (2009) An overview of chemical processes that damage cellular DNA: spontaneous hydrolysis, alkylation, and reactions with radicals. *Chem. Res. Toxicol. 22*, 1747–60.

(4) Swenberg, J. A., Lu, K., Moeller, B. C., Gao, L., Upton, P. B., Nakamura, J., and Starr, T. B. (2011) Endogenous versus exogenous DNA adducts: Their role in carcinogenesis, epidemiology, and risk assessment. *Toxicol. Sci. 120*, S130-45.

(5) Hoeijmakers, J. H. (2001) Genome maintenance mechanisms for preventing cancer. *Nature 411*, 366–74.

(6) Sancar, A., Lindsey-Boltz, L. A., Unsal-Kaçmaz, K., and Linn, S. (2004) Molecular mechanisms of mammalian DNA repair and the DNA damage checkpoints. *Annu. Rev. Biochem. 73*, 39–85.

(7) Schermerhorn, K. M., and Delaney, S. (2014) A chemical and kinetic perspective on base excision repair of DNA. *Acc. Chem. Res. 47*, 1238–1246.

(8) Delaney, S., Jarem, D. A., Volle, C. B., and Yennie, C. J. (2012) Chemical and biological consequences of oxidatively damaged guanine in DNA. *Free Radic. Res. 46*, 420–41.

(9) Chung, F. L., Chen, H. J., and Nath, R. G. (1996) Lipid peroxidation as a potential endogenous source for the formation of exocyclic DNA adducts. *Carcinogenesis 17*, 2105–11.

(10) Friedberg, E. C., Walker, G. C., Siede, W., and Wood, R. D. (2005) DNA Repair and Mutagenesis Second. American Society for Microbiology.

(11) Pandya, G. A., and Moriya, M. (1996) 1,N6-ethenodeoxyadenosine, a DNA adduct highly mutagenic in mammalian cells. *Biochemistry 35*, 11487–92.

(12) Chapman, J. R., Taylor, M. R. G., and Boulton, S. J. (2012) Playing the End Game: DNA Double-Strand Break Repair Pathway Choice. *Mol. Cell 47*, 497–510.

(13) Caldecott, K. W. (2008) Single-strand break repair and genetic disease. *Nat. Rev. Genet. 9*, 619–631.

(14) Chatterjee, N., and Walker, G. C. (2017) Mechanisms of DNA damage, repair, and mutagenesis. *Environ. Mol. Mutagen. 58*, 235–263.

(15) Prasad, R., Shock, D. D., Beard, W. A., and Wilson, S. H. (2010) Substrate channeling in mammalian base excision repair pathways: passing the baton. *J. Biol. Chem. 285*, 40479–88.

(16) Brooks, S. C., Adhikary, S., Rubinson, E. H., and Eichman, B. F. (2013) Recent advances in the structural mechanisms of DNA glycosylases. *Biochim. Biophys. Acta - Proteins Proteomics 1834*, 247–271.

(17) Friedman, J. I., and Stivers, J. T. (2010) Detection of damaged DNA bases by DNA glycosylase enzymes. *Biochemistry 49*, 4957–67.

(18) Esadze, A., and Stivers, J. T. (2018) Facilitated Diffusion Mechanisms in DNA Base Excision Repair and Transcriptional Activation. *Chem. Rev.* acs.chemrev.8b00513.

(19) Lindahl, T., Ljungquist, S., Siegert, W., Nyberg, B., and Sperens, B. (1977) DNA N-glycosidases: properties of uracil-DNA glycosidase from Escherichia coli. *J. Biol. Chem. 252*, 3286–94.

(20) Schormann, N., Ricciardi, R., and Chattopadhyay, D. (2014) Uracil-DNA glycosylases-structural and functional perspectives on an essential family of DNA repair enzymes. *Protein Sci. 23*, 1667–85.

(21) O'Brien, P. J., and Ellenberger, T. (2004) Dissecting the Broad Substrate Specificity of Human 3-Methyladenine-DNA Glycosylase. *J. Biol. Chem. 279*, 9750–9757.

(22) Lau, A. Y., Schärer, O. D., Samson, L., Verdine, G. L., and Ellenberger, T. (1998) Crystal Structure of a Human Alkylbase-DNA Repair Enzyme Complexed to DNA. *Cell 95*, 249–258.

(23) Slupphaug, G., Mol, C. D., Kavli, B., Arvai, A. S., Krokan, H. E., and Tainer, J. A. (1996) A nucleotide-flipping mechanism from the structure of human uracil-DNA glycosylase bound to DNA. *Nature 384*, 87–92.

(24) Parikh, S. S., Mol, C. D., Slupphaug, G., Bharati, S., Krokan, H. E., and Tainer, J. A. (1998) Base excision repair initiation revealed by crystal structures and binding kinetics of human uracil-DNA glycosylase with DNA. *EMBO J. 17*, 5214–26.

(25) Wibley, J. E. A., Waters, T. R., Haushalter, K., Verdine, G. L., and Pearl, L. H. (2003) Structure and specificity of the vertebrate anti-mutator uracil-DNA glycosylase SMUG1. *Mol. Cell 11*, 1647–59.

(26) Maiti, A., Morgan, M. T., Pozharski, E., and Drohat, A. C. (2008) Crystal structure of human thymine DNA glycosylase bound to DNA elucidates sequence-specific mismatch recognition. *Proc. Natl. Acad. Sci. U. S. A. 105*, 8890–5.

(27) Manvilla, B. A., Maiti, A., Begley, M. C., Toth, E. A., and Drohat, A. C. (2012) Crystal Structure of Human Methyl-Binding Domain IV Glycosylase Bound to Abasic DNA. *J. Mol. Biol. 420*, 164–175.

(28) Fromme, J. C., Banerjee, A., Huang, S. J., and Verdine, G. L. (2004) Structural basis for removal of adenine mispaired with 8-oxoguanine by MutY adenine DNA glycosylase. *Nature 427*, 652–656.

(29) Bruner, S. D., Norman, D. P. G., and Verdine, G. L. (2000) Structural basis for recognition and repair of the endogenous mutagen 8-oxoguanine in DNA. *Nature 403*, 859–866.

(30) Fromme, J. C., and Verdine, G. L. (2003) Structure of a trapped endonuclease III-DNA covalent intermediate. *EMBO J. 22*, 3461–3471.

(31) Zhu, C., Lu, L., Zhang, J., Yue, Z., Song, J., Zong, S., Liu, M., Stovicek, O., Gao, Y. Q., and Yi, C. (2016) Tautomerization-dependent recognition and excision of oxidation damage in base-excision DNA repair. *Proc. Natl. Acad. Sci. 113*, 7792–7797.

(32) Michaels, M. L., Tchou, J., Grollman, A. P., and Miller, J. H. (1992) A repair system for 8-oxo-7,8-dihydrodeoxyguanine. *Biochemistry 31*, 10964–8.

(33) Wiebauer, K., and Jiricny, J. (1990) Mismatch-specific thymine DNA glycosylase and DNA polymerase beta mediate the correction of G.T mispairs in nuclear extracts from human cells. *Proc. Natl. Acad. Sci. U. S. A. 87*, 5842–5.

(34) Maiti, A., and Drohat, A. C. (2011) Thymine DNA glycosylase can rapidly excise 5-formylcytosine and 5-carboxylcytosine: potential implications for active demethylation of CpG sites. *J. Biol. Chem. 286*, 35334–8.

(35) Kavli, B., Slupphaug, G., Mol, C. D., Arvai, A. S., Peterson, S. B., Tainer, J. A., and Krokan, H. E. (1996) Excision of cytosine and thymine from DNA by mutants of human uracil-DNA glycosylase. *EMBO J. 15*, 3442–7.

(36) Nash, H. M., Lu, R., Lane, W. S., and Verdine, G. L. (1997) The critical active-site amine of the human 8-oxoguanine DNA glycosylase, hOgg1: direct identification, ablation and chemical reconstitution. *Chem. Biol. 4*, 693–702.

(37) Hazra, T. K., Kow, Y. W., Hatahet, Z., Imhoff, B., Boldogh, I., Mokkapati, S. K., Mitra, S., and Izumi, T. (2002) Identification and characterization of a novel human DNA glycosylase for repair of cytosine-derived lesions. *J. Biol. Chem. 277*, 30417–20.

(38) Kavli, B., Sundheim, O., Akbari, M., Otterlei, M., Nilsen, H., Skorpen, F., Aas, P. A., Hagen, L., Krokan, H. E., and Slupphaug, G. (2002) hUNG2 is the major repair enzyme for removal of uracil from U:A matches, U:G mismatches, and U in single-stranded DNA, with hSMUG1 as a broad specificity backup. *J. Biol. Chem. 277*, 39926–36.

(39) Jiang, Y. L., Stivers, J. T., and Song, F. (2002) Base-flipping mutations of uracil DNA glycosylase: substrate rescue using a pyrene nucleotide wedge. *Biochemistry 41*, 11248–

54.

(40) Wong, I., Lundquist, A. J., Bernards, A. S., and Mosbaugh, D. W. (2002) Presteady-state analysis of a single catalytic turnover by Escherichia coli uracil-DNA glycosylase reveals a "pinch-pull-push" mechanism. *J. Biol. Chem. 277*, 19424–32.

(41) Stivers, J. T., and Jiang, Y. L. (2003) A Mechanistic Perspective on the Chemistry of DNA Repair Glycosylases. *Chem. Rev. 103*, 2729–2760.

(42) Xu, G., Herzig, M., Rotrekl, V., and Walter, C. A. (2008) Base excision repair, aging and health span. *Mech. Ageing Dev. 129*, 366–382.

(43) Robertson, A. B., Klungland, A., Rognes, T., and Leiros, I. (2009) DNA repair in mammalian cells: Base excision repair: the long and short of it. *Cell. Mol. Life Sci. 66*, 981–93.

(44) Cortázar, D., Kunz, C., Selfridge, J., Lettieri, T., Saito, Y., MacDougall, E., Wirz, A., Schuermann, D., Jacobs, A. L., Siegrist, F., Steinacher, R., Jiricny, J., Bird, A., and Schär, P. (2011) Embryonic lethal phenotype reveals a function of TDG in maintaining epigenetic stability. *Nature 470*, 419–23.

(45) Meira, L. B., Devaraj, S., Kisby, G. E., Burns, D. K., Daniel, R. L., Hammer, R. E., Grundy, S., Jialal, I., and Friedberg, E. C. (2001) Heterozygosity for the mouse Apex gene results in phenotypes associated with oxidative stress. *Cancer Res. 61*, 5552–7.

(46) Gu, H., Marth, J. D., Orban, P. C., Mossmann, H., and Rajewsky, K. (1994) Deletion of a DNA polymerase beta gene segment in T cells using cell type-specific gene targeting. *Science 265*, 103–6.

(47) Zhang, Y., and O'Brien, P. J. (2015) Repair of Alkylation Damage in Eukaryotic Chromatin Depends on Searching Ability of Alkyladenine DNA Glycosylase. *ACS Chem. Biol. 10*, 2606–15.

(48) Starcevic, D., Dalal, S., and Sweasy, J. B. (2004) Is there a link between DNA polymerase beta and cancer? *Cell Cycle 3*, 998–1001.

(49) Fishel, M. L., and Kelley, M. R. (2007) The DNA base excision repair protein Ape1/Ref-1 as a therapeutic and chemopreventive target. *Mol. Aspects Med. 28*, 375–95.

(50) Yang, J., Parsons, J., Nicolay, N. H., Caporali, S., Harrington, C. F., Singh, R., Finch, D., D'Atri, S., Farmer, P. B., Johnston, P. G., McKenna, W. G., Dianov, G., and Sharma, R. A. (2010) Cells deficient in the base excision repair protein, DNA polymerase beta, are hypersensitive to oxaliplatin chemotherapy. *Oncogene 29*, 463–8.

(51) Richmond, R. K., Sargent, D. F., Richmond, T. J., Luger, K., and Mäder, A. W. (2002) Crystal structure of the nucleosome core particle at 2.8 Å resolution. *Nature 389*, 251–260.

(52) Eickbush, T. H., and Moudrianakis, E. N. (1978) The histone core complex: an octamer assembled by two sets of protein-protein interactions. *Biochemistry 17*, 4955–64.

(53) Chua, E. Y. D., Vasudevan, D., Davey, G. E., Wu, B., and Davey, C. A. (2012) The mechanics behind DNA sequence-dependent properties of the nucleosome. *Nucleic Acids Res. 40*, 6338–6352.

(54) Hayes, J. J., Tullius, T. D., and Wolffe, A. P. (1990) The structure of DNA in a nucleosome. *Proc. Natl. Acad. Sci. U. S. A. 87*, 7405–9.

(55) Yang, J., and Narlikar, G. (2007) FRET-based methods to study ATP-dependent changes in chromatin structure. *Methods 41*, 291–295.

(56) Buning, R., and van Noort, J. (2010) Single-pair FRET experiments on nucleosome conformational dynamics. *Biochimie 92*, 1729–40.

(57) Lee, J. Y., Lee, J., Yue, H., and Lee, T.-H. (2015) Dynamics of nucleosome assembly and effects of DNA methylation. *J. Biol. Chem. 290*, 4291–303.

(58) Kim, J., Wei, S., Lee, J., Yue, H., and Lee, T. H. (2016) Single-Molecule Observation Reveals Spontaneous Protein Dynamics in the Nucleosome. *J. Phys. Chem. B 120*, 8925–8931.

(59) Polach, K. J., and Widom, J. (1999) Restriction enzymes as probes of nucleosome

stability and dynamics. *Methods Enzymol. 304*, 278–98.

(60) Anderson, J. D., and Widom, J. (2000) Sequence and position-dependence of the equilibrium accessibility of nucleosomal DNA target sites. *J. Mol. Biol. 296*, 979–987.

(61) Chen, Y., Tokuda, J. M., Topping, T., Sutton, J. L., Meisburger, S. P., Pabit, S. A., Gloss, L. M., and Pollack, L. (2014) Revealing transient structures of nucleosomes as DNA unwinds. *Nucleic Acids Res. 42*, 8767–76.

(62) Ngo, T. T. M., Zhang, Q., Zhou, R., Yodh, J. G., and Ha, T. (2015) Asymmetric unwrapping of nucleosomes under tension directed by DNA local flexibility. *Cell 160*, 1135–1144.

(63) Gansen, A., Felekyan, S., Kühnemuth, R., Lehmann, K., Tóth, K., Seidel, C. A. M., and Langowski, J. (2018) High precision FRET studies reveal reversible transitions in nucleosomes between microseconds and minutes. *Nat. Commun. 9*, 4628.

(64) Koyama, M., and Kurumizaka, H. (2018) Structural diversity of the nucleosome. *J. Biochem.*

(65) Pusarla, R.-H., and Bhargava, P. (2005) Histones in functional diversification. Core histone variants. *FEBS J. 272*, 5149–68.

(66) Azad, G. K., Swagatika, S., Kumawat, M., Kumawat, R., and Tomar, R. S. (2018) Modifying Chromatin by Histone Tail Clipping. *J. Mol. Biol. 430*, 3051–3067.

(67) Menoni, H., Gasparutto, D., Hamiche, A., Cadet, J., Dimitrov, S., Bouvet, P., and Angelov, D. (2007) ATP-dependent chromatin remodeling is required for base excision repair in conventional but not in variant H2A.Bbd nucleosomes. *Mol. Cell. Biol. 27*, 5949–56.

(68) Rodriguez, Y., Hinz, J. M., Laughery, M. F., Wyrick, J. J., and Smerdon, M. J. (2016) Site-specific Acetylation of Histone H3 Decreases Polymerase β Activity on Nucleosome Core Particles in Vitro. *J. Biol. Chem. 291*, 11434–45.

(69) Meas, R., Smerdon, M. J., and Wyrick, J. J. (2015) The amino-terminal tails of

histones H2A and H3 coordinate efficient base excision repair, DNA damage signaling and postreplication repair in Saccharomyces cerevisiae. *Nucleic Acids Res. 43*, 4990–5001.

(70) Beard, B. C., Stevenson, J. J., Wilson, S. H., and Smerdon, M. J. (2005) Base excision repair in nucleosomes lacking histone tails. *DNA Repair (Amst). 4*, 203–209.

(71) Hayes, J. J., and Lee, K. M. (1997) In vitro reconstitution and analysis of mononucleosomes containing defined DNAs and proteins. *Methods 12*, 2–9.

(72) Libertini, L. J., and Small, E. W. (1980) Salt induced transitions of chromatin core particles studied by tyrosine fluorescence anisotropy. *Nucleic Acids Res. 8*, 3517–34.

(73) Ober, M., and Lippard, S. J. (2007) Cisplatin damage overrides the predefined rotational setting of positioned nucleosomes. *J. Am. Chem. Soc. 129*, 6278–86.

(74) Mulvihill, D. J., Nichol Edamura, K., Hagerman, K. A., Pearson, C. E., and Wang, Y.-H. (2005) Effect of CAT or AGG interruptions and CpG methylation on nucleosome assembly upon trinucleotide repeats on spinocerebellar ataxia, type 1 and fragile X syndrome. *J. Biol. Chem. 280*, 4498–503.

(75) Luger, K., Rechsteiner, T. J., Flaus, A. J., Waye, M. M., and Richmond, T. J. (1997) Characterization of nucleosome core particles containing histone proteins made in bacteria. *J. Mol. Biol. 272*, 301–11.

(76) Sullivan, S. A., Aravind, L., Makalowska, I., Baxevanis, A. D., and Landsman, D. (2000) The Histone Database: a comprehensive WWW resource for histones and histone fold-containing proteins. *Nucleic Acids Res. 28*, 320–322.

(77) Lowary, P. T., and Widom, J. (1997) Nucleosome packaging and nucleosome positioning of genomic DNA. *Proc. Natl. Acad. Sci. U. S. A. 94*, 1183–8.

(78) Simpson, R. T., and Stafford, D. W. (1983) Structural features of a phased nucleosome core particle. *Proc. Natl. Acad. Sci. U. S. A. 80*, 51–5.

(79) Long, E. O., and Dawid, I. B. (1980) Repeated genes in eukaryotes. *Annu. Rev.*

Biochem. 49, 727–64.

(80) Prunell, A. (1983) Periodicity of exonuclease III digestion of chromatin and the pitch of deoxyribonucleic acid on the nucleosome. *Biochemistry 22*, 4887–94.

(81) Vasudevan, D., Chua, E. Y. D., and Davey, C. A. (2010) Crystal Structures of Nucleosome Core Particles Containing the “601” Strong Positioning Sequence. *J. Mol. Biol. 403*, 1–10.

(82) Dong, F., Hansen, J. C., and van Holde, K. E. (1990) DNA and protein determinants of nucleosome positioning on sea urchin 5S rRNA gene sequences in vitro. *Proc. Natl. Acad. Sci. U. S. A. 87*, 5724–8.

(83) Ura, K., Hayes, J. J., and Wolffe, A. P. (1995) A positive role for nucleosome mobility in the transcriptional activity of chromatin templates: restriction by linker histones. *EMBO J. 14*, 3752–65.

(84) Prasad, A., Wallace, S. S., and Pederson, D. S. (2007) Initiation of base excision repair of oxidative lesions in nucleosomes by the human, bifunctional DNA glycosylase NTH1. *Mol. Cell. Biol. 27*, 8442–53.

(85) Flaus, A., Luger, K., Tan, S., and Richmond, T. J. (1996) Mapping nucleosome position at single base-pair resolution by using site-directed hydroxyl radicals. *Proc. Natl. Acad. Sci. U. S. A. 93*, 1370–5.

(86) Lowary, P. T., and Widom, J. (1998) New DNA sequence rules for high affinity binding to histone octamer and sequence-directed nucleosome positioning. *J. Mol. Biol. 276*, 19–42.

(87) Bednar, J., Garcia-Saez, I., Boopathi, R., Cutter, A. R., Papai, G., Reymer, A., Syed, S. H., Lone, I. N., Tonchev, O., Crucifix, C., Menoni, H., Papin, C., Skoufias, D. A., Kurumizaka, H., Lavery, R., Hamiche, A., Hayes, J. J., Schultz, P., Angelov, D., Petosa, C., and Dimitrov, S. (2017) Structure and Dynamics of a 197 bp Nucleosome in Complex with Linker Histone H1. *Mol. Cell 66*, 384–397.e8.

(88) Cole, H. A., Tabor-Godwin, J. M., and Hayes, J. J. (2010) Uracil DNA glycosylase activity on nucleosomal DNA depends on rotational orientation of targets. *J. Biol. Chem. 285*, 2876–2885.

(89) Ye, Y., Stahley, M. R., Xu, J., Friedman, J. I., Sun, Y., McKnight, J. N., Gray, J. J., Bowman, G. D., and Stivers, J. T. (2012) Enzymatic excision of uracil residues in nucleosomes depends on the local DNA structure and dynamics. *Biochemistry 51*, 6028–6038.

(90) Nilsen, H., Lindahl, T., and Verreault, A. (2002) DNA base excision repair of uracil residues in reconstituted nucleosome core particles. *EMBO J. 21*, 5943–52.

(91) Bilotti, K., Tarantino, M. E., and Delaney, S. (2018) Human Oxoguanine Glycosylase 1 Removes Solution Accessible 8-Oxo-7,8-dihydroguanine Lesions from Globally Substituted Nucleosomes Except in the Dyad Region. *Biochemistry 57*, 1436–1439.

Chapter 2. Human OGG1 activity in nucleosomes is facilitated by transient unwrapping of DNA and is influenced by the local histone environment †

† Adapted from:

Bilotti, K., **Kennedy E.E.**, Li C., Delaney, S. (2017)

Human OGG1 activity in nucleosomes is facilitated by transient unwrapping of DNA and is influenced by the local histone environment.

DNA Repair 59, 1-8

I helped design the DNA substrates and experiments with K.B. I characterized the NCPs containing U lesions and the complementary hydroxyl radical footprinting. I carried out the UDG kinetics and assisted in the octamer reconstitution containing the tailless H2B with K.B. K.B. characterized the histone variant-containing NCPs, performed the hOGG1 kinetics, and the molecular modeling of hOGG1 and the NCP. K.B. and I analyzed the results and contributed to the presented interpretations. C.L. prepared the acetylated H2B and reconstituted the acetylated-H2B octamer. K.B. wrote the published manuscript with S.D.

2.1. Abstract

If unrepaired, damage to genomic DNA can cause mutations and/or be cytotoxic. Single base lesions are repaired via the base excision repair (BER) pathway. The first step in BER is the recognition and removal of the nucleobase lesion by a glycosylase enzyme. For example, human oxoguanine glycosylase 1 (hOGG1) is responsible for removal of the prototypic oxidatively damaged nucleobase, 8-oxo-7,8-dihydroguanine (8-oxoG). To date, most studies of glycosylases have used duplex DNA substrates. However, cellular DNA is packaged as repeating nucleosome units, with 145 base pair segments of DNA wrapped around histone protein octamers. Previous studies revealed inhibition of hOGG1 at the nucleosome dyad axis and in the absence of chromatin remodelers. In this study, we find that even in the absence of chromatin remodelers or external cofactors, hOGG1 can initiate BER at positions off the dyad axis and that this activity is facilitated by spontaneous and transient unwrapping of DNA from the histones. Additionally, we find that solution accessibility as characterized by hydroxyl radical footprinting is not fully predictive of glycosylase activity and that histone tails can suppress hOGG1 activity. We therefore suggest that local nuances in the nucleosome environment and histone-DNA interactions can impact glycosylase activity.

2.2. Introduction

Genomic DNA is under constant threat of damage from free radicals, radiation, and environmental toxins.[1] Persistent chemical modification of a nucleobase can be cytotoxic and/or mutagenic and is the underlying cause of aging and cancer.[1] Therefore, cells have developed a variety of essential repair pathways to remove lesions from DNA. Single base lesions are rectified via the base excision repair (BER) pathway, which is initiated by a glycosylase enzyme specific to the lesion. For example, the oxidation of guanine to 8-oxo-7,8-dihydroguanine (8-oxoG) is repaired in humans by oxoguanine

glycosylase 1 (hOGG1). Glycosylases bind the DNA and flip the lesion out of the base stack into the enzyme's active site. Glycosylases share a common S_N1 type mechanism for cleavage of the glycosidic bond at the lesion, ultimately resulting in an abasic site.[2–4]

The majority of studies to examine glycosylase activity have used duplex DNA as the substrate. While these studies provide essential mechanistic information about glycosylases, cellular DNA packaged as chromatin presents a more complex substrate context for repair *in vivo*.[5] The primary structural repeating unit of chromatin is the nucleosome. Individual nucleosomes, or nucleosome core particles (NCP), serve as a model system for the lowest-order element of DNA packaging. An NCP consists of 145-147 base pairs of duplex DNA wrapped around a protein core. The octameric protein core contains two copies each of the four histone proteins: H2A, H2B, H3, and H4. The histone proteins have unstructured lysine-rich tails which are subject to post-translational modification, such as acetylation.[6] The NCP contains a dyad axis of pseudosymmetry aligned with the central base pair of the wrapped DNA. The translational position of a base refers to its distance from the central base pair. Further, the rotational position of a base describes its rotational orientation relative to the histone core. Outward facing bases are solution accessible while bases facing inward to the histone core are sequestered.

Several factors have been proposed to impact the initiation of repair by glycosylases in packaged DNA substrates, including the steric bulk of the histone proteins and the specific position of the lesion. A recent review by Odell *et al*. summarized the studies to date and proposed a set of general tenets for glycosylase activity in NCPs.[5] First, spontaneous unwrapping of nucleosomal DNA transiently exposes sites that are normally occluded. Ensemble FRET measurements[7–9] and single molecule FRET techniques[10,11] have quantified the rates and extent of DNA end unwrapping. This dynamic motion ultimately results in increased accessibility of bases closer to the ends of DNA compared to bases at the dyad axis. Early work using restriction enzymes showed

increased accessibility of restriction sites closer to ends of nucleosomal DNA compared to restriction sites on the dyad axis.[12–15] This trend was also observed with the human glycosylase endonuclease III (hNTH1), which had increased excision of thymine glycol at the ends of the DNA compared to on the dyad axis;[13] interestingly, it was recently reported that human cells contain a factor that facilitates hNTH1 activity in NCP substrates.[16] Further, previous studies have revealed significant inhibition of several other glycosylases, including hOGG1, acting on lesions positioned at the dyad axis.[13,17,18] Notably, the abilities of uracil DNA glycosylase (UDG) and human alkyladenine glycosylase (AAG) to excise an outward facing lesion at the dyad axis were observed as exceptions.[17] Finally, it has been proposed that lesions with outward rotational position are more easily repaired than inward-facing lesions, though exceptions have been observed.[13,17,19–25] Most importantly, the general applicability of these principles to all glycosylases and lesions has yet to be fully explored.

In the case of hOGG1, inhibition has been observed in NCP substrates when the lesion is located at the dyad axis.[17,18,26] Activity of hOGG1 in NCP substrates has been observed upon addition of chromatin remodeling complexes.[18,26] and when the lesion is located in the linker region between two NCPs of a dinucleosome substrate.[26] Given the known importance of transient DNA unwrapping, hOGG1 activity with lesions of varied translational position warrants further exploration.

To investigate the role of DNA unwrapping on hOGG1 activity, we created site-specific NCP substrates with single base lesions incorporated off the dyad axis. The lesions were positioned approximately 20 base pairs from the end of the DNA within the region that is known to show dynamic unwrapping. To further investigate how the rotational position of a lesion impacts glycosylase activity, we incorporated lesions in positions of varying solution accessibility. Finally, we investigated the impact of the local

histone environment on hOGG1 activity via acetylation and omission of the histone H2B tail.

2.3. Experimental Procedures

2.3.1. Oligonucleotide Synthesis and Purification

Oligonucleotides were synthesized on a MerMade 4 (BioAutomation) DNA synthesizer using phosphoramidite chemistry. All synthesis reagents and phosphoramidites were purchased from Glen Research. The final trityl group was retained for an initial round of HPLC purification (Dynamax Microsorb C18 column, 10 × 250 mm; A = acetonitrile, B = 30 mM ammonium acetate; 5:95 to 35:65 A:B over 30 min at 3.5 mL/min). Following this first round of purification, oligonucleotides were incubated with 20% v/v aqueous acetic acid for 60 min at room temperature to remove the trityl group. For oligonucleotides containing only canonical bases or uracil (U), HPLC at 90°C was used for a second round of purification (Agilent PLRP-S column, 250 mm × 4.6 mm; A = 100 mM triethylammonium acetate [TEAA] in 5% aqueous MeCN, B = 100 mM TEAA in MeCN; 0:100 to 35:65 A:B over 35 min at 1 mL/min). For oligonucleotides containing 8-oxoG, incorporation of 8-oxoG was carried out according to Glen Research protocols. The trityl group was removed on the synthesizer before purification and 2-mercaptoethanol was included during cleavage of the oligonucleotide from the bead. Anion-exchange HPLC was used to purify the 8-oxoG-containing oligonucleotides (Dionex DNAPac PA100 anion-exchange column; A = 10% acetonitrile, B = 0.8 M ammonium acetate in 10% acetonitrile; 70:30 to 0:100 A:B over 35 min at 1 mL/min). Collected peaks were desalted by buffer exchange using centrifugal concentrators (Sartorius Vivaspin Turbo 15, 5 kDa MWCO).

2.3.2 Ligation of 145 mer Oligonucleotides

DNA substrates assembled for this study were designed using the synthetic 145 mer Widom 601 nucleosome positioning sequence[27] as a template (**Scheme S.2.1**). The two strands forming the duplex are differentiated as "I strand" and "J strand" based on the Widom 601 NCP crystal structure.[28] Specifically, we placed lesions in the "I strand."

We synthesized the DNA strands in shorter pieces for assembly into full-length 145 mer via enzymatic ligation. The short oligonucleotides were phosphorylated with T4 polynucleotide kinase (New England Biolabs) with an additional 2 mM ATP in the reaction buffer. Phosphorylated oligonucleotides were annealed to scaffold oligonucleotides in a 1:1 ratio by heating to 90 °C for 5 min followed by cooling to 25 °C at a rate of 1 °C/min. Next, the oligonucleotides were ligated for 3 h at room temperature using T4 Ligase (New England Biolabs). Full-length ligation products were purified by 8% denaturing PAGE (0.8 mm thickness). Electrospray ionization mass spectrometry was used to confirm the identity of the purified 145 mers. Oligonucleotide concentrations were determined by their absorbance at 260 nm using molar extinction coefficients calculated with the OligoAnalyzer tool (www.idtdna.com).

2.3.3. Glycosylase Expression and Purification

His6-tagged hOGG1 was recombinantly expressed in *E. coli* and purified as previously described.[17,29] SDS PAGE analysis showed hOGG1 purity to be >98%. *E. coli* UDG was purchased from New England Biolabs. The active site of *E. coli* UDG is over 55% identical and 73% similar to human UDG[30] leading to many previous studies to use *E. coli* UDG as a comparable alternative to using human UDG.[24] In addition, both types of UDG have similar competency for removing U from NCPs.[17,20,31] The total concentration of each enzyme was determined by Bradford assay with γ-globulin standards (Bio-Rad Laboratories).

2.3.4. Histone Proteins and Octamer Assembly

Expression and purification of canonical *Xenopus laevis* histone proteins and assembly of the histone octamer were performed according to the published method of Luger, et al.[32–34] Chemically acetylated H2B protein was prepared based on previously published methods,[35,36] which provides solution-accessible lysine residues as potential substrates. Briefly, 0.3 µmol of purified H2B was dissolved in 1 mL of freshly prepared 7 M urea solution with 500 mM ammonium acetate and 50 mM ammonium bicarbonate (pH 8.5). The mixture was kept on ice, and 1.5 µL of freshly prepared 10.6 M acetic anhydride was added every 15 min. Concurrently, the pH of the reaction was constantly adjusted to 8.0-8.5 with ammonium hydroxide. After 60 min, the reaction was quenched with 100 µL of 1 M Tris-HCl before transferring to a dialysis device for overnight dialysis into water with 2 mM 2-mercaptoethanol. Electrospray ionization mass spectrometry revealed that between 4-14 acetyl groups were added to H2B. The acetylated H2B protein was lyophilized and stored at -20 °C until used for octamer assembly. The tailless *Xenopus laevis* H2B protein (residues 24-122) was purchased from The Histone Source (Colorado State University).

2.3.5. Nucleosome Core Particle Reconstitution

NCPs were prepared by stepwise dialysis as reported previously.[17,31] Briefly, a Slide-a-Lyzer MINI dialysis device was equilibrated in buffer (10 mM Tris-HCl [pH 7.5], 1 mM EDTA, 1 mM dithiothreitol [DTT], 2 M NaCl) at 4 °C. Radiolabeled duplex (50 µL of 1 µM) was added to the dialysis device and allowed to incubate for 30 min before addition of histone octamer in a 1:1.05 molar ratio. The concentration of NaCl in the dialysis buffer was progressively lowered at 60 min intervals (1.2 M, 1.0 M, 0.6 M, 0 M). The final dialysis step was carried out for 3 h. Samples were filtered to remove precipitate and NCP formation was confirmed by 7% native PAGE (60:1 acrylamide:bisacrylamide; 0.25X TBE)

run for 3 h at 150 V in 4 °C. Only NCP preparations with less than 5% unincorporated duplex DNA (as determined by native gel) were used in the experiments.

2.3.6. Hydroxyl Radical Footprinting

Hydroxyl Radical Footprinting (HRF) procedures were based on previously published methods.[37,38] Briefly, 5 pmol of NCPs containing ^{32}P-radiolabeled DNA were suspended in 52.5 µL buffer (10 mM Tris-HCl [pH 7.5], 1 mM EDTA) and mixed with 7.5 µL each 10 mM Fe(II)-EDTA, 10 mM sodium ascorbate, and 0.12% w/v aqueous hydrogen peroxide. The reaction was incubated at room temperature for 10 min before quenching with the addition of 50 µL 1 mM EDTA in 25% w/v glycerol. The sample was immediately loaded on a pre-running 7% native PAGE (60:1 acrylamide:bisacrylamide, 0.25 X TBE) and electrophoresed for 3 h at 150 V at 4 °C. The band containing NCPs was excised and NCPs were eluted into buffer (300 mM sodium acetate [pH 8.0], 1 mM EDTA) overnight. The resulting eluent was concentrated (Sartorius Vivaspin Turbo 15, 5 kDa MWCO) and extracted twice against 25:24:1 phenol:chloroform:isoamyl alcohol (PCI; Sigma). An ethanol precipitation was performed with the addition of 20 µL co-precipitation reagent (0.5 mg/mL tRNA in 300 mM sodium acetate [pH 8.0], 1 mM EDTA). Samples were dissolved in formamide and run on an 8% denaturing PAGE. The gel was dried and exposed before phosphorimaging. The bands were quantitated using SAFA gel analysis software.[39]

2.3.7. Glycosylase Kinetics Experiments

Kinetics experiments were based on previously published protocols.[17] Briefly, radiolabeled, lesion-containing substrate (either duplex or NCP-incorporated) and glycosylase were prepared at 2X experimental concentration (final concentration 20 nM and 0.64 µM, respectively) in reaction buffer (20 mM Tris-HCl [pH 7.6], 25 mM NaCl, 75

mM KCl, 1 mM EDTA, 1 mM DTT, 200 μg/ml BSA). Following a temperature pre-equilibration at 37 °C for 2 min, equal volumes of substrate (8 μL) and glycosylase (8 μL) preparations were mixed for varying amounts of time before addition of 1 M NaOH quench (16 μL, final concentration 500 mM). For each time course a negative control sample (QC) was prepared by adding 1 M NaOH quench (16 μL) to substrate (8 μL) followed by addition of glycosylase (8 μL) before incubation at 37 °C for the duration of the longest time point. This control serves to reveal any pre-existing damage or incidental damage due to heating or sample work-up (generally less than 10%). Samples were heated to 90 °C for 2 min after addition of quench to induce a strand break at abasic sites. DNA was isolated from proteins by extraction with 25:24:1 PCI before desalting by ethanol precipitation. Samples were electrophoresed on an 8% denaturing PAGE, imaged by phosphorimagery (BioRad Pharos FX) and quantitated by densitometry. The fraction of product at each time point, (t), was determined by the formula

$$F_p(t) = \frac{\delta_p(t)}{\delta_s(t) + \delta_p(t)}$$

where $\delta_s(t)$ and $\delta_p(t)$ are the densities of the substrate and product bands, respectively, at time t. The product yield, $F_p(t)$, was corrected for pre-existing and incidental substrate damage using the following formula:

$$P(t) = \frac{F_p(t) - F_p(0)}{1 - F_p(0)}$$

where $F_p(0)$ is the fraction of product observed in the QC sample. The mean product yield from four independent trials (two separate NCP preparations with two trials each) was determined at each time point. The averaged data were fit to the modified first-order integrated rate law:

$$[P(t)] = [(\infty)](1 - e^{-k_{obs}t})$$

or

$$[P(t)] = [P1(\infty)]\left(1 - e^{-k_{obs},1t}\right) + [P2(\infty)](1 - e^{-k_{obs},2t})$$

where $[P(t)]$ is the concentration of product at time t, $[P(\infty)]$ is the maximum concentration of product, and $[P(0)]$ is the amount of product at time $t = 0$ (generally close to zero), using a nonlinear least squares regression (Kaleidagraph). Reaction rates, k_{obs}, were reported from the fits. A two-tailed student's *t* test was performed to obtain the *p* values for the tailless H2B NCPs and acetylated H2B NCPs in comparison to the canonical NCPs. We considered $p < 0.05$ to be significant.

2.3.8. Molecular Modeling

Molecular models were created in PyMOL (The PyMOL Molecular Graphics System, Version 1.74 Schrödinger, LLC.) to visualize hOGG1 binding to the 601 NCP. Structures of hOGG1-bound-NCPs were created by aligning the crystal structure of hOGG1 bound to DNA (PDB ID: 1ebm) with the 601 NCP crystal structure (PDB ID: 3lz0) as described previously.[17] The glycosylase surface was colored in PyMol according to proximity to the histone core (regions within 5 Å of the octamer are yellow; regions within 5-10 Å of the octamer are red; regions greater than 10 Å from the octamer are blue).

2.4. Results

2.4.1. Formation of Homogenous NCPs

In this study, we evaluated the impact of lesion position on BER in packaged DNA. Our DNA substrates were based on the Widom 601 positioning sequence, which binds in a single translational and rotational position around the histone octamer.[28,40] We used the Widom 601 NCP crystal structure[28] to guide our placement of DNA lesions off the dyad axis and in one of three rotational positions: out toward solution (OUT), approximately 90° from solution (MID), or in toward the histone core (IN) (**Figure 2.1.A**,**B**). These OUT, MID,

and IN positions correspond to locations -49, -52, and -54, respectively, on the “I strand,” which indicate the distance from the center of the DNA duplex, i.e. 49, 52, and 54 bp toward the 5'-end. (Alternatively, the lesion positions are 24, 21, and 19 bp away from the 5'-end of the DNA duplex, respectively.) A single 8-oxoG or U was incorporated at these sites during DNA synthesis (**Figure 2.1.C**). The complementary 601 strand was modified such that 8-oxoG was paired with C, and U was paired with G to mimic a deaminated C:G base pair. *Xenopus laevis* histone proteins were individually expressed in *E. coli*, purified, assembled into an octamer, and used to form NCPs following the salt dialysis method.[31,34] Histone octamers containing either a tailless or acetylated H2B protein were also used to assemble NCPs. A native gel showing representative reconstitutions of each NCP type is shown in **Figure 2.2.**

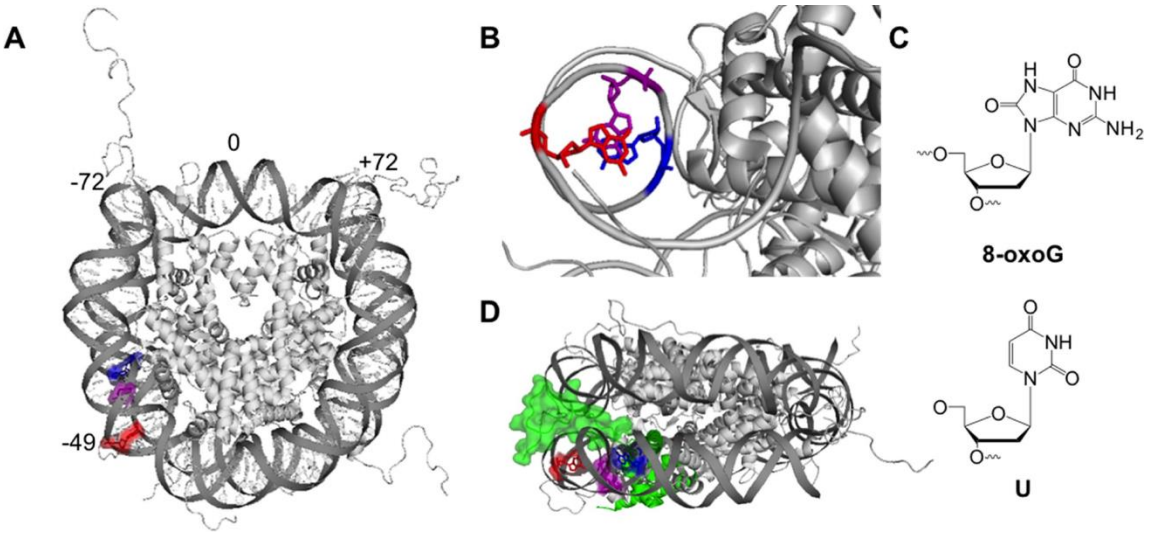

Figure 2.1. NCP structure and lesions used in this study. (A) Merged crystal structure of an NCP containing Widom 601 DNA (PDB ID: 3lz0) and histone octamer with tails (PDB ID: 1kx5) with off-dyad lesion locations highlighted using PyMol. The DNA strands are numbered such that 0 corresponds to center of the 145mer DNA, and the 5' end is base -72. The OUT, MID, and IN facing lesion positioned at base -49, -52, and -54, respectively. **(B)** Rotational positions of lesions (one DNA strand shown for simplicity). The location of the OUT facing lesion is highlighted in red, the MID facing lesion in purple, and the IN lesion in blue. **(C)** Lesions used in this study. **(D)** Side view of the NCP. The H2B tail is highlighted in green and represented in surface mode.

Figure 2.2. Representative native PAGE. Native PAGE was used for evaluating the reconstitution of canonical, tailless H2B, and acetylated H2B NCPs. Radiolabeled samples were loaded on a 1 mm thick 7% native gel (60:1 acrylamide:bisacrylamide, 0.25X TBE). The gel was run at 4°C for 3 hours at 150 V. Variable migration distances are observed for single strand, duplex, and NCP-incorporated DNA samples.

2.4.2. Hydroxyl Radical Footprinting Defines Rotational Position of Lesions

Hydroxyl radical footprinting (HRF) was used to characterize the solution accessibility of each lesion position. The HRF technique uses Fenton chemistry to generate hydroxyl radicals, which abstract a hydrogen atom from the DNA backbone to create a strand break.[38] A sample of duplex Widom 601 DNA treated with hydroxyl radicals shows an unbiased pattern of reactivity throughout the length of the DNA strand (**Figure 2.3.A**, DNA lane). In comparison, DNA incorporated into an NCP shows an oscillating pattern of damage (**Figure 2.3.A**, NCP lane). There are regions of protection and damage corresponding to the DNA wrapping in toward the histone core and out toward solution, respectively. Notably, the oscillatory pattern persists both upstream and downstream of

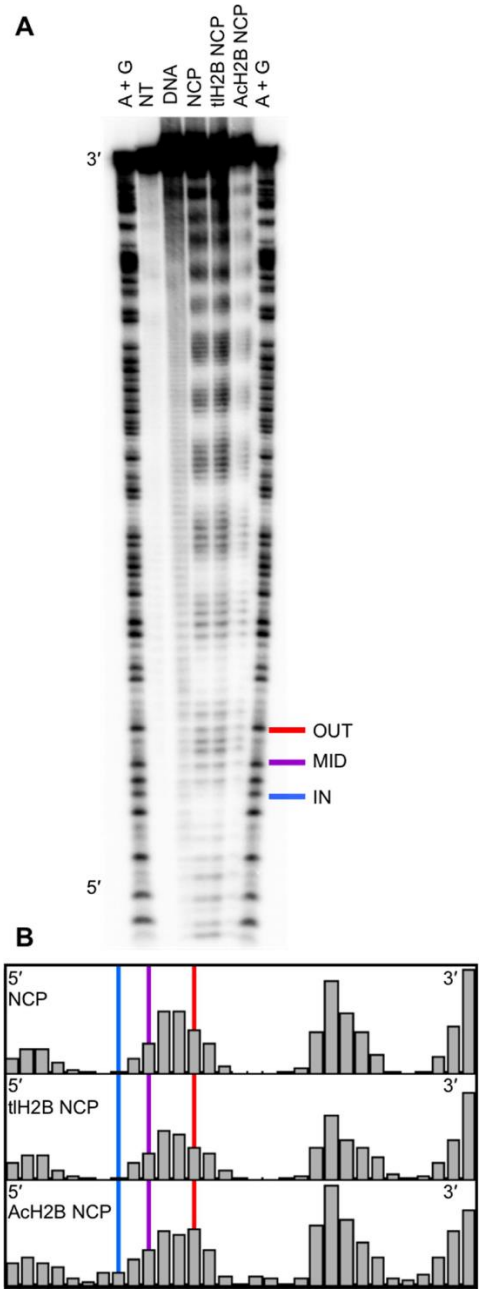

Figure 2.3. Hydroxyl Radical Footprinting of DNA in an NCP. (A) The hydroxyl radical footprinting experiment was analyzed by denaturing PAGE. The flanking "A+G" lanes display a ladder of the 601 DNA sequence created using Maxam Gilbert reactions. The "NT" lane shows a no treatment control. The "DNA" lane shows unbiased damage of hydroxyl radical treatment on duplex DNA. Hydroxyl radical treatment of canonical ("NCP"), tailless H2B octamer ("tlH2B"), and acetylated H2B octamer ("AcH2B NCP") NCPs reveals an oscillating pattern of damage. The location of OUT (red), MID (purple), and IN (blue) lesions in this study are highlighted. **(B)** Quantitation of band density of the footprinting using SAFA software to show relative solution accessibility. The vertical lines highlight the location of each lesion position.

the lesion positions, indicating that while this region is known to be more dynamic,[11] it is still in contact with the histone core and does not react like duplex DNA with hydroxyl radical treatment. The integrated band area at each base position,[39] and the relative reactivity of lesion positions is shown in **Figure 2.3.B**. This was further confirmed with HRF treatment of the complementary strand radiolabeled for visualization, shown in **Figure 2.4.** In addition, the incorporation of the lesions themselves did not change the expected solution accessibility at the observed rotational positions, as shown for U incorporation in the three rotational NCP positions in **Figure 2.5.** Indeed, the relative hydroxyl radical reactivity at the selected lesion positions correlates with predicted solution accessibility based on the Widom 601 NCP crystal structure (i.e. OUT > MID > IN).

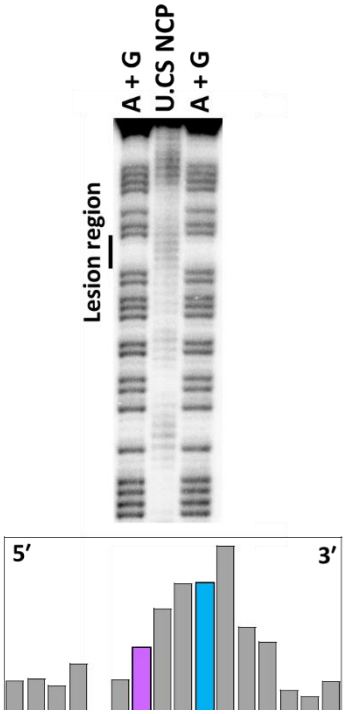

Figure 2.4. Hydroxyl radical footprinting in an NCP labeled for the nucleobases complementing the off-dyad U nucleobase positions. The hydroxyl radical footprinting experiment was analyzed by denaturing PAGE. The flanking "A+G" lanes display a ladder of the "J strand" of the 601 DNA sequence created using Maxam Gilbert reactions. The locations of the respective nucleobase complements of the observed OUT (dark red), MID (light purple), and IN (light blue) lesions in this study are highlighted in the quantitation of band densities that show relative solution accessibility.

Further, HRF was used to evaluate the impact of changes to histone proteins on the solution accessibility of the DNA bases. NCPs prepared using a histone octamer containing either tailless H2B or acetylated H2B histone proteins showed no systematic differences in the oscillating pattern or the relative solution accessibility of the studied OUT, MID, and IN positions when compared to the canonical histone octamer (**Figure 2.3.**).

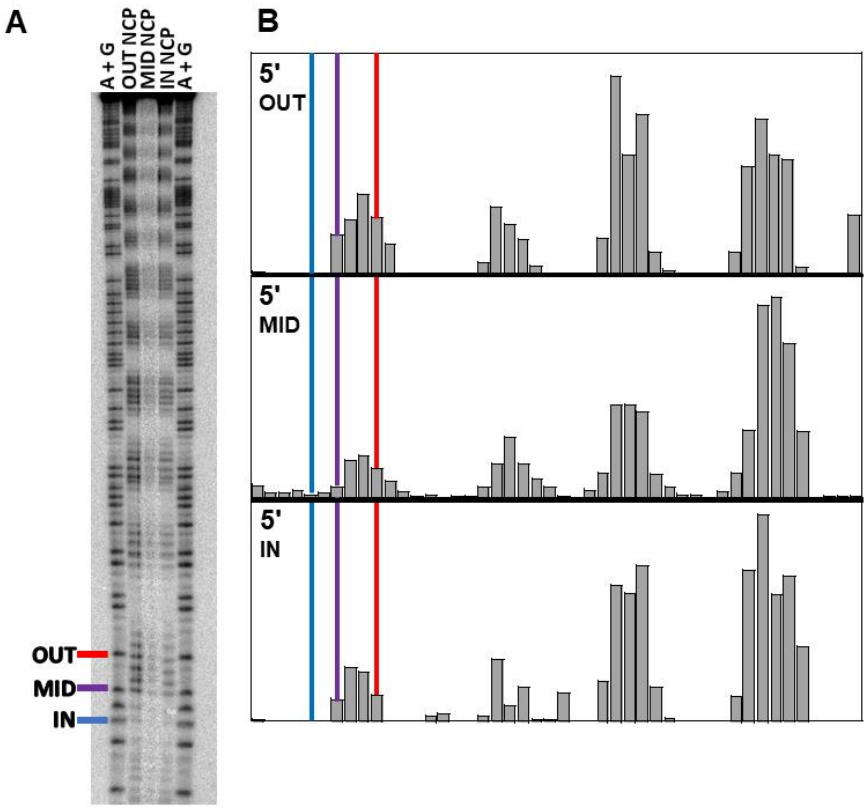

Figure 2.5. Hydroxyl radical footprinting of NCPs with U incorporated at indicated off-dyad positions. (A) The hydroxyl radical footprinting experiment was analyzed by denaturing PAGE (contrast adjusted for better visualization). The flanking "A+G" lanes display a ladder of the lesion-containing "I strand" of the undamaged 601 DNA sequence created using Maxam Gilbert reactions. Hydroxyl radical treatment of U-containing NCPs at the indicated rotational positions reveals an oscillating pattern of damage. The location of OUT (red), MID (purple), and IN (blue) U in this study are highlighted. **(B)** Quantitation of band density of the footprinting using SAFA software to show solution accessibility at U base positions indicated (colored lines) and surrounding region of gel.

2.4.3. Glycosylase Activity in NCPs with Off-Dyad Lesions

Kinetics experiments were performed to test the activity of glycosylase enzymes on NCP substrates. NCP substrates containing a single 8-oxoG or U lesion were incubated at 37 °C with hOGG1 or UDG before quenching with NaOH. Formation of product over time was monitored on denaturing PAGE gels (**Figure 2.6.**). In these experiments, a 32-fold excess of enzyme over substrate was used to ensure single-turnover conditions. We have previously shown that further increases in the excess of enzyme do not yield an increased rate of glycosylase activity in NCP substrates.[16] The observed rate (k_{obs}) therefore reflects the slowest step up to or including the chemistry step of glycosidic bond cleavage.

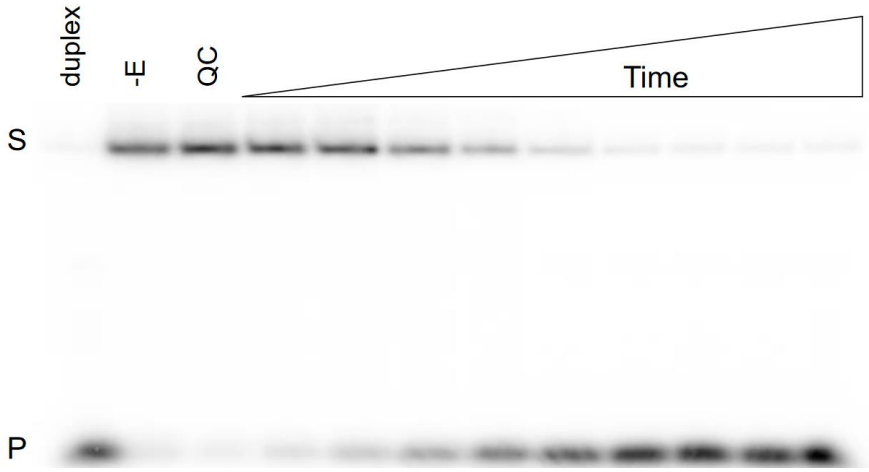

Figure 2.6. Representative denaturing PAGE. A representative denaturing PAGE showing the formation of product by UDG in a single turnover experiment. The conversion of the lesion containing NCP substrates (S) to nicked product (P) is observed with increasing time. A positive control of UDG acting on duplex ("duplex" lane) is included to verify the activity of UDG. The "–E" lane is a negative control prepared by incubating the NCP substrate in the absence of UDG at 37 °C for the duration of the longest time point. The "QC" lane is a second negative control that was prepared by adding 1 M NaOH quench (16 µL) to substrate (8 µL) followed by the immediate addition of UDG (8 µL) before incubation at 37 °C for the duration of the longest time point. As NaOH prevents glycosylase activity, this control serves to reveal any pre-existing damage or incidental damage. Radiolabeled samples were loaded on a 0.4 mm thick 8% denaturing sequencing gel. The gel was run for 45 min at 80 W to achieve adequate separation of substrate and product. The bands corresponding to substrate and product were quantified using densitometry.

Control experiments were performed in which duplex DNA substrates containing a single 8-oxoG or U lesion (the OUT facing lesion position is shown as a representative example) were converted to 87 and 99% product, respectively (**Figure 2.7.**). The data were fit to a single exponential, and the differences in k_{obs} and product formation for duplex DNA substrates of each lesion/glycosylase pair varied minimally with lesion position (data not shown).

For NCP substrates, we previously showed complete inhibition of hOGG1 activity on lesions located at the dyad axis, regardless of rotational position.[17] Interestingly, in the current work, we observe that activity of hOGG1 is restored on NCP substrates when the lesions are located off the dyad axis (**Figure 2.7.A**). Surprisingly, however, the product yield of these kinetic time courses does not correlate with the solution accessibility of the lesions as characterized by hydroxyl radical footprinting. The most product formation of 93% was observed at the MID facing lesion site and 49% product formation was observed for the IN facing lesion site. The most unanticipated result was the relative inhibition of hOGG1 at the most solution-accessible lesion tested in this experiment (OUT), which reached a maximum of 38% product (**Figure 2.7.A**, **Table 2.1.**). In contrast to the duplex substrates, the data for all NCP substrates were best fit to a double exponential model, reflecting a faster kinetic phase and a slower kinetic phase (**Table 2.1.**). While the product yield varies between different rotationally positioned substrates, the k_{obs} values are the same within error.

The unexpected pattern of glycosylase activity and solution accessibility was also manifested for another glycosylase, UDG, acting on the off-dyad lesions. However, for UDG, rather than observing differences in the amount of product, we observed differences in k_{obs}; while full product conversion was achieved for both the OUT and MID positions, U

at the MID position was excised approximately 10-fold faster than at the OUT position (**Figure 2.7.B**, **Table 2.1.**).

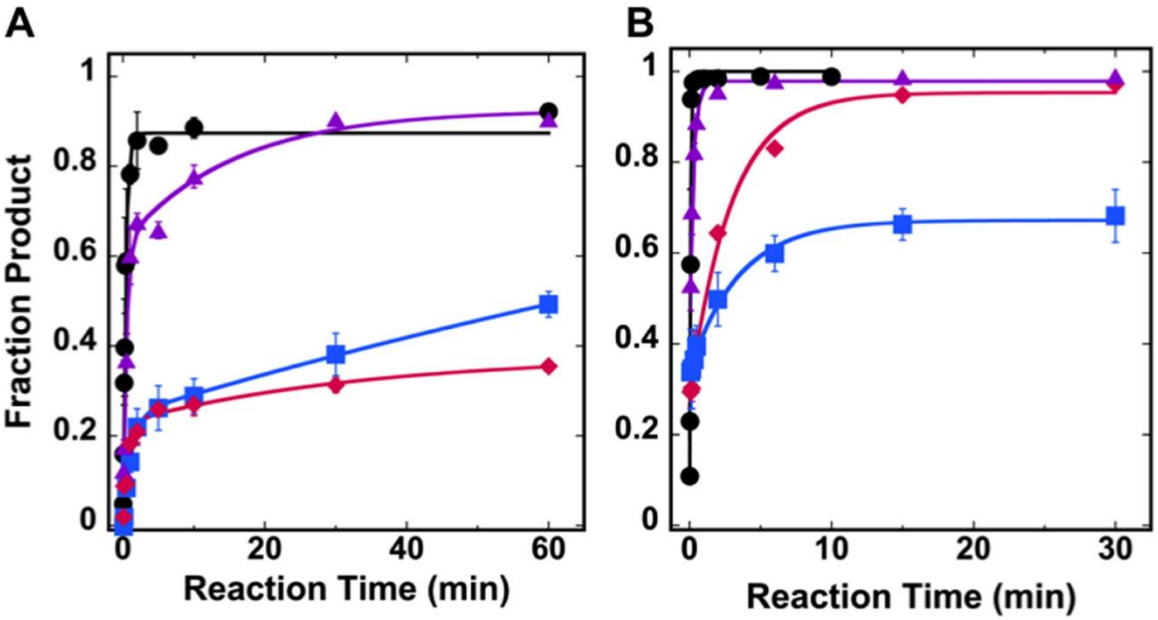

Figure 2.7. Single-turnover kinetic results for hOGG1 and UDG in NCP substrates. Kinetic time courses were performed to evaluate the activity of **(A)** hOGG1 or **(B)** UDG on either duplex DNA (●) or NCP substrates with off-dyad lesions. The NCP substrates contained lesions of varying rotational position: OUT (♦), MID(▲), or IN(■). Experiments were conducted using 20 nM NCP substrate and 0.64 μM glycosylase in 20 mM Tris-HCl (pH 7.6), 25 mM NaCl, 75 mM KCl, 1 mM EDTA, 1 mM DTT, 200 μg/mL BSA. Data for duplex substrates were fit to a single exponential equation; all NCP data were fit to a double exponential equation. Error bars represent the standard error (n=4).

Table 2.1. k_{obs} values determined for duplex DNA and NCP substrates

Enzyme	NCP	Substrate	k_{obs}/min (% product)
hOGG1	N/A	8-oxoG duplex	2.6 ± 0.2 (87%)
	canonical	8-oxoG^{OUT}	1.4 ± 0.4 (23%), 0.03 ± 0.03 (15%)
	canonical	8-oxoG^{MID}	2.0 ± 0.4 (63%), 0.06 ± 0.04 (30%)
	canonical	8-oxoG^{IN}	0.8 ± 0.1 (25%), N.R.[a] (≥ 24%)
	tailless H2B	8-oxoG^{OUT}	2.3 ± 0.4 (28%), 0.05 ± 0.02 (18%)
	acetylated H2B	8-oxoG^{OUT}	4.7 ± 1.4 (23%), 0.11 ± 0.03 (33%)
UDG	N/A	U duplex	12.6 ± 1.6 (99%)
	canonical	U^{OUT}	37.7 ± 33.4 (29%), 0.3 ± 0.05 (67%)
	canonical	U^{MID}	20.1 ± 5.3 (52%), 3.3 ± 0.6 (46%)
	canonical	U^{IN}	42.3 ± 19.9 (34%), 0.3 ± 0.04 (33%)

[a]N.R. indicates an undetermined k_{obs} value for this kinetic phase.

2.4.4. Glycosylase Activity in NCPs with H2B-Modified Octamers

Upon observing the disaccord between the solution accessibility of the lesions and the resulting glycosylase activity, we modeled the Widom 601 DNA wrapped around a histone core containing histone tails (PDB ID: 1kx5), which are present in our *in vitro* experiments. In this model we observed that our off-dyad lesions are near the H2B tail that protrudes between the superhelices (**Figure 2.1.D**). We hypothesized that interactions between the histone tail and the incoming glycosylase could explain the suppressed product yield of hOGG1 at the OUT lesion position as well as the slower k_{obs} for UDG.

To test the impact of the nearby H2B tail on hOGG1 activity, we created two modified histone octamers. First, we created NCPs using an octamer with chemically acetylated H2B proteins (**Figure 2.8.**), where addition of an acetyl group neutralizes the positive charge of lysine. In order to further test the steric impact of the H2B tail, we created

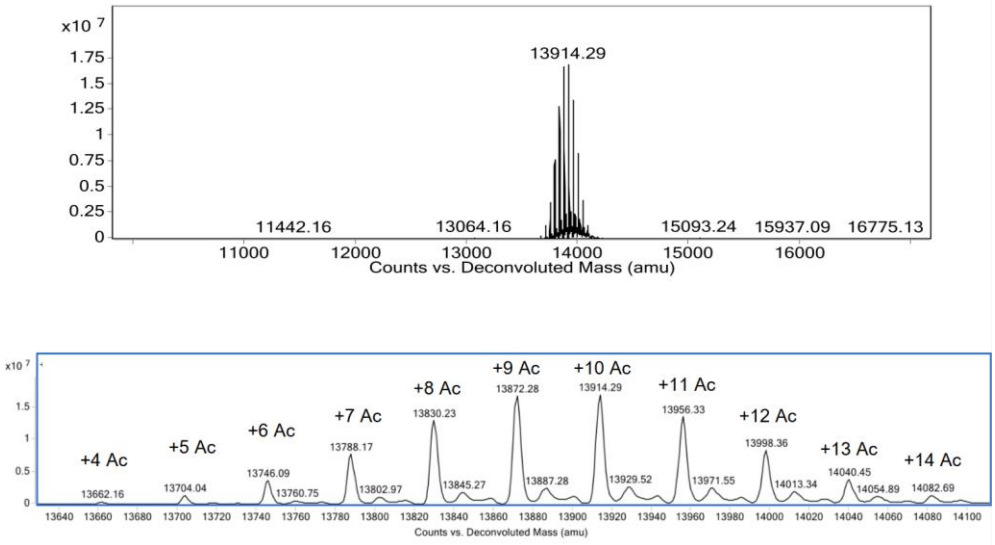

Figure 2.8. Acetylation of H2B. Electrospray ionization mass spectrometry was used to evaluate the acetylation of H2B. **(A)** Mass spectrometry reveals H2B acetylation. The peak at 13914.29 amu corresponds to the addition of 10 acetyl groups. **(B)** A zoomed-in view of the mass spectra reveals a distribution in the number of acetyl groups added. Peaks corresponding to the addition of 4-14 acetyl groups were observed.

NCPs using an octamer with tailless H2B proteins. We tested the activity of hOGG1 on these H2B-modified NCPs with an OUT facing 8-oxoG and compared product formation to the canonical NCP substrate (**Figure 2.9.**). While the tailless H2B NCP does not show a statistically significant increase in product formation, there is an increase in product with the acetylated H2B substrate (p = 0.0016).

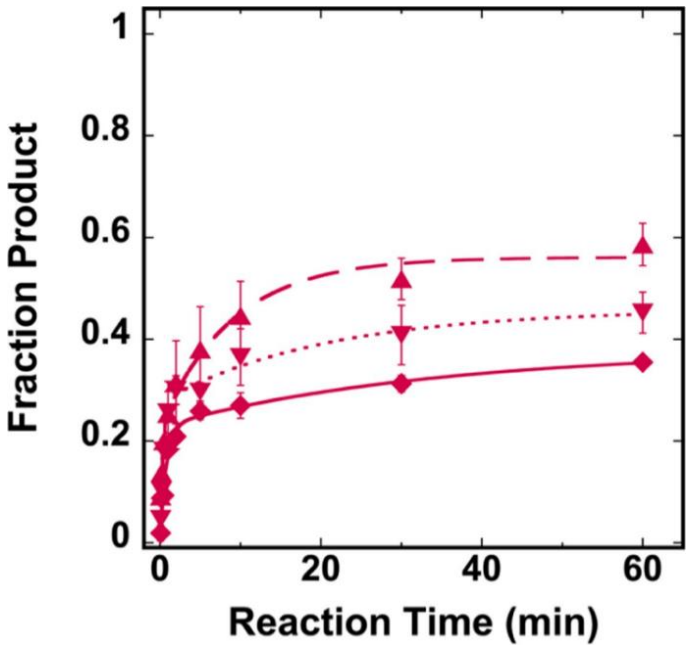

Figure 2.9. Single-turnover kinetic results for hOGG1 and 8-oxoG OUT NCP substrates with H2B modified NCPs. The octamer used to create the NCPs was varied to include a canonical octamer (♦, solid line), tailless H2B octamer (▼, short dashed line), or acetylated H2B octamer (▲, long dashed line). All data were fit to a double exponential equation. Error bars represent the standard error (n=4).

As a comparison point, we tested the impact of the H2B tail on the activity of UDG on off-dyad U lesions incorporated into the tailless H2B octamer. When the U was placed in the OUT off-dyad position in the tailless H2B octamer, the observed rate was comparable to that seen in the canonical octamer (**Figure 2.10.A**). We also observed UDG removal of the U IN off-dyad position in the tailless H2B octamer to test if enhanced product formation could be achieved with the missing tail. The observed rate and the

amount of product accumulation were comparable to those seen in the canonical octamer (**Figure 2.10.B.**).

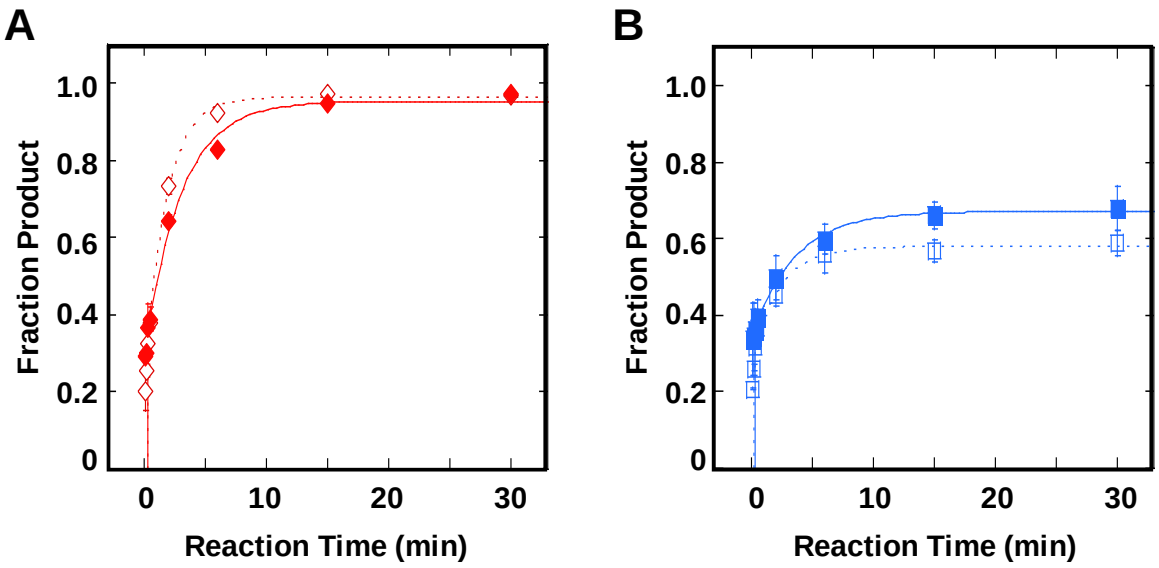

Figure 2.10. Single-turnover kinetics for the removal of off dyad U lesions by UDG in tailless H2B NCPs. Kinetic time courses were performed to evaluate the effect of the H2B tail on UDG in observed off-dyad positions. The U was placed in a tailless H2B NCP facing **(A)** OUT (◊, short dashed lines) or **(B)** IN (□, short dashed lines). All NCP data were fit to a double exponential equation. Error bars for tailless H2B data are the standard error calculated (n=2). Canonical NCP data (closed shapes, solid lines) for each position is duplicated from **Figure 2.7.B.** for comparison purposes.

2.5. Discussion

To investigate the role of DNA unwrapping on glycosylase activity, we created NCP substrates with single base lesions located approximately 20 base pairs from the end of the DNA. In general, activity of the tested enzymes increases when the lesions are moved closer to the DNA ends, relative to when the lesions are at the dyad. While hOGG1 was completely inhibited at the dyad axis regardless of the rotational position of the lesion,[17] product formation is observed at every off-dyad position studied here.

While the data for duplex DNA substrates fit well to a single exponential model, the kinetic data for the NCP substrates are more complex. For the off-dyad lesions, double

exponential models were required to fit the data for all lesion positions and glycosylases. We attribute the biphasic kinetics to the existence of two distinct substrate populations. Each NCP substrate shows a fast phase, which we attribute to a configuration that can be processed directly by the glycosylase. The slow kinetic phase for NCP substrates is generally two orders of magnitude slower than the fast phase. We attribute the slower phase to a population of NCPs that require a rate-limiting conformational change to adopt a structure permissive for repair. This conformational change is consistent with the transient unwrapping of DNA to expose the off-dyad lesion sites, and is not observed in experiments with lesions positioned on the dyad.[17] Previously, the Stivers group reported multiphasic kinetics in experiments with UDG excising U at sites off the dyad.[31]

As no crystal structures of glycosylase-bound NCPs have been reported, we used molecular modeling to analyze the interaction of the glycosylase and the NCP (**Figure 2.11.**). To generate these models, we merged the crystal structure of the 601 NCP with

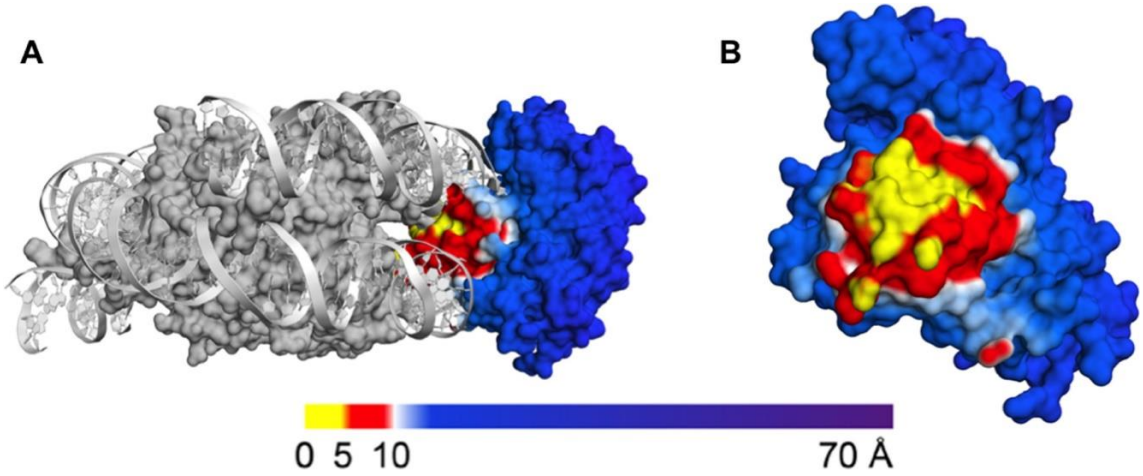

Figure 2.11. Molecular model of NCP-bound hOGG1. The NCP binding surface of hOGG1 was generated by merging the 601 NCP PDB (3lz0, gray) and hOGG1 bound to DNA (1ebm). **(A)** A side view of hOGG1 bound to the NCP is shown. **(B)** A front view of the binding surface of hOGG1 to NCPs with off dyad 8-oxoG OUT facing (base position -49) is shown and the NCP is hidden for clarity. The hOGG1 surface model is colored according to the distance to the histone core (regions less than 5 Å away from the octamer are yellow; regions within 5-10 Å of the octamer are red; region beyond 10 Å away from the octamer are blue).

the crystal structure of DNA-bound hOGG1. We chose to model the glycosylase-bound NCP using the 601 NCP crystal structure lacking histone tails[28] in order to avoid assigning static positions to the unstructured histone tails. The surface of the glycosylase was colored according to its proximity to the histone core as follows: regions within 5 Å of the octamer are yellow; regions within 5-10 Å of the octamer are red; regions greater than 10 Å away from the octamer are blue.[17]

Upon modeling hOGG1 bound to the NCP at the outward facing off-dyad lesion, we found the region near the enzyme's active site to have several amino acid residues within 5 Å of the octamer and an even larger region between 5-10 Å of the octamer. This region represents a significant steric clash between the histone core and hOGG1, which we might predict would prevent enzyme binding and, ultimately, excision of the lesion. However, 38% product formation is observed for hOGG1 at this off-dyad lesion position. The formation of product despite the potential for steric clash in a static model at this position emphasizes the contribution of DNA unwrapping and dynamics to hOGG1 accessibility in an NCP. This unwrapping off-dyad may also allow for hOGG1 to create the necessary 70° bend for cleavage of the *N*-glycosidic bond that was previously not possible on the dyad.[41]

There are conflicting reports on the correlation between solution accessibility of a lesion and enzyme activity in an NCP substrate.[13,17,19–25] We found that for hOGG1, the product yield for NCP substrates did not correlate with the solution accessibility of the lesions as determined by hydroxyl radical footprinting. Furthermore, while full product conversion was observed for both the OUT and MID position with UDG, the rate of excision at the MID position was ~10 times faster than at the OUT position. It is clear that solution accessibility as determined by hydroxyl radical footprinting is not able to predict all chemistry within an NCP. We therefore suggest that local nuances in the NCP environment and histone-DNA interaction have a significant impact on glycosylase activity

and may have a more influential role than solution accessibility at certain positions in the NCP. Other groups who have observed complex kinetics of UDG in NCP substrates have come to similar conclusions.[31]

We created a tailless H2B version of the histone octamer to test the influence of completely removing the histone tail on glycosylase activity. We found that for hOGG1, removing the H2B tails does lead to an increase in product formation, but is not considered statistically significant. Alternatively, UDG activity for off-dyad positions observed remained relatively unchanged when the H2B tail was absent. This might suggest that the H2B tail is interacting in a way with hOGG1 that is not observed for UDG. While we therefore conclude that the inhibition of hOGG1 is not completely derived from steric interference of the histone tail, the phenomenon of histone tail clipping *in vivo* by endopeptidases is an area of recent interest and has been observed in all histone proteins in several organisms.[42] It has been shown that histones lacking N-terminal tails allow for increased accessibility of nucleosomal DNA to transcription factors via increased unwrapping of DNA from the NCP.[43–45] Other BER enzymes have also shown varying levels of inhibition in NCP substrates due to the presence of histone tails.[46,47]

Histone proteins are also targets for post-translational modification, particularly acetylation at the positively charged lysine residues in the N-terminal tails. In this study, NCPs with acetylated H2B proteins showed an increase in hOGG1 product formation when compared to unmodified NCPs. While the H2B tail associates with the nearby DNA in unmodified NCPs, it has been shown that acetylation causes release of H2B tails from the DNA.[48] Further, FRET studies have shown that acetylation of histones facilitates DNA unwrapping.[49,50] We therefore attribute the significant increase in product formation to the neutralization of the lysine residues and resulting relaxation of the NCP structure. However, the incomplete recovery of product formation in acetylated H2B NCPs suggests

that electrostatic interference of the lysine residues on H2B is not the only contributing factor to hOGG1 inhibition at the OUT lesion position.

2.6. Conclusion

In summary, we demonstrate that hOGG1 can excise 8-oxoG from nucleosomal DNA in the absence of external cofactors or chromatin remodelers and that this activity is modulated by transient DNA unwrapping. We further demonstrate the complexity of the NCP environment, as we observe a disparity between solution accessibility and enzyme activity. Increased activity of hOGG1 in response to acetylation of H2B reveals intricacies in the NCP environment due to the electrostatic influence of the histone tails. A more complete understanding of BER in NCP substrates will require additional studies on the impact of histone modifications, chromatin remodeling complexes, and other cellular factors.

2.7. References

(1) Dizdaroglu, M. (2015) Oxidatively induced DNA damage and its repair in cancer. *Mutat. Res. Mutat. Res. 763*, 212–245.

(2) Werner, R. M., and Stivers, J. T. (2000) Kinetic Isotope Effect Studies of the Reaction Catalyzed by Uracil DNA Glycosylase: Evidence for an Oxocarbenium Ion−Uracil Anion Intermediate. *Biochemistry 39*, 14054–14064.

(3) McCann, J. A. B., and Berti, P. J. (2008) Transition-state analysis of the DNA repair enzyme MutY. *J. Am. Chem. Soc. 130*, 5789–97.

(4) Drohat, A. C., and Maiti, A. (2014) Mechanisms for enzymatic cleavage of the N-glycosidic bond in DNA. *Org. Biomol. Chem. 12*, 8367–8378.

(5) Odell, I. D., Wallace, S. S., and Pederson, D. S. (2013) Rules of engagement for base excision repair in chromatin. *J. Cell. Physiol. 228*, 258–66.

(6) Allfrey, V. G., Faulkner, R., and Mirsky, A. E. (2006) Acetylation and Methylation of Histones and Their Possible Role in the Regulation of RNA Synthesis. *Proc. Natl. Acad. Sci. 51*, 786–794.

(7) Li, G., and Widom, J. (2004) Nucleosomes facilitate their own invasion. *Nat. Struct. Mol. Biol. 11*, 763–9.

(8) Li, G., Levitus, M., Bustamante, C., and Widom, J. (2005) Rapid spontaneous accessibility of nucleosomal DNA. *Nat. Struct. Mol. Biol. 12*, 46–53.

(9) Tims, H. S., Gurunathan, K., Levitus, M., and Widom, J. (2011) Dynamics of Nucleosome Invasion by DNA Binding Proteins. *J. Mol. Biol. 411*, 430–448.

(10) Tomschik, M., Zheng, H., Holde, K. van, Zlatanova, J., and Leuba, S. H. (2005) Fast, long-range, reversible conformational fluctuations in nucleosomes revealed by single-pair fluorescence resonance energy transfer. *Proc. Natl. Acad. Sci. 102*, 3278–3283.

(11) Wei, S., Falk, S. J., Black, B. E., and Lee, T. H. (2015) A novel hybrid single molecule approach reveals spontaneous DNA motion in the nucleosome. *Nucleic Acids Res. 43*,

e111.

(12) Anderson, J. D., and Widom, J. (2000) Sequence and position-dependence of the equilibrium accessibility of nucleosomal DNA target sites. *J. Mol. Biol. 296*, 979–987.

(13) Prasad, A., Wallace, S. S., and Pederson, D. S. (2007) Initiation of base excision repair of oxidative lesions in nucleosomes by the human, bifunctional DNA glycosylase NTH1. *Mol. Cell. Biol. 27*, 8442–53.

(14) Polach, K. J., and Widom, J. (1999) Restriction enzymes as probes of nucleosome stability and dynamics. *Methods Enzymol. 304*, 278–98.

(15) Linxweiler, W., and Hörz, W. (1984) Reconstitution of mononucleosomes: characterization of distinct particles that differ in the position of the histone core. *Nucleic Acids Res. 12*, 9395–413.

(16) Pederson, D. S., Sweasy, J. B., Wallace, S. S., Averill, A. M., Marsden, C. G., and Maher, R. L. (2017) Human cells contain a factor that facilitates the DNA glycosylase-mediated excision of oxidized bases from occluded sites in nucleosomes. *DNA Repair (Amst). 57*, 91–97.

(17) Olmon, E. D., and Delaney, S. (2017) Differential Ability of Five DNA Glycosylases to Recognize and Repair Damage on Nucleosomal DNA. *ACS Chem. Biol. 12*, 692–701.

(18) Menoni, H., Gasparutto, D., Hamiche, A., Cadet, J., Dimitrov, S., Bouvet, P., and Angelov, D. (2007) ATP-dependent chromatin remodeling is required for base excision repair in conventional but not in variant H2A.Bbd nucleosomes. *Mol. Cell. Biol. 27*, 5949–56.

(19) Hinz, J. M., Rodriguez, Y., and Smerdon, M. J. (2010) Rotational dynamics of DNA on the nucleosome surface markedly impact accessibility to a DNA repair enzyme. *Proc. Natl. Acad. Sci. U. S. A. 107*, 4646–51.

(20) Nilsen, H., Lindahl, T., and Verreault, A. (2002) DNA base excision repair of uracil residues in reconstituted nucleosome core particles. *EMBO J. 21*, 5943–52.

(21) Beard, B. C., Wilson, S. H., and Smerdon, M. J. (2003) Suppressed catalytic activity of base excision repair enzymes on rotationally positioned uracil in nucleosomes. *Proc. Natl. Acad. Sci. U. S. A. 100*, 7465–70.

(22) Odell, I. D., Barbour, J.-E., Murphy, D. L., Della-Maria, J. A., Sweasy, J. B., Tomkinson, A. E., Wallace, S. S., and Pederson, D. S. (2011) Nucleosome disruption by DNA ligase III-XRCC1 promotes efficient base excision repair. *Mol. Cell. Biol. 31*, 4623–32.

(23) Odell, I. D., Newick, K., Heintz, N. H., Wallace, S. S., and Pederson, D. S. (2010) Non-specific DNA binding interferes with the efficient excision of oxidative lesions from chromatin by the human DNA glycosylase, NEIL1. *DNA Repair (Amst). 9*, 134–43.

(24) Cole, H. A., Tabor-Godwin, J. M., and Hayes, J. J. (2010) Uracil DNA glycosylase activity on nucleosomal DNA depends on rotational orientation of targets. *J. Biol. Chem. 285*, 2876–2885.

(25) Rodriguez, Y., and Smerdon, M. J. (2013) The Structural Location of DNA Lesions in Nucleosome Core Particles Differentially Influence Accessibility of Base Excision Repair Enzymes. *J. Biol. Chem. 19*, 13863–13875.

(26) Menoni, H., Shukla, M. S., Gerson, V., Dimitrov, S., and Angelov, D. (2012) Base excision repair of 8-oxoG in dinucleosomes. *Nucleic Acids Res. 40*, 692–700.

(27) Lowary, P. T., and Widom, J. (1998) New DNA sequence rules for high affinity binding to histone octamer and sequence-directed nucleosome positioning. *J. Mol. Biol. 276*, 19–42.

(28) Vasudevan, D., Chua, E. Y. D., and Davey, C. A. (2010) Crystal Structures of Nucleosome Core Particles Containing the “601” Strong Positioning Sequence. *J. Mol. Biol. 403*, 1–10.

(29) Jarem, D. A., Wilson, N. R., and Delaney, S. (2009) Structure-dependent DNA damage and repair in a trinucleotide repeat sequence. *Biochemistry 48*, 6655–63.

(30) Xiao, G., Tordova, M., Jagadeesh, J., Drohat, A. C., Stivers, J. T., and Gilliland, G. L. (1999) Crystal structure of Escherichia coli uracil DNA glycosylase and its complexes with uracil and glycerol: structure and glycosylase mechanism revisited. *Proteins 35*, 13–24.

(31) Ye, Y., Stahley, M. R., Xu, J., Friedman, J. I., Sun, Y., McKnight, J. N., Gray, J. J., Bowman, G. D., and Stivers, J. T. (2012) Enzymatic excision of uracil residues in nucleosomes depends on the local DNA structure and dynamics. *Biochemistry 51*, 6028–6038.

(32) Luger, K., Rechsteiner, T. J., and Richmond, T. J. (1999) Expression and purification of recombinant histones and nucleosome reconstitution. *Methods Mol. Biol. 119*, 1–16.

(33) Luger, K., Rechsteiner, T. J., and Richmond, T. J. (1999) Preparation of nucleosome core particle from recombinant histones. *Methods Enzymol. 304*, 3–19.

(34) Dyer, P. N., Edayathumangalam, R. S., White, C. L., Bao, Y., Chakravarthy, S., Muthurajan, U. M., and Luger, K. (2003) Reconstitution of Nucleosome Core Particles from Recombinant Histones and DNA. *Methods Enzymol. 375*, 23–44.

(35) Bheda, P., Swatkoski, S., Fiedler, K. L., Boeke, J. D., Cotter, R. J., and Wolberger, C. (2012) Biotinylation of lysine method identifies acetylated histone H3 lysine 79 in Saccharomyces cerevisiae as a substrate for Sir2. *Proc. Natl. Acad. Sci. U. S. A. 109*, E916-25.

(36) Parsons, X. H., Garcia, S. N., Pillus, L., and Kadonaga, J. T. (2003) Histone deacetylation by Sir2 generates a transcriptionally repressed nucleoprotein complex. *Proc. Natl. Acad. Sci. U. S. A. 100*, 1609–14.

(37) Hayes, J. J., Tullius, T. D., and Wolffe, A. P. (1990) The structure of DNA in a nucleosome. *Proc. Natl. Acad. Sci. U. S. A. 87*, 7405–9.

(38) Jain, S. S., and Tullius, T. D. (2008) Footprinting protein–DNA complexes using the hydroxyl radical. *Nat. Protoc. 3*, 1092–1100.

(39) Das, R., Laederach, A., Pearlman, S. M., Herschlag, D., and Altman, R. B. (2005)

SAFA: semi-automated footprinting analysis software for high-throughput quantification of nucleic acid footprinting experiments. *RNA 11*, 344–54.

(40) Chua, E. Y. D., Vasudevan, D., Davey, G. E., Wu, B., and Davey, C. A. (2012) The mechanics behind DNA sequence-dependent properties of the nucleosome. *Nucleic Acids Res. 40*, 6338–6352.

(41) Bruner, S. D., Norman, D. P. G., and Verdine, G. L. (2000) Structural basis for recognition and repair of the endogenous mutagen 8-oxoguanine in DNA. *Nature 403*, 859–866.

(42) Zhou, P., Wu, E., Alam, H. B., and Li, Y. (2014) Histone cleavage as a mechanism for epigenetic regulation: current insights and perspectives. *Curr. Mol. Med. 14*, 1164–72.

(43) Vitolo, J. M., Thiriet, C., and Hayes, J. J. (2000) The H3-H4 N-terminal tail domains are the primary mediators of transcription factor IIIA access to 5S DNA within a nucleosome. *Mol. Cell. Biol. 20*, 2167–75.

(44) Vettese-Dadey, M., Walter, P., Chen, H., Juan, L. J., and Workman, J. L. (1994) Role of the histone amino termini in facilitated binding of a transcription factor, GAL4-AH, to nucleosome cores. *Mol. Cell. Biol. 14*, 970–81.

(45) Godde, J. S., Nakatani, Y., and Wolffe, A. P. (1995) The amino-terminal tails of the core histones and the translational position of the TATA box determine TBP/TFIIA association with nucleosomal DNA. *Nucleic Acids Res. 23*, 4557–64.

(46) Beard, B. C., Stevenson, J. J., Wilson, S. H., and Smerdon, M. J. (2005) Base excision repair in nucleosomes lacking histone tails. *DNA Repair (Amst). 4*, 203–209.

(47) Chafin, D. R., Vitolo, J. M., Henricksen, L. A., Bambara, R. A., and Hayes, J. J. (2000) Human DNA ligase I efficiently seals nicks in nucleosomes. *EMBO J. 19*, 5492–5501.

(48) Fu, I., Cai, Y., Geacintov, N. E., Zhang, Y., and Broyde, S. (2017) Nucleosome Histone Tail Conformation and Dynamics: Impacts of Lysine Acetylation and a Nearby Minor Groove Benzo[a]pyrene-Derived Lesion. *Biochemistry 56*, 1963–1973.

(49) Kim, J., Wei, S., Lee, J., Yue, H., and Lee, T. H. (2016) Single-Molecule Observation Reveals Spontaneous Protein Dynamics in the Nucleosome. *J. Phys. Chem. B 120*, 8925–8931.

(50) Kim, J., Lee, J., and Lee, T.-H. (2015) Lysine Acetylation Facilitates Spontaneous DNA Dynamics in the Nucleosome. *J. Phys. Chem. B 119*, 15001–15005.

2.8. Appendix: Supplementary Information

Scheme S.2.1. Oligonucleotide sequences used in this work. The 145mer oligonucleotides were synthesized as three component oligonucleotides. Each strand was divided into a 45mer, a 40mer, and a 60mer, as indicated by the vertical lines. The component oligonucleotides were assembled for ligation using the scaffolds listed. The table below details the base identity at locations X (lesion strand) or Y (complement strand) explored in this study.

145mer lesion strand (numbering based on "I strand" of Vasudevan et. al.)[28]:
5′– ATC AGA ATC CCG GTG CCG X^{-54}GX^{-52} CCX^{-49} CTC AAT TGG
TCG TAG ACA GCT |CTA GCA CCG CTT AAA CGC ACG TAC GCG
CTG TCC CCC GCG T|TT TAA CCG CCA AGG GGA TTA CTC CCT
AGT CTC CAG GCA CGT GTC AGA TAT ATA CAT CGA T –3′

Scaffold 1: 5′– TTT AAG CGG TGC TAG AGC TGT CTA CGA CCA –3′

Scaffold 2: 5′– CCC TTG GCG GTT AAA ACG CGG GGG ACA GCG –3′

145mer complement strand (numbering based on "J strand" of Vasudevan et. al.)[28]:
5′– ATC GAT GTA TAT ATC TGA CAC GTG CCT GGA GAC TAG
GGA GTA ATC|CCC TTG GCG GTT AAA ACG CGG GGG ACA GCG
CGT ACG TGC G|TT TAA GCG GTG CTA GAG CTG TCT ACG ACC
AAT TGA GY^{+49}G GY^{+52}C Y^{+54}CG GCA CCG GGA TTC TGA T –3′

Scaffold 3: 5′– TTT AAC CGC CAA GGG GAT TAC TCC CTA GTC –3′

Scaffold 4: 5′– CTA GCA CCG CTT AAA CGC ACG TAC GCG CTG –3′

Substrate	X^{-49}	Y^{+49}	X^{-52}	Y^{+52}	X^{-54}	Y^{+54}
8-oxoG^{OUT}	8-oxoG	C	G	C	G	C
8-oxoG^{MID}	G	C	8-oxoG	C	G	C
8-oxoG^{IN}	G	C	G	C	8-oxoG	C
U^{OUT}	U	G	C	G	C	G
U^{MID}	C	G	U	G	C	G
U^{IN}	C	G	C	G	U	G

Chapter 3. The architectural nuances of nucleosomes revealed by global repair profiling of human alkyladenine DNA glycosylase †

† Adapted from:

Kennedy E.E., Li C., Delaney, S. (2019)

Manuscript Submitted.

I designed the experiments in collaboration with C.L. I performed all the experiments and analyzed the results. I wrote the submitted manuscript with S.D.

3.1. Abstract

Alkyladenine DNA glycosylase (AAG) is the only known human glycosylase capable of excising alkylated purines from DNA, including the highly mutagenic 1,N^6-ethenoadenine (εA) lesion. Here we examine AAG's ability to excise εA from a nucleosome core particle (NCP), which is the primary repeating unit of DNA packaging in eukaryotes. Using chemical synthesis techniques, we assembled a global population of NCPs in which A is replaced with εA. While each NCP contains no more than one εA lesion, the total population contains εA in 49 distinct geometric positions. Using this global εA-containing NCP system, we obtained kinetic parameters of AAG throughout the NCP architecture. We observed monophasic reaction kinetics across the NCP, but varying amounts of AAG excision. AAG activity is correlated with solution accessibility and local histone architecture. Notably, we identified some highly solution-accessible lesions that are not repaired well, and an increase in repair within the region of asymmetric unwrapping of the nucleosomal DNA end. These observations support *in vivo* work and provide molecular-level insight into the relationship between repair and NCP architecture.

3.2. Introduction

Despite its being the code of life, DNA has a physiochemical composition that makes it susceptible to modification and decomposition by endogenous and exogenous sources.[1] Failure to rectify these modifications can result in mutagenic consequences such as cancer.[2] The repair of nucleobase lesions can be accomplished with the base excision repair (BER) pathway. BER is initiated by a glycosylase enzyme specialized for removing a particular lesion(s).[3] Most glycosylases use a base-flipping mechanism to extrude the lesion from the helix and catalyze *N*-glycosidic bond cleavage, resulting in an abasic site.[4] Interestingly, alkyladenine DNA glycosylase (AAG) is the only known human glycosylase that removes alkylated nucleobases, including 3-methyladenine, 7-

methylguanine, and 1,N^6-ethenoadenine (εA).[5,6] Specifically, εA can be generated by environmental exposure to vinyl chloride, or by attack of endogenous lipid peroxidation products (**Figure 3.1.A**).[7] The current study focuses on the removal of εA by AAG.

Many prior studies characterized glycosylase activity using short oligonucleotide duplex substrates. However, eukaryotic DNA is highly packaged, presenting a more complicated environment for repair *in vivo*. The primary repeating unit of chromatin is the nucleosome core particle (NCP) (**Figure 3.1.B,**) with 70-90% of genomic DNA packaged as such.[8] NCPs consist of 145-147 bp of DNA wrapped in ~1.7 left-handed superhelical turns around an octameric core of histone proteins.[9] The histone core contains two copies of each histone, H2A, H2B, H3, and H4, with two-fold rotational symmetry about a dyad

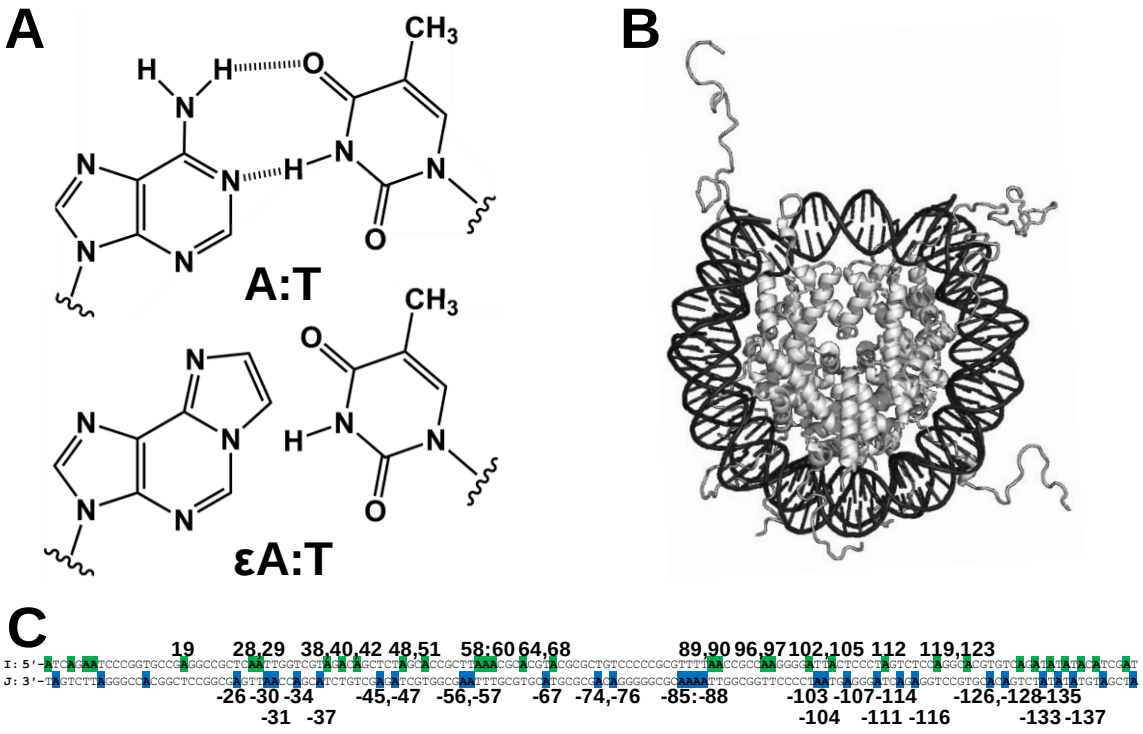

Figure 3.1. Representations of lesions, NCP, and DNA sequence. (A) An A:T bp and mutagenic εA:T bp. **(B)** Representation of an NCP. **(C)** The 145 bp Widom 601 duplex. Locations of A in sequence are highlighted in the I strand (green) and J strand (blue). Base pairs are numbered starting from the 5'-end of the I strand, with the J strand nucleobase indicated by a negative.

axis. As a consequence of wrapping around the histone core, the DNA becomes structurally distorted and locally stretched.[10–12] The presence of the histones also means that there are regions of DNA that are sterically blocked while other regions are physically more accessible to DNA-binding proteins.[13,14]

The geometric position of a nucleobase in an NCP can be described in two ways: the rotational position and the translational position. Rotational positioning of a nucleobase refers to its helical orientation; i.e. if the lesion is facing outward toward solution, or inward toward the histone core. Translational positioning refers to the location of the nucleobase relative to the dyad axis. It has been shown that nucleobases located toward the ends of the DNA have increased solution accessibility compared with those near the dyad region due to transient and spontaneous DNA unwrapping.[13,15]

Previous studies have shown that geometric positioning of a lesion and local histone environment can modulate glycosylase activity on an NCP.[16] Most of these previous studies created NCPs containing a site-specific lesion. To obtain information about activity in other NCP regions, additional site-specific lesion-containing NCPs were created with the lesion in a different geometric position. These initial experiments showed that each local histone environment had varying effects on glycosylase activity beyond solution accessibility. Because every nucleobase in an NCP inherently has a unique microenvironment, no lesion location can be used as a representative of repair in a packaged DNA context. Furthermore, although studies using site-specific lesions in NCPs are informative, it would be time-consuming and impractical to study DNA repair across the entirety of the nuanced NCP architecture containing 145-147 bp in this manner.

With these considerations in mind, we recently designed a global system for simultaneous study of multiple lesion positions, and therefore probing of multiple NCP microenvironments, to describe glycosylase activity across an NCP.[17] Global lesion-containing DNA is prepared by chemical synthesis using a building block mixture of the

lesion of interest and the unmodified nucleobase that maximizes the number of strands containing 0 or 1 lesion throughout the sequence. Reconstitution of NCPs using global lesion-containing duplex and histone octamer creates a population of NCPs with the lesion positioned in a variety of well-defined translational and rotational positions. Here, we utilize the global system to substitute εA for A in either the I or J strand of the Widom 601 NCP[11] to study excision by AAG in a total of 49 distinct geometric positions (**Figure 3.1.C**, **Scheme S.3.1.**). Whereas our previous work qualitatively described repair of 8-oxo-7,8-dihydroguanine lesions in NCPs, our current work elevates the global system to provide kinetic parameters to describe εA excision by AAG in duplex controls and NCPs.

3.3. Experimental Procedures

3.3.1. Global εA-containing 145 mer oligonucleotide synthesis and purification

All oligonucleotides used in this study were synthesized on a MerMade 4 DNA synthesizer (BioAutomation). All phosphoramidites and reagents were purchased from Glen Research. We utilized the 145 bp Widom 601 nucleosome positioning sequence for duplex and NCP assembly (**Scheme S.3.1.**).[18] Base pairs are numbered starting from the 5'-end of the I strand, with the J strand designated with a negative (-) (**Figure 3.1.C**). The 145 mer oligonucleotides containing global εA were synthesized on 1,400 Å controlled pore glass beads using phosphoramidites with ultramild protecting groups and deprotected according to the manufacturer's specifications. εA was substituted for A throughout the DNA on either the I strand or J strand of the Widom 601 sequence to ultimately have at most one εA:T bp per duplex. To accomplish this, we used methods similar to our recent report.[17] Briefly, a mixture of εA and A phosphoramidites was used during the synthesis with the molar ratio determined by the Poisson distribution (λ= 0.355), such that 95% of the DNA population contains either 0 or 1 εA lesion per 145 mer

oligonucleotide. The final trityl group was removed on the synthesizer. The DNA was cleaved from the beads by incubation in NH_4OH at room temperature for 2 h and purified by 8% denaturing PAGE run for 5 h at 80 W. A small portion of the synthesized DNA was radiolabeled and was loaded in lanes adjacent to where the unlabeled DNA was loaded. The region of the gel that co-migrated with a 145 mer standard was excised and "crushed and soaked"[19] overnight in 15 mL elution buffer (300 mM sodium acetate [pH 8.0], 1 mM EDTA) with gentle shaking (80 rpm) at 37 °C. The buffer containing the eluted DNA was passed through a 0.22 μm cellulose acetate syringe filter and was concentrated and desalted with many ethanol precipitations. The concentrations of the PAGE-purified oligonucleotides were determined by their absorbance at 260 nm using molar extinction coefficients for the undamaged Widom 601 sequences obtained using the OligoAnalyzer tool on www.idtdna.com.

The incorporation of εA at A sites was confirmed by cleavage by AAG. Specifically, the εA-containing 145 mer strand was 5'-radiolabeled using T4 kinase (New England Biolabs) and γ-^{32}P-ATP (Perkin Elmer) and annealed to its respective undamaged complement to form duplex (see below). The εA-containing duplex (DUP) was then incubated with AAG for 1 h at 37 °C, followed by the addition of equal volume of 1 M NaOH and incubation at 90 °C for 3 min. Samples were supplemented with 40 μL co-precipitation agent (0.5 mg/mL tRNA in 300 mM NaOAc [pH 8.0], 1 mM EDTA) and subsequently desalted with two ethanol precipitations. Samples were prepared for separation on 12% denaturing PAGE in a 1:1 mixture of formamide and water. Cleavage at each A position confirms that the εA lesions are present as expected.

3.3.2. Ligation strategy to synthesize undamaged 145 mer oligonucleotide complementary to εA-containing strands

The 145 mer oligonucleotides complementary to the εA-containing oligonucleotides were prepared by ligating short component oligonucleotides. The component oligonucleotides for ligation were synthesized using standard phosphoramidite protecting groups with the final trityl group retained for reverse-phase HPLC purification at 90 °C (Agilent PLRP-S column, 250 mm × 4.6 mm; A = 100 mM triethylammonium acetate [TEAA] in 5% aqueous MeCN, B = 100 mM TEAA in MeCN; 5:95 to 35:65 A:B over 30 min, 35:65 to 5:95 A:B over 5 min at 1 mL/min). The trityl group was then removed with incubation in 20% v/v aqueous glacial acetic acid for 1 h at room temperature, followed by a second HPLC purification at 90 °C (Agilent PLRP-S column, 250 mm × 4.6 mm; A = 100 mM triethylammonium acetate [TEAA] in 5% aqueous MeCN, B = 100 mM TEAA in MeCN; 0:100 to 15:85 A:B over 35 min, 15:85 to 35:65 A:B over 5 min at 1 mL/min). Electrospray ionization mass spectrometry was used to verify the identity of the component oligonucleotides.

Component oligonucleotides were used in ligation (**Scheme S.3.2.**). Five nmol of each component oligonucleotide 2 and 3 were 5'-phosphorylated in the presence of 2 mM ATP using T4 kinase (New England Biolabs). Phosphorylated component oligonucleotides were combined in equal amounts with component 1 and a 5% excess of two scaffolding oligonucleotides, s12 and s23, in annealing buffer (10 mM Tris-HCl pH 8.0, 50 mM NaCl, 1 mM EDTA). The strands were annealed by heating to 90 °C for 5 min followed by cooling to room temperature at a rate of 1 °C/min. The annealed component oligonucleotides were ligated together overnight at room temperature using T4 ligase (New England Biolabs). The ligated 145 mer oligonucleotides were purified by denaturing PAGE as described above for the εA-containing 145 mer.

3.3.3. Formation of global εA-containing duplex (DUP)

The 145 mer oligonucleotides containing εA lesions were 5'-radiolabeled for visualization. The global εA-containing I strand was annealed with the J strand 145 mer that lacked εA lesions. Similarly, the J strand oligonucleotide containing εA lesions was annealed with the undamaged I strand. DUP was formed by mixing the radiolabeled εA-containing strand with the complementary strand in a 1:1.07 ratio in annealing buffer and heating to 90 °C for 5 min followed by cooling to room temperature at a rate of 1 °C/min. DUP formation was confirmed on a 7% native PAGE (60:1 acrylamide : bisacrylamide; 0.25x TBE). The samples were loaded using 5% (v/v) glycerol in 10 mM Tris-HCl (pH 7.5), 1mM EDTA and run for 3 h at 160 V at 4 °C. Only DUP containing ≤ 5% single-strand DNA were used in further studies.

3.3.4. Reconstitution of global εA nucleosome core particles (NCPs)

Recombinant *Xenopus laevis* histones were individually expressed and purified, and subsequently assembled into octamers.[20,21] NCPs were reconstituted by dialyzing the radiolabeled εA-containing DUP population and histone octamer together via salt gradient, as described previously.[17] Briefly, a 10% molar excess of histone octamer was gently added to 25 µL of 1 µM radiolabeled εA-containing 145 bp DUP in buffer (10 mM Tris-HCl [pH 7.5], 1 mM EDTA, 1 mM dithiothreitol [DTT], 2 M NaCl, 500 µg/mL BSA) in a Slide-a-Lyzer dialysis device (0.1 mL capacity, 3.5 kDa MWCO; Thermo Fisher Scientific). The dialysis device started in a buffer of 10 mM Tris-HCl (pH 7.5), 1 mM EDTA, 1mM dithiothreitol (DTT), 2 M NaCl at 4 °C. At 1 h intervals, the device was placed in analogous buffers containing decreasing concentrations of NaCl (1.2 M, 1.0 M, 0.6 M, 0 M). The final dialysis in 0 M NaCl proceeded for 3 h before the reconstitution was filtered with a 0.22 µm cellulose acetate centrifuge tube filter (Corning Costar) to remove precipitates. NCP formation and relative purity were analyzed using a 7% native PAGE (60:1 acrylamide:

bisacrylamide; 0.25x TBE) run for 3 h at 160 V in 4 °C. Only NCPs containing ≤ 5% DUP were used in further studies.

We tested for bias of εA incorporation into NCPs to address the concern of εA enrichment or depletion as a function of εA location. We reconstituted global εA-containing DUP into NCPs and then subsequently removed the histone proteins by extraction with an equal volume of 25:24:1 phenol:chloroform:isoamyl alcohol (PCI) and subsequent ethanol precipitation to create “freed DUP”. The freed DUP was incubated with a 30-fold excess of AAG for 2 h at 37 °C in 20 mM Tris-HCl (pH 7.6), 50 mM NaCl, 150 mM KCl, 1 mM EDTA, 1 mM DTT, 200 μg/mL BSA. Samples were quenched with the addition of an equal volume of 1 M NaOH supplemented with internal references (**Scheme S.3.3.**). An equal volume of PCI was added and the aqueous layer was subjected to two ethanol precipitations. The samples were prepared in a 1:1 mixture of formamide and water for separation on a 12% denaturing PAGE to resolve the 5' end of εA positions (ranging from 28-68). Quantitation of band intensity was determined by SAFA.[22] The density measurements for all lanes was normalized to the internal references; the 23 mer internal reference was used for the 5'-ends of the sequences (ranging from fragment lengths 9-68) and the 92 mer internal reference was used for the 3'-ends of the sequences (ranging from fragment lengths 70-132). The amount of background damage from the -E sample was subtracted from AAG-treated samples. The resulting amount of cleavage due to AAG activity observed in the freed DUP substrate was compared with analogous conditions of the same DUP population that had never been incorporated into NCPs. The ratio of εA excision in the freed DUP substrate was compared with εA excision in the unincorporated DUP to quantify equal distribution of εA lesions across the NCP populations. A ratio of 1 indicates that the amount of cleavage in the freed DUP is equal to that in the unincorporated DUP, and therefore present in equal amounts in both DUP substrates.

3.3.5. Hydroxyl radical footprinting (HRF)

HRF was carried out using previously-published conditions to establish relative solution accessibility of nucleobase positions in NCPs under single-hit conditions.[10,23] Briefly, 7.5 µL of each 1 mM Fe(II)-EDTA, 10 mM sodium ascorbate, and 0.12% w/v aqueous hydrogen peroxide were gently combined with 5 pmol NCPs in a total of 52.5 µL buffer (10 mM Tris-HCl [pH 7.5], 1 mM EDTA). The reaction proceeded at room temperature for 10 min in the dark and was quenched with the addition of 16 µL 50 mM EDTA in 25% v/v glycerol. The quenched sample was immediately loaded onto a 7% native PAGE (60:1 acrylamide: bisacrylamide; 0.25x TBE) and run for 3 h at 160 V at 4 °C. Gel bands containing the NCP species were excised and NCPs were eluted into buffer (0.3 M NaOAc, 1 mM Tris-HCl [pH 8.0], 1 mM EDTA) for 16-20 h at 37 °C with gentle shaking (80 rpm). The NCP eluent was concentrated using a centrifugal concentrator (Sartorius Vivaspin Turbo 15, 5 kDa MWCO) and filtered using a 0.22 µm cellulose acetate centrifuge tube filter (Corning Costar). The sample was extracted twice with equal volume additions of PCI to remove histone proteins, and the resulting aqueous phase was concentrated by SpeedVac evaporation. Following the addition of 40 µL co-precipitation agent (0.5 mg/mL tRNA in 300 mM NaOAc [pH 8.0], 1 mM EDTA), samples were desalted with two ethanol precipitations. Samples were prepared in a 1:1 mixture of formamide and water for denaturing PAGE. Cleavage fragments were resolved after splitting the sample into two halves. Each half was loaded onto separate denaturing PAGE (12% gel for 5'-end fragments, 8% for 3'-end fragments).[24,25] Denaturing PAGE were visualized by phosphorimagery (Bio-Rad PharosFX).

Bands resulting from HRF cleavage were quantitated using SAFA gel analysis software.[22] The more solution-accessible a nucleobase position is to hydrogen abstraction, the stronger the intensity of the corresponding cleavage fragment. Categorization of solution accessibilities of nucleobases were determined as a ratio of

band intensity at a given position relative to the highest band intensity within the helical turn. Highly solution-accessible (HIGH) positions were defined as those with a ratio greater than 0.7; medium solution-accessible (MID) positions with a ratio range from 0.3-0.7; solution-inaccessible (LOW) positions were defined as those with a ratio less than 0.3.

3.3.6. AAG kinetics on global εA-containing DNA

AAG was purchased from New England Biolabs. The total concentration of AAG was determined by the Bradford method using bovine γ-globulin standards (Bio-Rad Laboratories). All AAG concentrations given below or in figure captions are total enzyme concentrations.

Reactions were initiated after the DNA substrate and AAG were pre-equilibrated at 37 °C for 2 min by combining an equal volume of 26.6 nM DNA substrate (DUP or NCP) and 0.8 μM AAG for a final experimental sample of 13.3 nM DNA and 0.4 μM AAG in 20 mM Tris-HCl (pH 7.6), 50 mM NaCl, 150 mM KCl, 1 mM EDTA, 1 mM DTT, 200 μg/mL BSA. The reactions were incubated at 37 °C for 5, 15, 30, 60, 90, 120, or 180 min before they were quenched with an equal volume of 1 M NaOH supplemented with the radiolabeled internal references and incubated at 90 °C for 3 min. Timepoints were initiated in such a way that all samples were quenched at the same time before immediate sample workup; this process was used to avoid extended incubation of εA lesions in NaOH after quenching which could result in degradation and false-positive results of AAG-catalyzed cleavage.[26,27] After incubation with NaOH, an equal volume of PCI was added followed by 40 μL of co-precipitation agent (0.5 mg/mL tRNA in 300 mM NaOAc [pH 8.0], 1 mM EDTA) and the samples were subsequently desalted with two ethanol precipitations. The (-E) sample was not incubated with AAG but instead an equivalent volume of reaction buffer was added and incubated at 37 °C for 180 min, quenched, and subsequently worked up like the rest of the samples. Any incidental damage due to experimental

conditions or workup was revealed by this sample which was used for a background subtraction for AAG-treated samples.

After the final ethanol precipitation all samples were resuspended in a 1:1 mixture of formamide and water and split in half. Each half was loaded onto separate denaturing PAGE (12% gel for 5'-end fragments; 8% for 3'-end fragments). The PAGE gels were visualized by phosphorimagery on a Bio-Rad PharosFX and quantified by SAFA.[22] The internal references served as a loading control and also allowed us to account for loss of εA cleavage products due to sample workup, especially smaller fragments that have a decreased ability to precipitate.[28] Accordingly, the band intensities in each lane were normalized to an internal reference. The 23 mer internal reference was used for the 5'-end fragments (ranging from 9-68) and the 92 mer internal reference was used for the 3'-ends fragments (ranging from 70-132). After this normalization the band intensity in the -E lane was subtracted from the AAG-treated samples.

As a result of the global lesion substitution, <1% of the DNA population is available as a substrate at each εA position. Therefore, the exposure time needed for phosphorimagery leads to overexposure of the parent band which then cannot be accurately quantified and used as a reference point to determine the amount of cleavage product at each εA. To address this technical challenge, we defined the amount of product observed with the DUP control after 180 min as the theoretical maximum amount of product at a given lesion position (DUP_{180}). Therefore, product accumulation at time *t* is represented as a ratio relative to DUP_{180}. In DUP, product accumulation at time *t* is represented as DUP_t/DUP_{180}, where DUP fraction product is normalized to 1.0 for the 180 min sample. In NCPs, product accumulation at time *t* is represented as NCP_t/DUP_{180}, where a ratio of 1.0 indicates the εA is removed completely, as in DUP. Replicate data at each observed εA position were averaged for every timepoint, and then fit to a single exponential model $y(t) = y_{\max}\left(1 - e^{-k_{\mathrm{obs}}t}\right)$, where y_{max} is the amplitude of the reaction's

fit, k_{obs} is the observed rate constant, and t is time. Error bars shown are calculated standard errors (SE) from 3-10 replicates for each εA position at each timepoint: $SE = \frac{\sigma}{\sqrt{n}}$, where σ is the standard deviation of the population and n is the number of replicates.

We confirmed that AAG retains full activity during the 180 min time course. The activity of AAG pre-incubated for 180 min (3 h sample) at 37 °C under experimental conditions was compared to that of AAG directly added (0 h sample) to global εA-containing DUP. After addition, the reactions proceeded for 1 h at 37 °C before quenching with NaOH supplemented with radiolabeled internal references and sample workup as described above. Cleavage products resulting from εA excision were resolved on a 12% denaturing PAGE to resolve the 5'-end fragments and quantified by SAFA.[22] After normalization using the 53 mer internal reference and background subtraction of the -E data the ratio of product formation for the 180 min sample relative to the 0 h sample was determined. A ratio of 1 indicates that after 180 min at 37 °C AAG retains full activity.

3.3.7. Molecular modeling of NCP

A crystal structure modeling the Widom 601 sequence wrapped around a *X. laevis* histone octamer with histone tails was created using the "merge" function in PyMOL (**Figure 3.1.B**). The NCP crystal structure containing the Widom 601 sequence but lacks histone tails (PDB ID: 3lz0) was merged with an NCP crystal structure containing the alpha-satellite DNA sequence but containing the histone tails (PDB ID: 1kx5) by aligning the overlapping histone protein amino acid sequences. The Widom 601 duplex and the histone octamer containing the histone tails were combined and merged to create a new, separate PyMOL object.

3.4. Results

3.4.1. AAG activity on global εA-containing duplex

After confirming εA incorporation into our global population (**Figure 3.2.A,B**), we first measured εA excision by AAG as a function of time in a 145 bp global duplex control (DUP). DUP was assembled with one εA-containing 145 mer annealed to an undamaged complementary strand. Due to the relatively small amounts of each lesion-containing substrate resulting from global εA substitutions relative to the total DNA population, we defined the amount of excised product observed after 180 min as the maximal product accumulation at a given lesion site. We chose an 180 min time course based on previous experiments and AAG's slow activity,[1–4] and confirmed that AAG retains full activity over the 180 min (**Figure 3.3.A,B**). Therefore, product accumulation at time *t* is represented as a ratio relative to product accumulation at 180 min (DUP_t/DUP_{180}) (**Figure 3.4.A,B, Figure 3.5.A**, **Figure 3.6.A**). Monophasic fits of reaction progress at each lesion site in DUP (**Figure 3.5.B**, closed symbols)

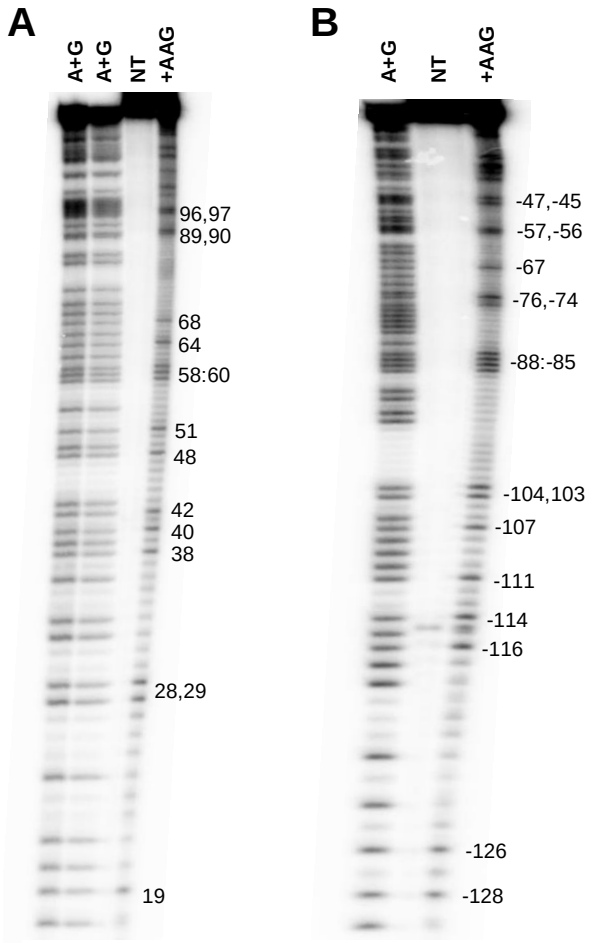

Figure 3.2. Confirmation of εA substitutions for A in Widom 601 I and J strands. The εA was incorporated separately in the **(A)** I and **(B)** J strands. The A+G lanes display a sequence ladder created using Maxam-Gilbert reactions using Widom 601 sequences lacking εA lesions. NT lanes show corresponding untreated I or J strand. The +AAG lanes are DNA duplexes containing εA in either the I or J strand treated with AAG for 1 h at 37 °C and quenched with the addition of NaOH to create strand breaks at AAG-generated abasic sites. In both PAGE images, the parent band was partially

determined the observed rate (k_{obs}) of AAG excision at the 49 εA positions in DUP, which ranges from 0.030-0.091 min^{-1} (**Table 3.1** for all k_{obs} values). These k_{obs} values are comparable to previous reports for site-specific εA lesions in both short oligonucleotide duplexes[2,3] and 145 bp duplex.[1]

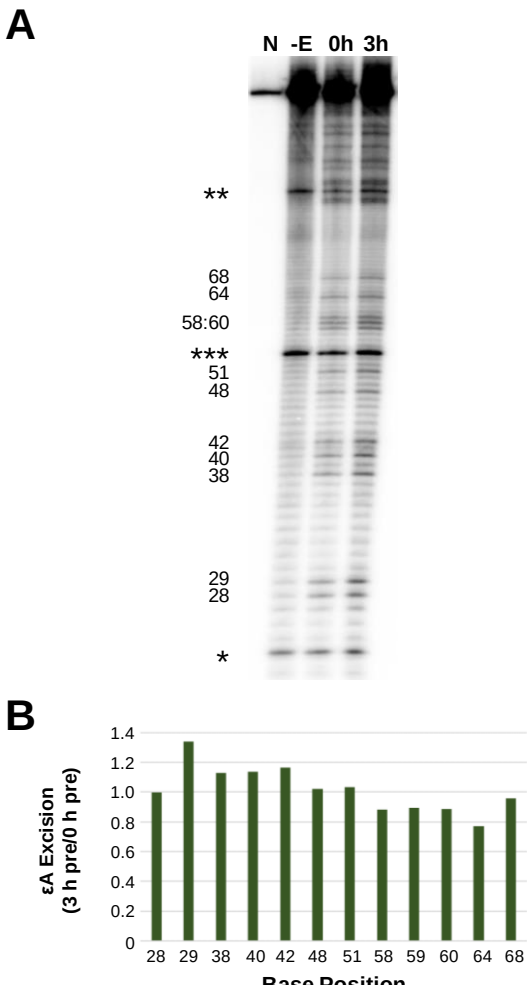

Figure 3.3. AAG retains full activity for 180 min. (A) AAG was either added directly (0 h lane) or pre-incubated at 37 °C under experimental conditions for 180 min (3 h lane) before incubation with global εAI DUP. After AAG addition, the reaction proceeded for 1 h at 37 °C before quenching with NaOH and sample workup for loading on denaturing PAGE. Three internal references, a 23 mer (*), 92 mer (**), and 53 mer (***) used for quantitation are indicated. The N lane shows the DUP sample without any treatment. The -E lane is quenched with NaOH to show any damage due to experimental conditions and workup. **(B)** Quantification of AAG activity at various positions in DUP, shown as a ratio of εA excision seen in the 3 h pre-incubation sample to the amount of εA excision seen in the 0 h sample. A ratio of 1 indicates that pre-incubation of AAG for 3 h before reaction does not influence its activity.

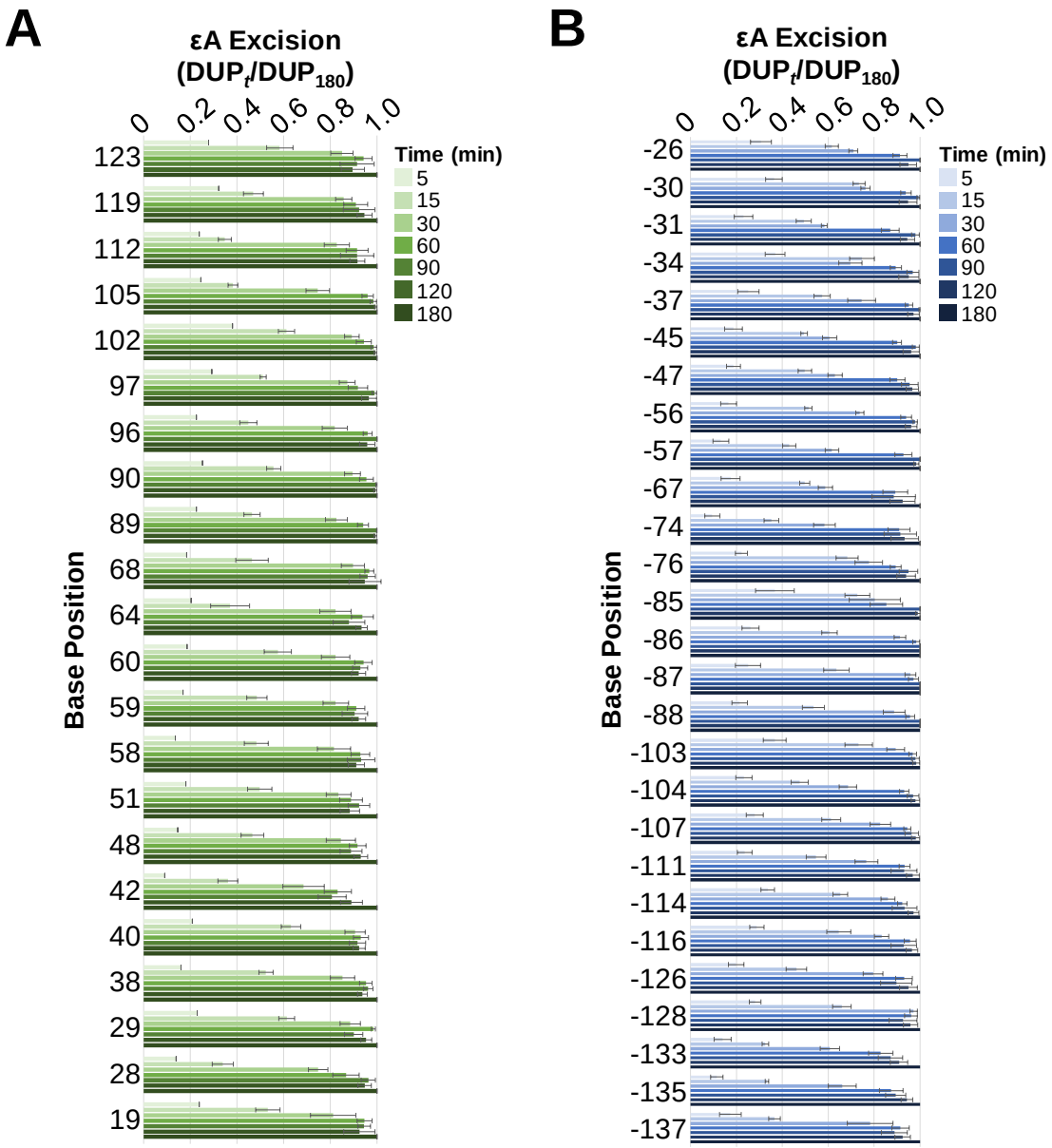

Figure 3.4. Quantitation of εA excision over time in global DUP. Lesions removed from the **(A)** I strand and **(B)** J strand from observed positions. Product accumulation at time *t* is represented as a ratio relative to product accumulation at 180 min (DUP_t/DUP_{180}), the defined maximal product. Error bars are calculated standard errors (n= 3-10).

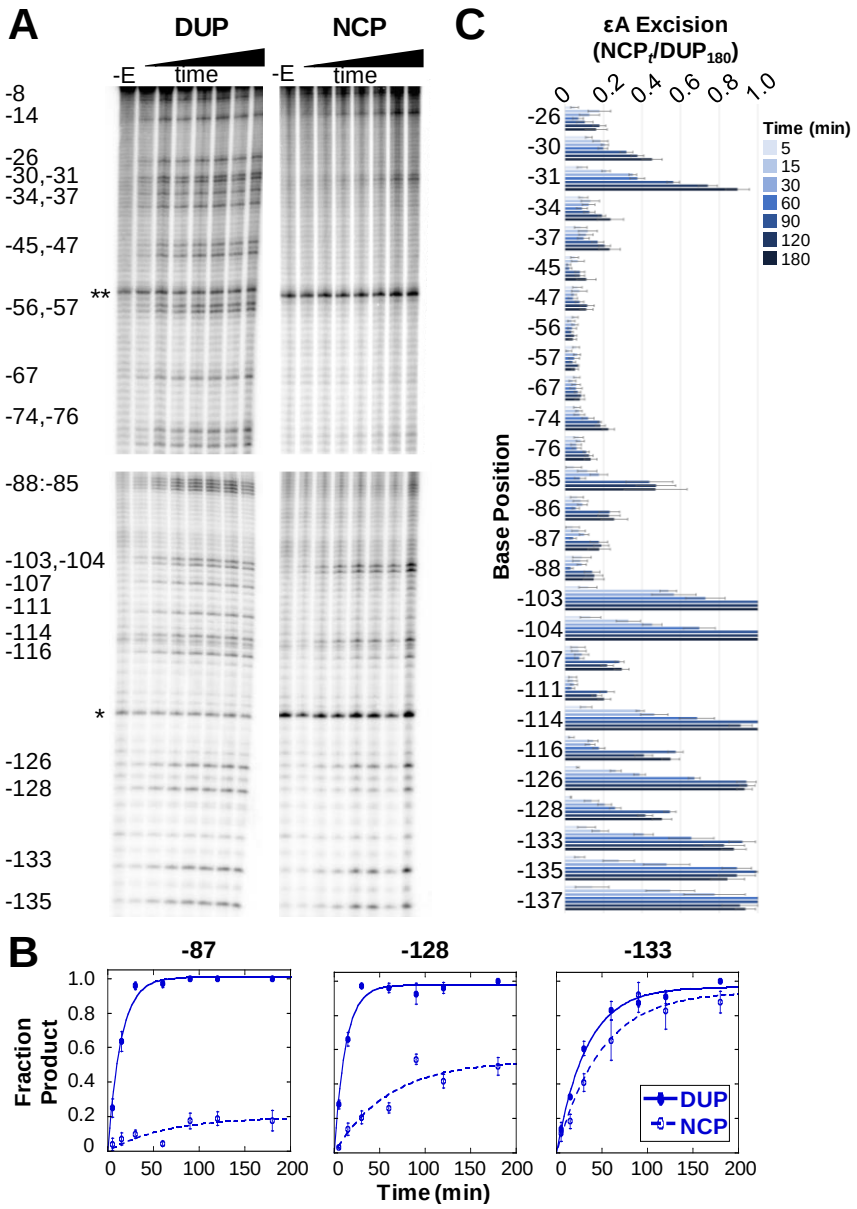

Figure 3.5. Single-turnover kinetic time course experiments of εA excision on the J strand by AAG. (A) Representative PAGE gels showing εA excision on the J strand of DUP (left) and NCP (right). DNA samples only treated with NaOH (-E lanes) show incidental damage from experimental conditions and sample workup. Two internal references, a 23 mer (*) and 92 mer (**), used for quantitation are indicated. Four separate gels are shown, indicated by the spaces between the images, with each gel cropped for alignment. The top two panels are aligned to show DUP and NCP data for positions -8 to -76. The bottom two panels are aligned to show data for positions -85 to -135. **(B)** Selected kinetic fits showing examples of low (site -87), medium (site -128), and high (position -133) amounts of εA excision on DUP (closed symbols) and NCPs (open symbols). **(C)** Quantitation of εA excision over time on the J strand in NCPs. Error bars are calculated standard errors (n= 3-10). Analogous activity on the I strand in NCPs is shown in **Figure 3.6.**

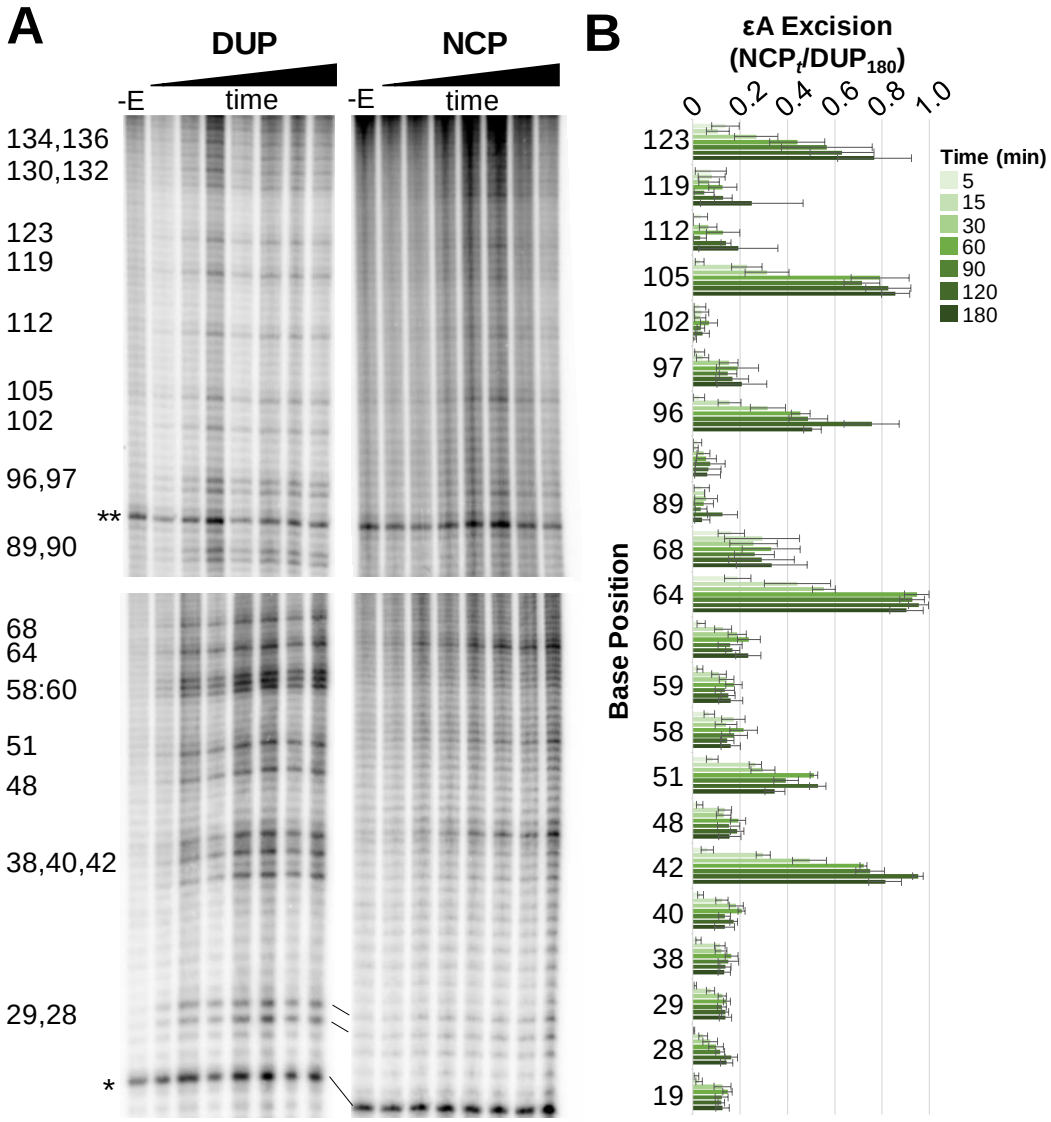

Figure 3.6. Single-turnover kinetic time course experiments of εA excision on the I strand by AAG. (A) Representative PAGE gels showing εA excision on the J strand of DUP (left) and NCP (right). DNA samples only treated with NaOH (-E lanes) show incidental damage from experimental conditions and sample workup. Two internal references, a 23 mer (*) and 92 mer (**), used for quantitation are indicated. Four separate gels are shown, indicated by the spaces between the images, with each gel cropped for alignment. The top two panels are aligned to show DUP and NCP data for positions -8 to -76. The bottom two panels are aligned to show data for positions -85 to -135. **(B)** Selected kinetic fits showing examples of low (site -87), medium (site -128), and high (position -133) amounts of εA excision on DUP (closed symbols) and NCPs (open symbols). **(C)** Quantitation of εA excision over time on the J strand in NCPs. Error bars are calculated standard errors (n= 3-10).

3.4.2. AAG activity on global εA-containing NCPs

We next prepared global εA-containing NCP populations to examine AAG activity in packaged DNA (**Figure 3.7.**). We previously reported[17,21,30] extensive control experiments to determine strategies that minimize, to the greatest extent possible, unincorporated DNA in NCP preparations. Only NCP preparations with ≤ 5% DUP are used in experiments. In this work, the upper bound of contaminating DUP used in NCP experiments is the lowest amount of εA excision observed at a single site: site -56 has an average accumulation of 4% (**Figure 3.8.**). Therefore, DUP cannot account for more than 4% of the reported NCP product in excision experiments.

Product accumulation in the NCP was determined at time *t* as a ratio relative to maximal product accumulation, NCP_t/DUP_{180} (**Figure 3.5.A,C**, **Figure 3.6.B**). Unlike AAG excision from DUP, not all εA lesions in NCPs were fully excised by 180 min; 30/49 sites

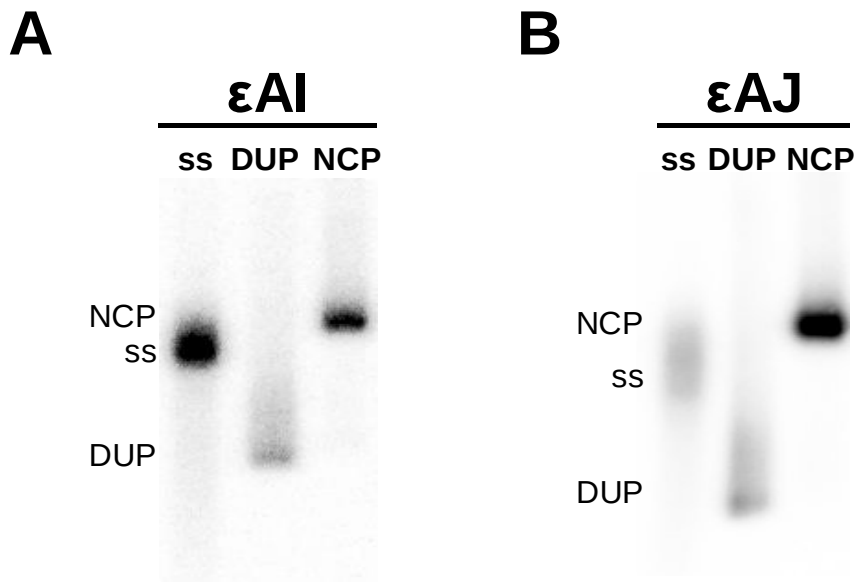

Figure 3.7. Formation of global εA-containing DUP and NCPs. Representative native PAGE gels showing differential migrations of global εA-containing single-strand (ss), DUP, and NCPs on the (**A**) I strand and (**B**) J strand. When εA was in the I strand it was paired with the J strand lacking damage. When εA was in the J strand, it was paired with I strand lacking damage. Only DUP preparations having ≤ 5% single-strand DNA were used in further studies. Similarly, only NCP preparations having ≤ 5% DUP were used in further studies.

had less than 30% excision (**Figure 3.8.**). We next obtained k_{obs} describing AAG excision of εA from the global NCPs. As observed for DUP, excision of εA across NCPs displayed monophasic behavior (**Figure 3.5.B**, open symbol). In addition, k_{obs} values across NCPs are comparable to those observed in DUP and to those obtained for a site- specific lesion in an NCP (**Table 3.1**).[21]

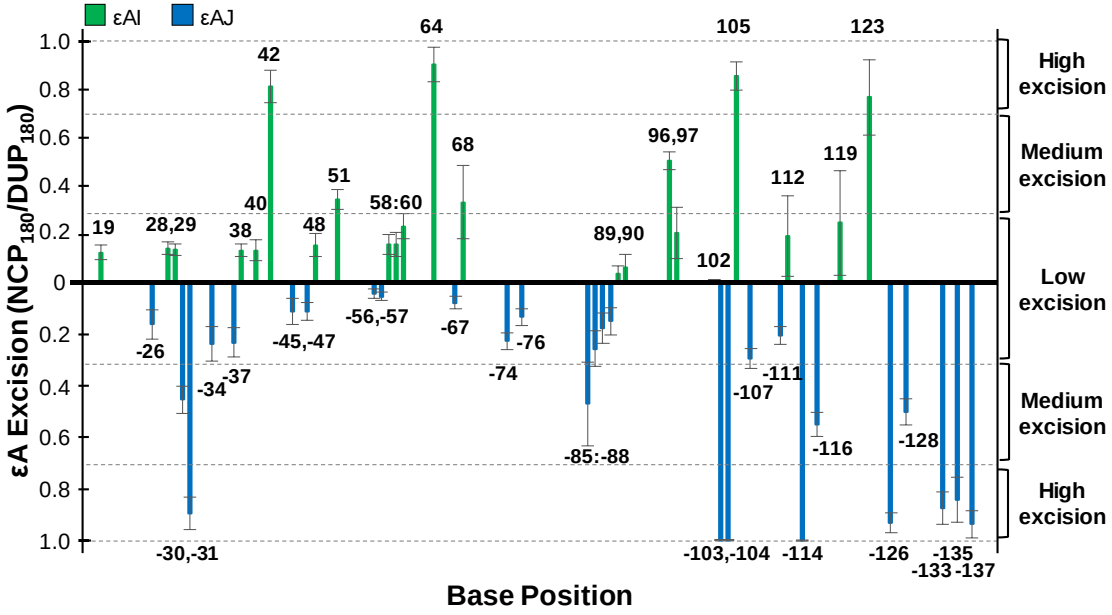

Figure 3.8. Quantitative assessment of relative AAG activity in NCPs. Relative AAG activity at each NCP position was categorized based on the average product accumulation after 180 min. Low εA excision is defined as product accumulation < 0.3, medium εA excision ranges between 0.3-0.7, and high εA excision is defined as > 0.7. A ratio of 1 represents full repair in NCPs as seen in DUP. Error bars are calculated standard errors (n= 3-10).

3.4.3. Relationships between AAG activity and solution accessibility of εA lesions in NCPs

We performed hydroxyl radical footprinting (HRF) to characterize solution accessibility of nucleobases in global NCPs (**Figure 3.9.**, shaded gray area; **Figure S.3.10.A-D** for gels). εA positions with high (HIGH), medium (MID), and low (LOW) solution accessibilities were grouped based on the ratios of accessibility to the maximal

Base Position	DUP k_{obs} (min^{-1})	DUP Frac. pdt.	DUP R^2 fit	NCP k_{obs} (min^{-1})	NCP Frac. pdt.	NCP R^2 fit
19	0.057	0.965	0.991	0.044	0.133	0.817
-26	0.060	0.965	0.955	n. d.	< 0.18	n. d.
28	0.037	0.990	0.977	0.019	0.157	0.950
29	0.067	0.970	0.977	0.054	0.139	0.932
-30	0.086	0.954	0.933	0.017	0.435	0.705
-31	0.038	0.979	0.967	0.009	1.092	0.949
-34	0.089	0.930	0.861	n. d.	< 0.240	n. d.
-37	0.054	0.988	0.992	n. d.	< 0.240	n. d.
38	0.054	0.982	0.979	0.073	0.146	0.884
40	0.070	0.957	0.970	0.087	0.167	0.727
42	0.036	0.930	0.964	0.027	0.880	0.966
-45	0.038	0.991	0.983	n. d.	< 0.120	n. d.
-47	0.040	0.984	0.988	n. d.	< 0.120	n. d.
48	0.051	0.958	0.963	0.070	0.171	0.842
51	0.055	0.943	0.970	0.052	0.443	0.785
-56	0.046	0.990	0.995	n. d.	< 0.055	n. d.
-57	0.034	1.020	0.992	n. d.	< 0.065	n. d.
58	0.050	0.965	0.974	n.d.	< 0.220	n. d.
59	0.052	0.955	0.977	0.073	0.156	0.907
60	0.059	0.960	0.984	0.068	0.201	0.785
64	0.046	0.964	0.949	0.038	0.953	0.962
-67	0.039	0.952	0.971	n. d.	< 0.085	n. d.
68	0.053	0.990	0.963	n. d.	< 0.335	n. d.
-74	0.031	0.994	0.987	0.015	0.232	0.866
-76	0.068	0.948	0.965	n. d.	< 0.230	n. d.
-85	0.088	0.951	0.925	0.008	0.660	0.786
-86	0.065	1.007	0.993	0.009	0.322	0.728
-87	0.070	1.007	0.983	n. d.	< 0.190	n. d.
-88	0.056	1.007	0.987	n. d.	< 0.150	n. d.
89	0.048	1.005	0.989	n. d.	< 0.130	n. d.
90	0.060	1.001	0.989	0.045	0.066	0.911
96	0.048	1.000	0.984	0.023	0.621	0.867
97	0.059	0.983	0.976	0.036	0.187	0.852
102	0.076	0.983	0.973	n. d.	< 0.070	n. d.
-103	0.091	0.980	0.997	0.032	0.998	0.928
-104	0.043	0.993	0.994	0.021	1.068	0.974
105	0.041	1.013	0.980	0.021	0.899	0.942
-107	0.065	0.977	0.998	0.009	0.370	0.749
-111	0.054	0.969	0.995	0.007	0.292	0.718
112	0.046	0.963	0.938	n. d.	< 0.193	n. d.
-114	0.079	0.957	0.988	0.023	1.015	0.957
-116	0.071	0.964	0.993	0.010	0.677	0.808
119	0.059	0.958	0.950	n. d.	< 0.260	n. d.
123	0.068	0.945	0.981	0.012	0.854	0.975
-126	0.049	0.964	0.983	0.019	1.025	0.976
-128	0.080	0.976	0.970	0.017	0.537	0.887
-133	0.031	0.965	0.991	0.021	0.939	0.963
-135	0.033	0.982	0.988	0.031	0.944	0.945
-137	0.043	0.962	0.965	0.053	0.971	0.969

Table 3.1. k_{obs} values for εA excision by AAG. Product accumulation over time was characterized by monophasic kinetic fits by Kaleidagraph to yield k_{obs} and % product values for εA positions on the I strand (green rows) and J strand (blue rows) of the global εA-containing DNA substrates. Fields displaying "n. d." were unable to be determined based on the small amounts of product accumulation observed.

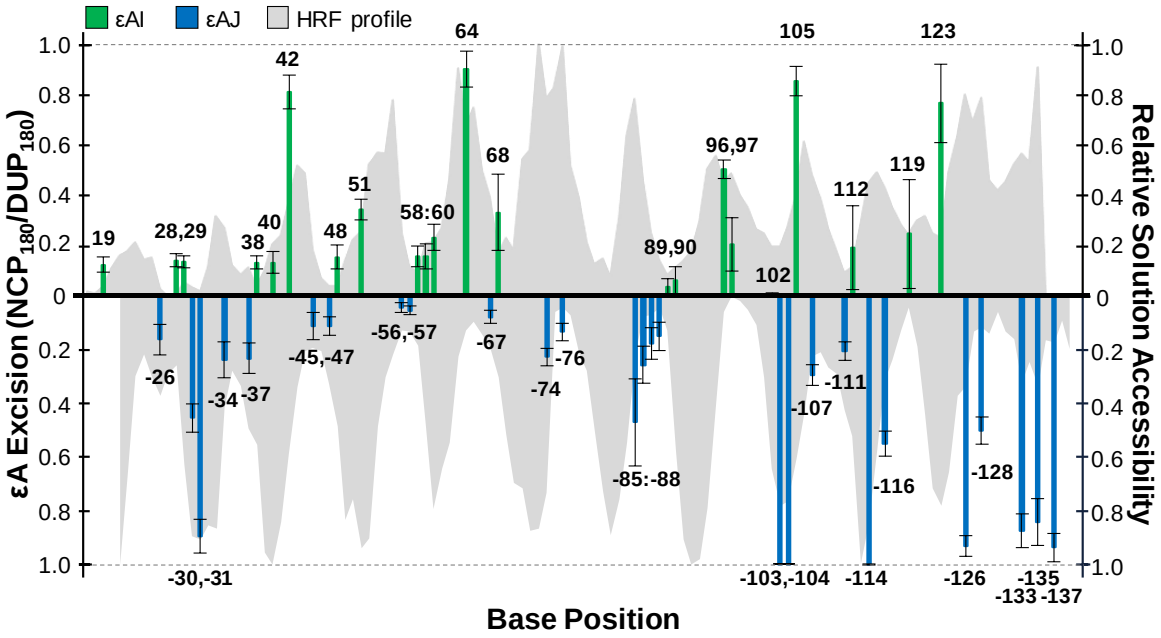

Figure 3.9. Relationship between AAG activity on and solution accessibility of εA positions in the NCP. The amount of AAG excision after 180 min is shown as bars at each εA position along the I strand (green) and J strand (blue). Error bars represent the standard error (n = 3-10). The HRF profile characterizes relative reactivity as a function of base position and is depicted as gray area in the background.

Table 3.2. Solution accessibilities of εA positions in NCPs.

Solution Accessibility	HRF Ratio[a]	Positions
LOW	0-0.3	19, -26, 28, 29, 38, -45, 48, -56, -57, 58, 59, 60, -67, 68, -76, -86, -87, 88, 89, 90, -107, 112, 123, -128
MID	0.3-0.7	-34, -37, 40, -47, 51, -85, 102, -111, -116, 119, -126, -137
HIGH	0.7-1.0	-30, -31, 42, 64, -74, 96, 97, -103, -104, 105, -114, -133, -135

[a] The HRF ratio is the ratio of band intensity at a given cleavage fragment in the HRF profile relative to the highest band intensity within the associated helical turn. This ratio represents the amount of solution accessibility of the nucleobase position relative to the most solution-accessible nucleobase position within the helical turn. LOW was defined as having a ratio of less than 0.3, MID as 0.3-0.7, and HIGH as more than 0.7.

accessibility within a helical turn of the HRF profile (**Table 3.2.**). Overall, we found the extent of εA excision from NCPs by AAG is highly correlated with solution accessibility. About half of the HIGH positions, i.e. sites 42, 64, -103, -104, 105, -114, had maximal εA

excision (90-100%). Conversely, minimal amounts of product were observed at most LOW positions, with no greater than 20% εA excision. MID positions had low to moderate εA excision, ranging from 10-60%.

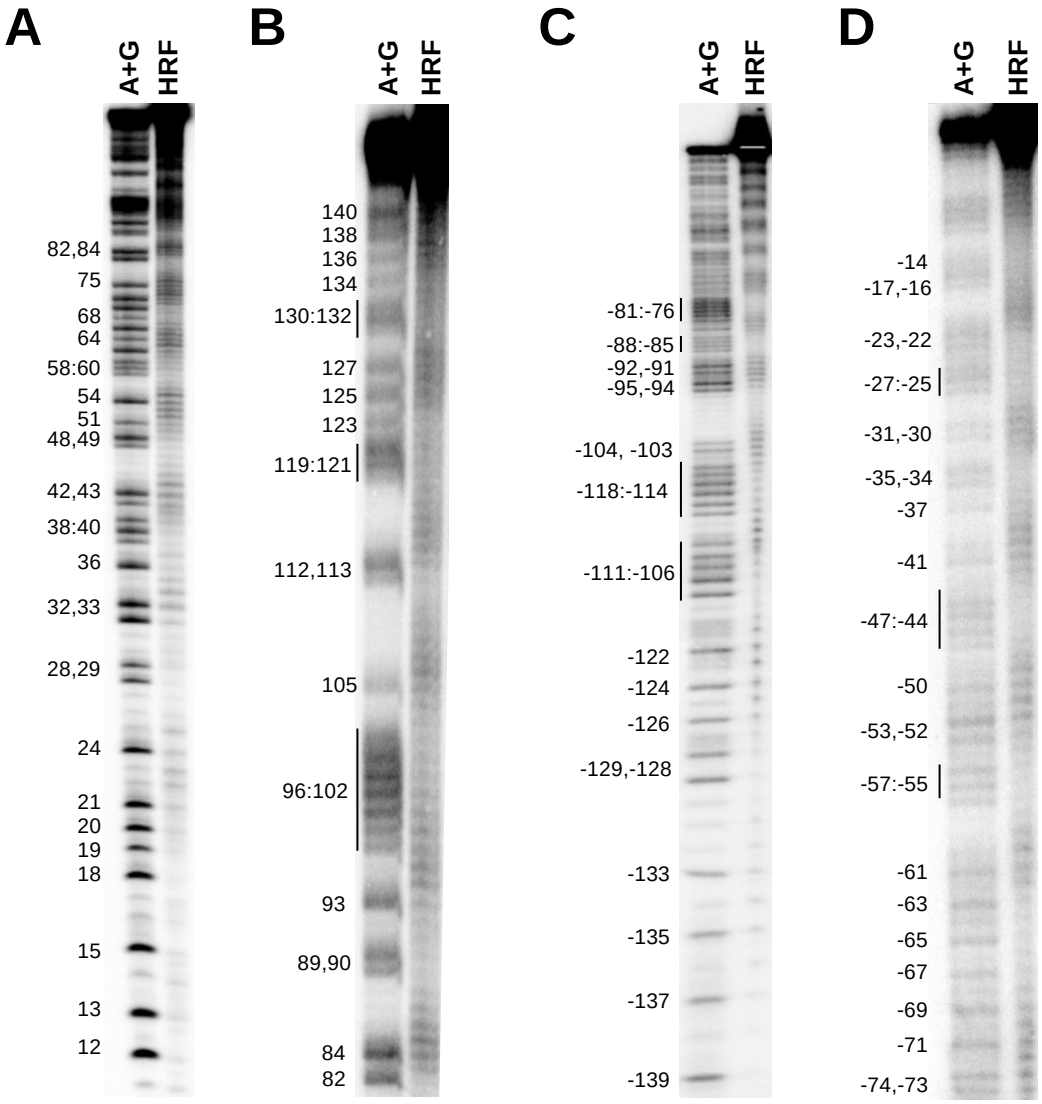

Figure 3.10. HRF denaturing PAGE gels to characterize nucleobase solution accessibilities in global εA-containing NCPs shown in Figure 3 of the main text. The HRF reaction on the global εA-containing I strand NCPs of the **(A)** 5'-end and **(B)** 3'-end are shown in the respective HRF lanes. The HRF reaction on the global εA-containing J strand NCPs of the **(C)** 5'-end and **(D)** 3'-end are shown in the respective HRF lanes. The A+G lanes display a sequence ladder created using Maxam-Gilbert reactions using undamaged Widom 601 sequences.

Interestingly, these experiments with global εA lesion NCPs reveal exceptions to the correlation between solution accessibility and AAG activity. Specifically, there are instances of HIGH positions that are inefficiently excised by AAG. For example, position -74 only had 20% εA excision observed. Sites -30, 96, and 97 are also HIGH positions that are also inefficiently excised by AAG, but have the additional feature of each being adjacent to a site where εA is more readily excised. For instance, AAG excised 40% of εA at position -30, but nearly quantitative conversion to product was observed at position -31. All other consecutive-run εA positions observed, such as 28 and 29; 58 through 60; 89 and 90; -57 and -56; -85 through -88; and -103 and -104, have εA excision correlated with relative solution accessibility as expected.

In addition to seeing a decreased in AAG activity in HIGH positions, we also observed instances of increased AAG activity despite solution accessibility characterization. Specifically, we observe increased activity in our global εA NCPs from base pair 123 to the DNA end, regardless of solution accessibility (**Figure 3.9.**). At least 60% excision of εA was observed at LOW positions, where similar solution-accessible positions elsewhere in the NCP, like positions 28, 29, -45, 48, 59, -67, -88, had at most 30% excision. MID positions on this end, such as 123, 126, -135, showed at least 80% εA excision, while MID positions on the other end, such as 19, -24, -34, had at most 20%.

3.5. Discussion

To investigate the effects of the histone octamer on repair of AAG on NCPs, we created a global population of εA-containing NCPs to observe AAG activity on a variety of translational and rotational positions in 49 distinct positions. Compared with DUP, we find a suppressed amount of activity across the Widom 601 duplex when incorporated into the NCPs (Compare **Figure 3.4.** with **Figures 3.5.** and **3.6.**), indicating that the presence of the histone octamer interferes with AAG activity. We verified that all DNA containing εA

lesions formed NCPs and there was no bias in NCP formation based on the geometric position of the lesion (**Figure 3.11.**); therefore, a lack of excision from NCPs is due to a lack of AAG activity.

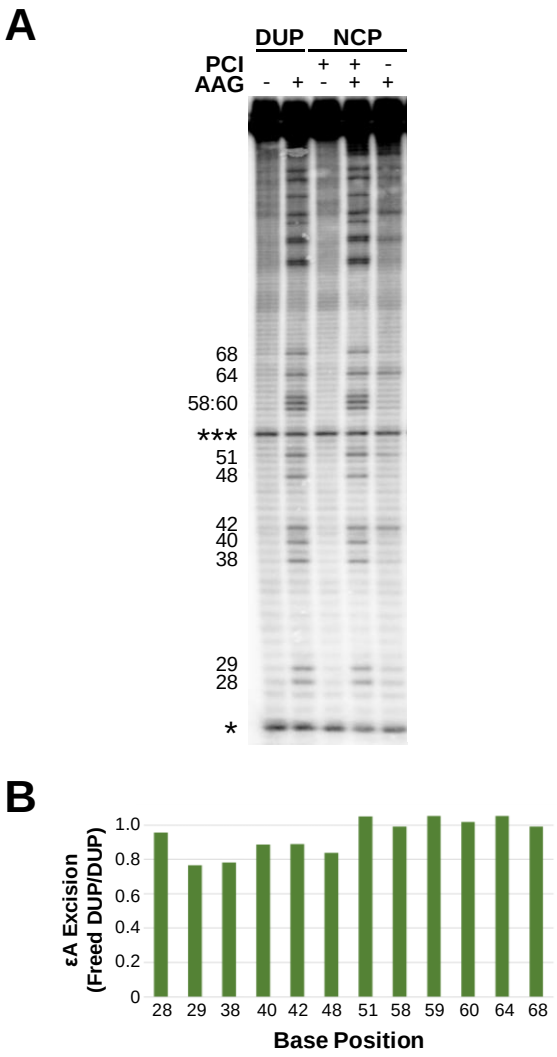

Figure 3.11. Non-biased incorporation of εA-containing DNA into NCPs. NCPs were assembled with global εA-containing I strand DUP, and then separated from histone octamers using a PCI extraction to create "freed DUP." AAG was incubated with freed DUP for 2 h at 37 °C and with DUP never incorporated into an NCP to compare differences in AAG activity. Different amounts of εA excision between the two samples would suggest biased incorporation of εA lesions during NCP reconstitution. **(A)** Denaturing PAGE gel of reactions for quantitative comparison. Two internal references, a 23 mer (*) and 53 mer (***) used for quantitation are indicated. – AAG lanes were only treated with NaOH to show any damage due to experimental conditions and workup. The freed DUP samples are indicated with + PCI designations. **(B)** Quantification of εA excision in each DUP substrate. A ratio of 1 indicates that the amount of cleavage in the freed DUP is equal to that in the unincorporated DUP.

In addition to quantifying relative amounts of εA excision by AAG as a function of position in the NCP, we also determined kinetic parameters observing excision accumulation over time at each position. We observed monophasic behavior of AAG across the sequence in NCPs, as in DUP. This characteristic, paired with the varying amounts of εA excision in NCPs, may reveal the subpopulations of NCPs that are conformationally competent for AAG activity. Previous kinetic characterizations of human glycosylases hOGG1 and UNG2 acting on site-specific lesion NCP systems revealed multiphasic kinetics (≥2 phases) for removal of lesions in some positions, which was attributed to conformation changes in the NCP.[30,31] Considering AAG's slower rate of glycosylase activity compared with hOGG1 and UNG2, the monophasic behavior observed across the NCP suggests that analogous conformational changes cannot be resolved on this time-scale.

We next characterized the relationships between AAG activity and solution accessibility of the εA lesions to better understand how the histone octamer influenced activity. Like many site-specific lesioned NCP systems studying glycosylase activity have described previously,[16] we too found a strong correlation between activity and solution accessibility of the NCP at a majority of the positions observed (**Figure 3.9.**). The overall correlation between glycosylase activity and solution accessibility observed in these *in vitro* chromatin experiments is consistent with *in vivo* observations. A report[32] using yeast mapped alkylation damage and its subsequent repair by the yeast homolog of AAG across the genome. The examination of 10,000 strongly-positioned NCPs in the genome revealed decreased repair in less solution-accessible sites. Another recent study[33] reported that somatic mutational rates in ~3,500 human tumors are enriched in sequences packaged by NCPs. Further, a subset of tumor types had a relative increase in mutation rates where minor grooves faced the histone core, specifically attributed to decreased repair at less-accessible positions. A reduction of AAG activity observed here within chromatin may

lead to this imbalance in DNA damage and repair that could cause mutagenicity and genetic instability described *in vivo.*[32,34] Indeed, it has been shown that DNA packaged in an NCP has been shown to be as susceptible as unpackaged DNA to alkylating agents.[35] We have observed in this work that AAG can remove εA lesions from HIGH positions, but has minimal activity on LOW positions. These results may suggest that εA repair by AAG at LOW positions *in vivo* may require additional nuclear factors, such as histone variants, histone post-translational modifications, and/or chromatin remodelers to increase access to LOW-positioned lesions.[14,36]

However, we did find some exceptions to this correlation between AAG activity and εA lesion solution accessibility that we attribute to a variety of architectural features of the NCP. In our initial survey, we observed a broader range of εA excision at MID positions. Upon consultation with an NCP representation of the Widom 601 duplex wrapped around the histone octamer, we noticed that the MID positions with less than 20% εA excision are located near histone tails; sites -34, -37, -47, -111 are closest to the base of an H2A tail, and position 119 is similarly near an H2B tail. Indeed, other glycosylases[30,37] and BER enzymes[38] have shown variable amounts of inhibition due to histone tails. The proximity of histone tails to certain positions may interfere with AAG in similar ways to reduce activity.

Next, we noted some HIGH positions that showed decreased AAG activity. The first such position is -74, where there was only 20% εA excision. Position -74 is located near the dyad axis, and the surrounding DNA around this dyad region has been shown to have different characteristics from the rest of the NCP. Any combination of these characteristics, including less DNA-histone dynamics,[15] a straighter conformation, and being underwound[10] may contribute to suppressed AAG activity. Indeed, we[17,21] and others [31,39,40] have found that repair of lesions in the ~20-bp of DNA centered at the dyad region is suppressed relative to other regions of the NCP. *In vivo* observations have also

shown these patterns of decreased BER within the dyad region of strongly-positioned NCPs.[32] Sites -30, 96, and 97 were also HIGH positions where AAG showed decreased activity. Specifically, sites -30 and -31 had differing amounts of εA excision, which may be due to the potential influence of the unstructured tails of nearby H2B and/or H2A (**Figure 3.12.A**). Additionally, these two positions are close to superhelical location (SHL) 5, a location in nucleosomal DNA known for stretching and disrupted base stacking.[12] This DNA stretching could influence the -30 position, to decrease AAG excision relative to position -31. Similarly, positions 96 and 97 had decreased εA excision, and may be influenced by nearby H2B and/or H4 tails (**Figure 3.12.B**), or nearby DNA stretching

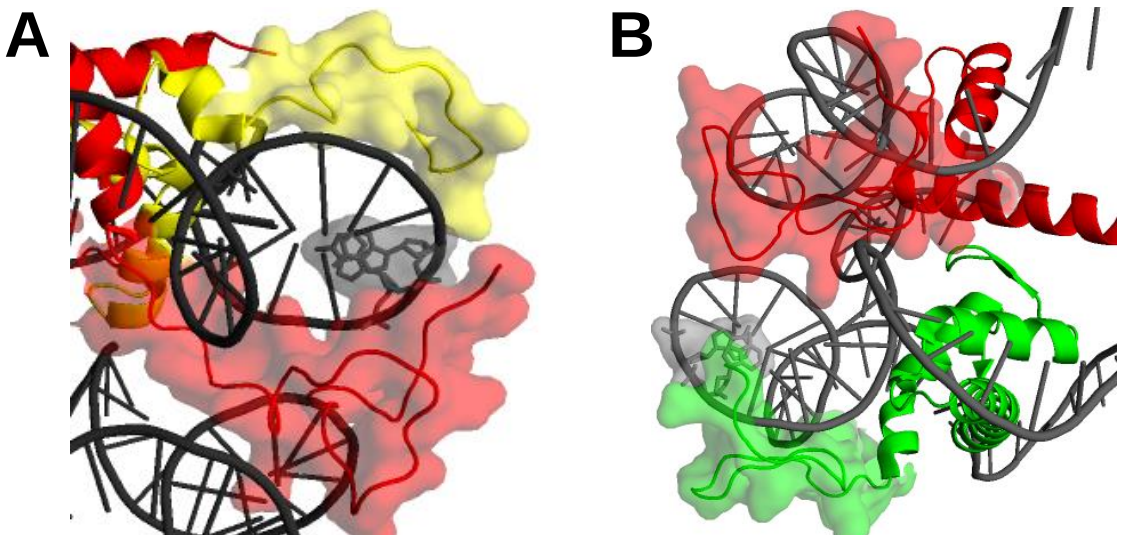

Figure 3.12. Proximity of histone tails to HIGH positions with low AAG activity. Zoom-in views of NCP crystal structure showing proximity of histone tails that may be within the potential area of effect on HIGH positions with decreased AAG activity. **(A)** Positions -30 and -31 (shown as gray sticks with a surface overlay) are in proximity to the nearby tails of H2A (yellow) and/or H2B (red). **(B)** Positions 96 and 97 (shown as gray sticks with a surface overlay) are similarly near the tails of H4 (green) and H2B (red). Only the histones and lesion-containing strand are shown for simplicity. The histone tails are shown with a surface overlay for emphasis. A merged NCP crystal structure of the Widom 601 duplex (PDB code 3lz0) and histone octamer with tails (PDB 1kx5) was created for these images using PyMOL.

between SHL ±1 to ±2 that results in severe kinking[12] to prevent AAG activity. The differential εA excision by AAG in the described positions emphasizes the effects of subtle, local NCP microenvironments unique to each nucleobase position and highlights the complexities that DNA packaging into an NCP presents for a glycosylase. Instances of decreased AAG activity in HIGH positions create an imbalance between damage and repair that can contribute to mutagenic signatures,[33] and describe potential hotspots in the packaged genome for persistent alkylation damage due to a deficiency in repair.

Finally, we observed increased AAG activity from base pair 123 to the end of the sequence in the global εA-containing NCPs regardless of solution accessibility. Although both ends of the DNA in NCPs have been shown to spontaneously and transiently unwrap to allow for increased access to nucleobases, one end is known to be more dynamic than the other. This asymmetric characteristic has been characterized previously *in vitro* with FRET studies to show asymmetric DNA-histone dynamics at the ends.[41–43] However, we directly observe the consequence of this asymmetric unwrapping in our global εA NCPs, with increased AAG activity toward the end known to unwrap preferentially in the 601 NCP.[42,43] These results are consistent with *in vivo* observations of higher levels of BER-related repair asymmetric to the dyad in genomic DNA.[32]

3.6. Conclusion

In summary, we determined the repair profile and various kinetic parameters in global DUP and NCPs to observe εA excision by AAG activity at 49 distinct geometric positions. AAG activity across the DUP had maximal amounts of excision, but varying amounts of activity across the NCP architecture. We show that the presence of the histone octamer, and therefore the packaging of DNA into chromatin, modulates repair by AAG. Although AAG's monophasic kinetic behavior remained consistent across the NCP, we observed interesting relationships between the amounts of εA excision and NCP

architecture. More specifically, we observed a general correlation between AAG activity and solution accessibility in the NCPs. However, we observed a few exceptions to this correlation, including HIGH positions with low repair likely due to distinct NCP microenvironments that suppress AAG activity, and increased εA removal at the DNA end that asymmetrically unwraps. Our characterizations of AAG excision of εA in global NCPs have revealed interesting microenvironments that inhibit repair that could not be appreciated previously in site-specific lesion NCPs. Future studies using this global NCP system could provide a more comprehensive understanding of the nuanced relationships between NCP architecture and DNA repair in cells.

3.7. References

(1) Lindahl, T. (1993) Instability and decay of the primary structure of DNA. *Nature 362*, 709–715.

(2) Helleday, T., Eshtad, S., and Nik-Zainal, S. (2014) Mechanisms underlying mutational signatures in human cancers. *Nat. Rev. Genet. 15*, 585–98.

(3) Schermerhorn, K. M., and Delaney, S. (2014) A chemical and kinetic perspective on base excision repair of DNA. *Acc. Chem. Res. 47*, 1238–1246.

(4) Brooks, S. C., Adhikary, S., Rubinson, E. H., and Eichman, B. F. (2013) Recent advances in the structural mechanisms of DNA glycosylases. *Biochim. Biophys. Acta - Proteins Proteomics 1834*, 247–271.

(5) Lee, C.-Y. I., Delaney, J. C., Kartalou, M., Lingaraju, G. M., Maor-Shoshani, A., Essigmann, J. M., and Samson, L. D. (2009) Recognition and processing of a new repertoire of DNA substrates by human 3-methyladenine DNA glycosylase (AAG). *Biochemistry 48*, 1850–61.

(6) Samson, L. D., Essigmann, J. M., Delaney, J. C., Lingaraju, G. M., Lee, C.-Y. I., Maor-Shoshani, A., and Kartalou, M. (2009) Recognition and Processing of a New Repertoire of DNA Substrates by Human 3-Methyladenine DNA Glycosylase (AAG) † . *Biochemistry 48*, 1850–1861.

(7) Swenberg, J. A., Lu, K., Moeller, B. C., Gao, L., Upton, P. B., Nakamura, J., and Starr, T. B. (2011) Endogenous versus exogenous DNA adducts: Their role in carcinogenesis, epidemiology, and risk assessment. *Toxicol. Sci. 120*, S130-45.

(8) Segal, E., and Widom, J. (2009) What controls nucleosome positions? *Trends Genet. 25*, 335–343.

(9) Richmond, R. K., Sargent, D. F., Richmond, T. J., Luger, K., and Mäder, A. W. (2002) Crystal structure of the nucleosome core particle at 2.8 Å resolution. *Nature 389*, 251–260.

(10) Hayes, J. J., Tullius, T. D., and Wolffe, A. P. (1990) The structure of DNA in a nucleosome. *Proc. Natl. Acad. Sci. U. S. A. 87*, 7405–9.

(11) Vasudevan, D., Chua, E. Y. D., and Davey, C. A. (2010) Crystal Structures of Nucleosome Core Particles Containing the “601” Strong Positioning Sequence. *J. Mol. Biol. 403*, 1–10.

(12) Chua, E. Y. D., Vasudevan, D., Davey, G. E., Wu, B., and Davey, C. A. (2012) The mechanics behind DNA sequence-dependent properties of the nucleosome. *Nucleic Acids Res. 40*, 6338–6352.

(13) Anderson, J. D., and Widom, J. (2000) Sequence and position-dependence of the equilibrium accessibility of nucleosomal DNA target sites. *J. Mol. Biol. 296*, 979–987.

(14) Rodriguez, Y., Hinz, J. M., and Smerdon, M. J. (2015) Accessing DNA damage in chromatin: Preparing the chromatin landscape for base excision repair. *DNA Repair (Amst). 32*, 113–119.

(15) Kim, J., Wei, S., Lee, J., Yue, H., and Lee, T. H. (2016) Single-Molecule Observation Reveals Spontaneous Protein Dynamics in the Nucleosome. *J. Phys. Chem. B 120*, 8925–8931.

(16) Kennedy, E. E., Caffrey, P. J., and Delaney, S. (2018) Initiating base excision repair in chromatin. *DNA Repair (Amst). 71*, 87–92.

(17) Bilotti, K., Tarantino, M. E., and Delaney, S. (2018) Human Oxoguanine Glycosylase 1 Removes Solution Accessible 8-Oxo-7,8-dihydroguanine Lesions from Globally Substituted Nucleosomes Except in the Dyad Region. *Biochemistry 57*, 1436–1439.

(18) Lowary, P. T., and Widom, J. (1998) New DNA sequence rules for high affinity binding to histone octamer and sequence-directed nucleosome positioning. *J. Mol. Biol. 276*, 19–42.

(19) Sambrook, J., and Russell, D. W. (2006) Isolation of DNA Fragments from Polyacrylamide Gels by the Crush and Soak Method. *Cold Spring Harb. Protoc.*

(Sambrook, J., and Russell, D., Eds.) *2006*, pdb.prot2936.

(20) Luger, K., Rechsteiner, T. J., and Richmond, T. J. (1999) Expression and purification of recombinant histones and nucleosome reconstitution. *Methods Mol. Biol. 119*, 1–16.

(21) Olmon, E. D., and Delaney, S. (2017) Differential Ability of Five DNA Glycosylases to Recognize and Repair Damage on Nucleosomal DNA. *ACS Chem. Biol. 12*, 692–701.

(22) Das, R., Laederach, A., Pearlman, S. M., Herschlag, D., and Altman, R. B. (2005) SAFA: semi-automated footprinting analysis software for high-throughput quantification of nucleic acid footprinting experiments. *RNA 11*, 344–54.

(23) Jain, S. S., and Tullius, T. D. (2008) Footprinting protein–DNA complexes using the hydroxyl radical. *Nat. Protoc. 3*, 1092–1100.

(24) Maxam, A. M., and Gilbert, W. (1977) A new method for sequencing DNA. *Proc. Natl. Acad. Sci. U. S. A. 74*, 560–4.

(25) Maxam, A. M., and Gilbert, W. (1980) Sequencing end-labeled DNA with base-specific chemical cleavages. *Methods Enzymol. 65*, 499–560.

(26) Speina, E., Cieśla, J. M., Wójcik, J., Bajek, M., Kuśmierek, J. T., and Tudek, B. (2001) The Pyrimidine Ring-opened Derivative of 1,N 6-Ethenoadenine Is Excised from DNA by the Escherichia coli Fpg and Nth Proteins. *J. Biol. Chem. 276*, 21821–21827.

(27) Hedglin, M., and O'Brien, P. J. (2008) Human alkyladenine DNA glycosylase employs a processive search for DNA damage. *Biochemistry 47*, 11434–11445.

(28) Shaytan, A. K., Xiao, H., Armeev, G. A., Wu, C., Landsman, D., and Panchenko, A. R. (2017) Hydroxyl-radical footprinting combined with molecular modeling identifies unique features of DNA conformation and nucleosome positioning. *Nucleic Acids Res. 45*, 9229–9243.

(29) O'Brien, P. J., and Ellenberger, T. (2004) Dissecting the Broad Substrate Specificity of Human 3-Methyladenine-DNA Glycosylase. *J. Biol. Chem. 279*, 9750–9757.

(30) Bilotti, K., Kennedy, E. E., Li, C., and Delaney, S. (2017) Human OGG1 activity in

nucleosomes is facilitated by transient unwrapping of DNA and is influenced by the local histone environment. *DNA Repair (Amst). 59*, 1–8.

(31) Ye, Y., Stahley, M. R., Xu, J., Friedman, J. I., Sun, Y., McKnight, J. N., Gray, J. J., Bowman, G. D., and Stivers, J. T. (2012) Enzymatic excision of uracil residues in nucleosomes depends on the local DNA structure and dynamics. *Biochemistry 51*, 6028–6038.

(32) Mao, P., Brown, A. J., Malc, E. P., Mieczkowski, P. A., Smerdon, M. J., Roberts, S. A., and Wyrick, J. J. (2017) Genome-wide maps of alkylation damage, repair, and mutagenesis in yeast reveal mechanisms of mutational heterogeneity. *Genome Res. 27*, 1674–1684.

(33) Pich, O., Muiños, F., Sabarinathan, R., Reyes-Salazar, I., Gonzalez-Perez, A., and Lopez-Bigas, N. (2018) Somatic and Germline Mutation Periodicity Follow the Orientation of the DNA Minor Groove around Nucleosomes. *Cell 175*, 1074–1087.e18.

(34) Levine, R. L., Yang, I. Y., Hossain, M., Pandya, G. A., Grollman, A. P., and Moriya, M. (2000) Mutagenesis induced by a single 1,N6-ethenodeoxyadenosine adduct in human cells. *Cancer Res. 60*, 4098–4104.

(35) Trzupek, J. D., Gottesfeld, J. M., and Boger, D. L. (2006) Alkylation of duplex DNA in nucleosome core particles by duocarmycin SA and yatakemycin. *Nat. Chem. Biol. 2*, 79–82.

(36) Pederson, D. S., Sweasy, J. B., Wallace, S. S., Averill, A. M., Marsden, C. G., and Maher, R. L. (2017) Human cells contain a factor that facilitates the DNA glycosylase-mediated excision of oxidized bases from occluded sites in nucleosomes. *DNA Repair (Amst). 57*, 91–97.

(37) Beard, B. C., Stevenson, J. J., Wilson, S. H., and Smerdon, M. J. (2005) Base excision repair in nucleosomes lacking histone tails. *DNA Repair (Amst). 4*, 203–209.

(38) Chafin, D. R., Vitolo, J. M., Henricksen, L. A., Bambara, R. A., and Hayes, J. J. (2000)

Human DNA ligase I efficiently seals nicks in nucleosomes. *EMBO J. 19*, 5492–5501.

(39) Cole, H. A., Tabor-Godwin, J. M., and Hayes, J. J. (2010) Uracil DNA glycosylase activity on nucleosomal DNA depends on rotational orientation of targets. *J. Biol. Chem. 285*, 2876–2885.

(40) Rodriguez, Y., and Smerdon, M. J. (2013) The Structural Location of DNA Lesions in Nucleosome Core Particles Differentially Influence Accessibility of Base Excision Repair Enzymes. *J. Biol. Chem. 19*, 13863–13875.

(41) Chen, Y., Tokuda, J. M., Topping, T., Sutton, J. L., Meisburger, S. P., Pabit, S. A., Gloss, L. M., and Pollack, L. (2014) Revealing transient structures of nucleosomes as DNA unwinds. *Nucleic Acids Res. 42*, 8767–76.

(42) Ngo, T. T. M., Zhang, Q., Zhou, R., Yodh, J. G., and Ha, T. (2015) Asymmetric unwrapping of nucleosomes under tension directed by DNA local flexibility. *Cell 160*, 1135–1144.

(43) Gansen, A., Felekyan, S., Kühnemuth, R., Lehmann, K., Tóth, K., Seidel, C. A. M., and Langowski, J. (2018) High precision FRET studies reveal reversible transitions in nucleosomes between microseconds and minutes. *Nat. Commun. 9*, 4628.

3.8. Appendix: Supplementary Information

Scheme S.3.1. Widom 601 sequences. I and J strand designations are based on the crystal structure of Vasudevan, *et a*l. for the Widom 601 NCP.[11]

I strand:

5′-ATC AGA ATC CCG GTG CCG AGG CCG CTC AAT TGG TCG TAG ACA GCT CTA GCA CCG CTT AAA CGC ACG TAC GCG CTG TCC CCC GCG TTT TAA CCG CCA AGG GGA TTA CTC CCT AGT CTC CAG GCA CGT GTC AGA TAT ATA CAT CGA T

J strand:

5′- ATC GAT GTA TAT ATC TGA CAC GTG CCT GGA GAC TAG GGA GTA ATC CCC TTG GCG GTT AAA ACG CGG GGG ACA GCG CGT ACG TGC GTT TAA GCG GTG CTA GAG CTG TCT ACG ACC AAT TGA GCG GCC TCG GCA CCG GGA TTC TGA T

Scheme S.3.2. Ligation strategy for complementary 145 mer oligonucleotides lacking damage. Each 145 mer is assembled by the ligation of three component oligonucleotides. Components 2 and 3 are 5'-phosphorylated and combined with component 1 and two scaffold oligonucleotides s12 and s23 for annealing. Annealed strands are subsequently ligated to create the full-length strands. When global εA was in the I strand, it was annealed to the non-lesion-containing J strand. Similarly, when global εA was in the J strand, it was annealed to the non-lesion-containing I strand.

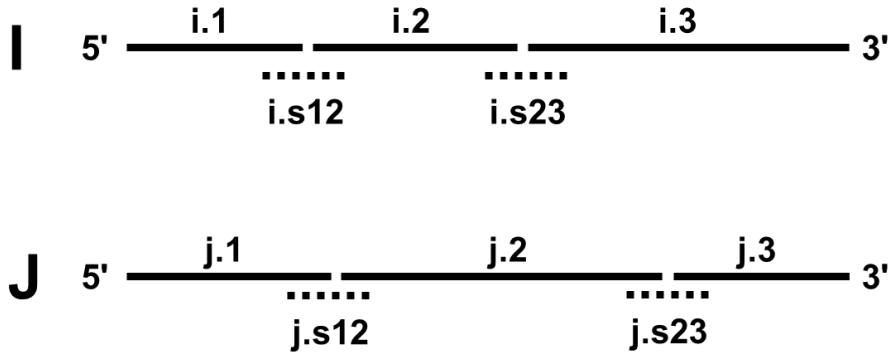

Component	Length	Sequence (5' to 3')
i.1	35mer	ATCAGAATCCCGGTGCCGAGGCCGCTCAATTGGTC
i.2	45mer	GTAGACAGCTCTAGCACCGCTTAAACGCACGTACGCGCTGTCCCC
i.3	65mer	CGCGTTTTAACCGCCAAGGGGATTACTCCCTAGTCTCCAGGCACGTGTCAGATATATACATCGAT
i.s12	32mer	GTGCTAGAGCTGTCTACGACCAATTGAGCGGC
i.s23	26mer	GGCGGTTAAAACGCGGGGGACAGCGC
j.1	45mer	ATCGATGTATATATCTGACACGTGCCTGGAGACTAGGGAGTAATC
j.2	65mer	CCCTTGGCGGTTAAAACGCGGGGGACAGCGCGTACGTGCGTTTAAGCGGTGCTAGAGCTGTCTAC
j.3	35mer	GACCAATTGAGCGGCCTCGGCACCGGGATTCTGAT
j.s12	30mer	TTTAACCGCCAAGGGGATTACTCCCTAGTC
j.s23	32mer	GCCGCTCAATTGGTCGTAGACAGCTCTAGCAC

Scheme S.3.3. Sequences of internal reference oligonucleotides.

23 mer:

5′-ATC AGA ATC CCG GTG CCG AGG CC

92 mer:

5′-ATC AGA ATC CCG GTG CCG AGG CCG CTC AAT TGG TCG TAG ACA GCT CTA GCA CCG CTT AAA CGC ACG TAC GCG CTG TCC CCC GCG TTT TAA CC

53 mer:

5′-ATC GAT GTA TAT ATC TGA CAC GTG CCT GGA GAC TAG GGA GTA ATC CCC TTG

Chapter 4. Finding a damaged needle in a packaged haystack: Observing uracil DNA glycosylase processivity in the nucleosome core particle

I designed and performed all the experiments and analyzed the results discussed here.

4.1. Abstract

Before base excision repair (BER) can be initiated with the cleavage of the N-glycosidic bond of a lesion nucleobase, glycosylases must first search for and find the rare lesions among billions of undamaged nucleobases. This crucial process is not fully understood and is a topic of interest in the DNA repair field. In the nucleus, both three-dimensional (volume-wide) and one-dimensional (local) searches must take place for efficient probing of the genome. Of particular interest is a glycosylase's one-dimensional transfer, or its processivity. Processivity is described as relative contributions from both associative transfer ("sliding" close to the phosphate backbone) and dissociative transfer (small "hopping" and re-binding events). Previous *in vitro* studies on duplex have shown that multiple factors influence the relative contribution of each mode of one-dimensional transfer. However, the genomic DNA is packaged into nucleosome core particle (NCP) subunits, which likely influence glycosylase searching and initiating BER. In this study, we set out to determine how glycosylase processivity is influenced by DNA packaging in two-site NCP substrates. We find that the presence of the histone octamer core strongly inhibits the associative transfer mode to favor dissociative transfer in NCPs.

4.2. Introduction

In the course of a typical day, a single cell deals with ~10,000 spontaneously-generated lesions that could potentially threaten its very existence.[1] Without efficient repair of these lesions, the genetic information that the DNA contains is endangered. The task of finding nucleobase lesions belongs to the DNA glycosylases belonging to the base excision repair (BER) pathway. On the scale of the human genome, glycosylase searching for lesions is a monumental task akin to looking for a needle in a haystack, since there are also ~12,000,000,000 undamaged nucleobases. To further complicate matters, 70-90% of the human genome is packaged into NCPs for compaction into the nucleus, which may

compromise repair activities.[2,3] Specifically, it is not understood how BER, the main pathway responsible for repairing modified nucleobase lesions, is initiated by glycosylase searching in the packaged genome environment. Once the lesion is found, the minimal kinetic scheme of glycosylases can begin, and the subsequent treatment by downstream BER enzymes. Once the job of the glycosylase is finished, the glycosylase then seeks out its next damaged needle in the genomic haystack to repeat the process. Unlike other repair pathways, BER substrates are typically non-bulky, like uracil (U), 8-oxo-7,8-dihydroguanine, and abasic sites, and are therefore not as disruptive to the local DNA environment as bulkier lesions, like thymine dimers repaired by nucleotide excision repair, for easy recognition.

It is widely accepted in the field that the most efficient means of searching the genome *in vivo* includes relative contributions of both longer-range three-dimensional diffusion, and shorter-range one-dimensional diffusion. Previous studies of glycosylase searching have focused on one-dimensional transfer, specifically the movement between two lesions during a single DNA encounter event, known as processivity. There are two main modes of processivity: associated diffusion (traditionally referred to as “sliding”) and dissociative transfer (traditionally referred to as “hopping”) (**Figure 4.1.**).[4] Associative transfer is characterized by a glycosylase maintaining near-constant contact with the DNA structure in such a way that follows the helical turning,[5,6] while not necessarily reliant on the electrostatics of the phosphate backbone to do so.[5,7,8] This mode of transfer is advantageous in scanning local stretches of DNA, but becomes more tedious and slower as distances between lesions increase. On the other hand, dissociative transfer is made up of more transient, micro-dissociations from the DNA where the glycosylase is still near enough to rebind with high probability. This mode of transfer is helpful in decreasing the overall searching volume over longer distances, where the probability of encountering another lesion upon re-binding is less likely. These two modes are thought to work

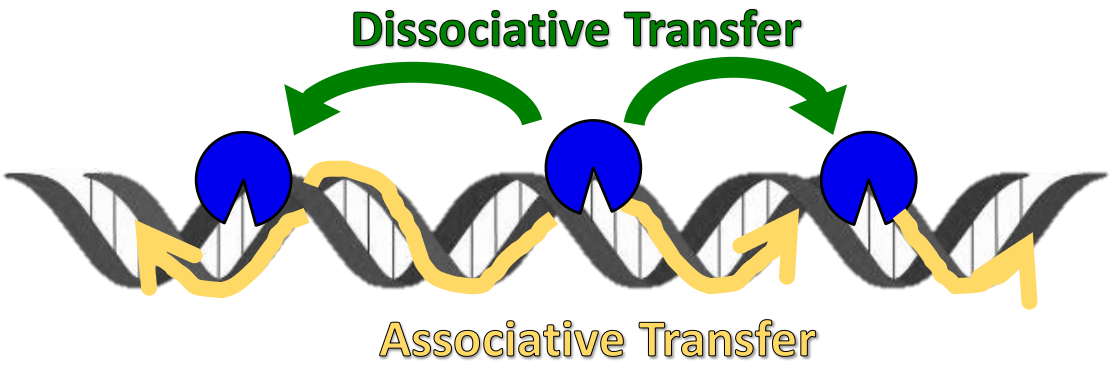

Figure 4.1. Associative vs. dissociative transfer on DNA duplex. After cleavage of the first lesion, the glycosylase (blue crescent) travels to the second lesion site along the DNA (dark gray) using either associative transfer (yellow arrows) or dissociative transfer (green arrows). Associative transfer is characterized by close contact with the helical turning of the DNA strand, while dissociative transfer is characterized by micro-dissociations and re-bindings.

together for fast, efficient searching of lesions among undamaged DNA before replication takes place to lock in the mutagenicity of lesions left unrepaired. We know that these two modes of processivity occur, but we do not know the relative contributions of each under various environmental conditions and DNA contexts.

Previous studies have been conducted to characterize processivity in duplex systems with a few glycosylases, such as human oxoguanine glycosylase (hOGG1),[9–13] human alkyladenine DNA glycosylase (AAG),[6,14–16] and uracil DNA glycosylases (UDG).[5,7,8,17–20] In general, UDG is one of the most-studied and therefore best-understood of the glycosylases[21–25] and is an attractive candidate for processivity studies in a new context. In the experiments discussed in this chapter, we wish to expand upon these transfer systems and apply them in an NCP system to examine how the presence of the histone octamer core affects searching and processivity. We used two-site NCP ensemble systems to observe the relative contributions of associative and dissociative transfer of UDG in packaged DNA under different environmental conditions to mimic those found in the nucleus. The results show that dissociative transfer is the major mode of one-

dimensional transfer in packaged DNA to navigate the presence of the histone octamer core.

4.3. Experimental Procedures

4.3.1. Oligonucleotide synthesis and purification

Oligonucleotides were synthesized on a MerMade 4 (BioAutomation) DNA synthesizer using standard phosphoramidite chemistry. All synthesis reagents and phosphoramidites were purchased from Glen Research. The final trityl group was retained after synthesis for use in the initial HPLC purification 90 °C (Agilent PLRP-S column, 250 mm × 4.6 mm; A = 100 mM triethylammonium acetate [TEAA] in 5% aqueous MeCN, B = 100 mM TEAA in MeCN; 5:95 to 35:65 A:B over 30 min, 35:65 to 5:95 A:B over 5 min at 1 mL/min). The trityl group was removed with incubation in 20% v/v aqueous glacial acetic acid for 1 h at room temperature, followed by a second HPLC purification at 90°C (Agilent PLRP-S column, 250 mm × 4.6 mm; A = 100 mM triethylammonium acetate [TEAA] in 5% aqueous MeCN, B = 100 mM TEAA in MeCN; 0:100 to 15:85 A:B over 35 min, 15:85 to 35:65 A:B over 5 min at 1 mL/min). Electrospray ionization mass spectrometry was used to verify the identity of the prepared oligonucleotides.

4.3.2. Ligation of full-length 145/146 mer oligonucleotides

Full-length 145 mer (Widom 601 sequence)[26] or 146 mer (5S sequence)[27] oligonucleotides used in studies were synthesized in shorter pieces and ligated together enzymatically (**Schemes S.4.1 and S.4.2** for 601 145 mers, **Schemes S.4.3 and S.4.4** for 5S 146 mers) The short oligonucleotides were phosphorylated with T4 polynucleotide kinase (New England Biolabs) and subsequently annealed to scaffold oligonucleotides in a 1:1.1 ratio by heating to 90 °C for 5 min followed by cooling to room temperature at a rate of 1°C/min. The annealed oligonucleotides were then ligated using T4 ligase (New

England Biolabs) for 3 h at room temperature. Full-length ligation products were purified using an 8% denaturing PAGE (0.8 m thick). Concentrations of the retrieved full-length purified oligonucleotides were determined by their absorbance at 260 nm using molar extinction coefficients calculated with the IDT OligoAnalyzer tool (www.idtdna.com).

4.3.3. Enzymes and histone proteins

E. coli UDG, uracil DNA glycosylase inhibitor (UGI), and human single-strand-selective monofunctional uracil DNA glycosylase 1 (SMUG1) were purchased from New England Biolabs. We used *E. coli* UDG in our studies because it has an active site that is over 55% identical and 73% similar to human UDG (UNG2)[24] and has been used in many previous studies as an acceptable alternative to using UNG2.[28] In addition, both enzymes have similar competency for removing U from NCPs.[26,29–31] Human apurinic/apyrimidinic endonuclease 1 (APE1) was expressed and purified as previously reported.[32] The total concentration of each enzyme was determined by the Bradford method using γ-globulin standards (Bio-Rad Laboratories). All concentrations reported here are total enzyme concentrations.

Recombinant *Xenopus laevis* histones were individually expressed and purified, and subsequently assembled into octamers for use in NCP reconstitutions.[26,33,34]

4.3.4. Duplex substrate preparation

Full-length oligonucleotides containing U lesions were 5'-radiolabeled for visualization. The processive products of the substrate containing two U on the same 145 mer strand (UUsame) contained an internal radiolabel located between the two U lesions for direct visualization of the double-cleavage product (**Schemes S.4.1. and S.4.2.**). Taking the Widom 601 ligation as an example, we applied the internal radiolabel by splitting the 145mer ligation into two component strands, i.1 and i.2, each containing a U

lesion. In a five nmol-scale ligation, a portion of the i.2 population (~10%) was 5'-radiolabeled using T4 kinase and ^{32}P-γ-ATP (Perkin Elmer); the remaining population was phosphorylated with 10 mM cold ATP. The two strands were ligated and gel-purified as described above. The oligonucleotide containing the two U and the internal radiolabel was annealed to its J-strand complement in a 1:1.05 ratio to form duplex.

For substrate preparation of the duplex with one U in each strand of duplex (UUopp), the full-length oligonucleotides were 5'-radiolabeled after ligation and combined in equal amounts of radioactive signal for relative quantitation of excision. Cold U-containing oligonucleotides were supplemented to reach the desired duplex concentration before annealing in a final 1:1 ratio.

All duplex formations took place in annealing buffer (10mM Tris-HCl pH 8.0, 50 mM NaCl, 1 mM EDTA) that was heated to 90 °C for 5 min followed by cooling to room temperature at a rate of 1 °C/min. Duplex formation was confirmed on a 7% native PAGE (60:1 acrylamide : bisacrylamide; 0.25x TBE) run for 3 h at 160 V in 4 °C to separate single-strand DNA and duplex species. Only duplex preparations containing ≤ 5% single-strand DNA were used in duplex studies.

4.3.5. Nucleosome core particle (NCP) reconstitution

NCPs were prepared by stepwise dialysis as previously described.[26] The duplex to be reconstituted was gently mixed with the histone octamer in a 10% molar excess to 25 µL of 1 µM duplex in buffer (10 mM Tris-HCl [pH 7.5], 1 mM EDTA, 1 mM dithiothreitol [DTT], 2 M NaCl, 500 µg/mL BSA) in a Slide-a-Lyzer dialysis device (0.1 mL capacity, 3.5 kDa MWCO; Thermo Fisher Scientific). The dialysis device started in a buffer of 10mM Tris-HCl (pH 7.5), 1 mM EDTA, 1 mM dithiothreitol (DTT), 2 M NaCl at 4 °C. At 1 h intervals, the device was placed in analogous buffers containing decreasing concentrations of NaCl (1.2 M, 1.0 M, 0.6 M, 0 M). The final dialysis in 0 M NaCl (R0

buffer) proceeded for 3 h before the reconstitution was filtered to remove precipitated species. Successful NCP formation and relative purity were confirmed using a 7% native PAGE (60:1 acrylamide: bisacrylamide; 0.25x TBE) that ran for 3 h at 160 V in 4°C to separate NCP and duplex species. Only NCPs containing ≤ 5% duplex were used in further studies. In the case of the NCPs containing the 5S sequence templates, the NCPs were heat-shifted (incubated in R0 buffer at 40°C for a minimum of 30 min) to a single translational species[34,35] before use in further experiments, unless otherwise specified.

4.3.6. Hydroxyl radical footprinting (HRF)

The HRF reaction was carried out using previously described conditions in order to establish relative solution accessibilities of nucleobase positions in NCPs.[26,36] Briefly, 7.5 µL of each 1 mM Fe(II)-EDTA, 10 mM sodium ascorbate, and 0.12% w/v aqueous hydrogen peroxide were gently combined per 5 pmol NCPs containing ^{32}P-end-labeled DNA in a total of 52.5 µL R0 buffer. The mixture incubated at room temperature for 10 min in the dark, and then the reaction was quenched with the addition of 16 µL 50 mM EDTA in 25% v/v glycerol. The quenched sample was immediately loaded on a 7% native PAGE (60:1 acrylamide: bisacrylamide; 0.25x TBE) and run for 3 h at 160 V in 4 °C to separate the NCP and duplex species. Gel bands containing the NCP species were incised, and NCPs were eluted into buffer (0.3 M NaOAC, 1 mM Tris-HCl [pH 8.0], 1 mM EDTA) between 16-20 h at 37 °C with gentle shaking. The reacted NCP eluent was concentrated using a centrifugal concentrator (Sartorius Vivaspin Turbo 15, 5 kDa MWCO) and filtered with a cellulose acetate membrane (Thermo Scientific). The sample was extracted twice using 25:24:1 phenol:chloroform:isoamyl alcohol (PCI; Sigma) to remove the proteins, and the resulting aqueous phase was concentrated by Speedvac evaporation. Following the addition of 40 µL co-precipitation agent (0.5 mg/mL tRNA in 300 mM sodium acetate [pH 8.0], 1 mM EDTA), samples were desalted with two ethanol precipitations. Cleavage

fragments were resolved after splitting the sample onto two denaturing PAGE (12% gel for 5'-end, 8% for 3'-end visualization) with accompanying Maxam Gilbert's (A+G) sequencing ladder for reference, and imaged by phosphorimagery. Relative strand cleavage at base positions were quantitated using SAFA gel analysis software.[37]

4.3.7. Processivity assays

Determination of processivity in duplex and NCP substrates was modeled after previously published protocols.[6,8,18] Briefly, radiolabeled U-containing substrate (either duplex or NCP) and glycosylase were prepared at 2x experimental concentration (final concentrations: 40 nM substrate, 200 pM UDG; substrate is in 200-fold excess) in reaction buffer. Reaction buffer for low-salt conditions was 10 mM NaCl, 20 mM Tris-HCl (pH 7.6), 10 mM EDTA, 200 mg/mL BSA, 1 mM DTT. Reactions that took place in high-salt conditions occurred in an analogous buffer containing 100 mM NaCl. Reactions containing a final concentration of 10 mM free uracil were prepared with 20 mM uracil in the substrate pot before mixing with UDG.

Following a temperature pre-equilibration at 37 °C for 2 min, equal volumes of substrate and UDG were mixed and incubated for varying amounts of time (0.5, 1, 2, 5, 10, 20, 30, 60 min, unless otherwise indicated) before quenching the reaction with the addition of 0.1 U UGI. Each time course included a quench control sample (QC) that was prepared by adding the UGI to the substrate before UDG addition and subsequently incubated at 37 °C for the duration of the longest timepoint. This control shows that the amount of UGI added is sufficient to prevent further chemistry and potentially a false-positive of processivity. For reactions exploring SMUG1 processivity activity in NCPs, samples were instead quenched with the addition of an equal volume of the final reaction worth of PCI for an immediate separation and extraction of protein. (SMUG1 cannot be quenched with UGI because the inhibitor is only specific for binding the UDG catalytic

site.[38]) SMUG1 samples were then ethanol-precipitated before the addition of APE1 and subsequent workup.

After quenching, all samples were subsequently treated with 18.5 nM APE1 (unless otherwise specified) for 1 h at 37 °C to cleave strands at the resulting abasic sites from UDG activity (APE1 reaction buffer: 20 mM NaCl, 20 mM Tris-HCl [pH 7.6], 200 mg/mL BSA, 1mM DTT, 10 mM $MgCl_2$). Proteins were then digested with the addition of 1/5 volume of 2.5% (v/v) SDS, 250 mM EDTA, and 2.5 mg/mL fresh proteinase K, incubated at 37 °C overnight. In some cases, protein extraction was performed using an equal volume of PCI and subsequent ethanol precipitation to further clean up samples.

Samples were then prepared for electrophoresis to separate substrate and product species. UUsame samples were prepared in formamide and water for electrophoresis on a 10% denaturing PAGE to separate substrate and product. UUopp samples were resuspended in water and split into two: half of the samples were prepared in formamide and water for electrophoresis on a 10% denaturing PAGE, and the other half of the samples were prepared in R0 buffer and 5% (v/v) glycerol for electrophoresis on a 10% native PAGE (60:1 acrylamide: bisacrylamide; 0.25x TBE) and run for 3.5 h at 150 V at room temperature. PAGE results were visualized by phosphorimagery (Bio-Rad Pharos FX). Preliminary observations of processivity capabilities was determined qualitatively by the relative amounts of processive product appearance.

4.4. Results

4.4.1. General approach for observing processivity

To observe processivity of a glycosylase, the substrate for study contains two lesion sites in such a way that relative amounts of chemistry acting on both sites in a single

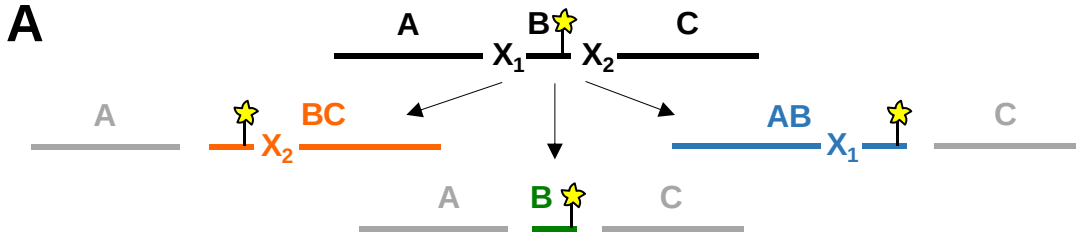

B

$$P_{proc} = \frac{[B]}{[B] + [AB] + [BC]}$$

Figure 4.2. Example of experimental substrate set-up and quantitation for observing processivity. (A) An experimental substrate with an internal radiolabel (star) present between two lesions, X_1 and X_2 for visualization of unique cleavage products. Cleavage at X_1 results in the visualization of product BC (orange). Cleavage at X_2 results in the visualization of AB (light blue). Products BC and AB are single-cleavage products. Cleavage at both lesions result in the visualization of double-cleavage product B (green). **(B)** Quantitation of processivity (P_{proc}) is a ratio of the amount of double-cleavage products to the amounts of all products observed.

enzyme-binding event can be determined (**Figure 4.2.**). Therefore, the substrate is designed so that one can distinguish between events when either one lesion is removed, the other lesion is removed, or both lesions are removed during a single binding event. As an example, **Figure 4.2.A** shows a length of DNA containing two lesions, X_1 and X_2, with an internal radiolabel for visualization of all chemistry events that may occur. Glycosylase activity alone at a lesion forms an abasic site. The addition of APE1 converts the abasic sites to strand cleavages to generate unique fragments. Here, cleavage at only site X_1 results in the visualization of product BC, cleavage at only site X_2 results in the visualization of product AB, and cleavage at both sites results in the visualization of product B. Products BC and AB are the result of single-cleavage events, when the glycosylase removes only one lesion in a binding event. Product B is the result of a double-cleavage event and is indicative of processivity taking place. The probability of

processivity, P_{proc}, is quantified using the ratio of the amounts of observed double-cleavage products relative to all cleavage products (**Figure 4.2.B**). The theoretical maximum of P_{proc} is a ratio of 1, which represents the scenario of a glycosylase always removing both lesions in a single binding event.

In these assays, it is imperative to use multiple turnover (MTO) conditions, where [UDG]<<[DNA], for correct interpretation of observing processivity.[6,39] By limiting amounts of UDG, the probability of two UDG binding the same DNA substrate to remove both lesions is reduced, and therefore limits the chance for a false-positive output of processivity. An additional safeguard against the observations of false-positive processive products is to track only the first 10-25% of total product accumulation.[6,40,41] The reasoning for this is to minimize the possibility of UDG's removing the second lesion from a single-cleavage intermediate.[40] For the described processivity studies below, the DNA substrate was in 200-fold excess over UDG.

Using a DNA substrate containing two uracil lesions, UDG processivity assays are initiated with the addition of UDG to DNA and incubated for various amounts of time before quenching. The reaction is quenched using an excess of uracil DNA glycosylase inhibitor (UGI), a small protein specific for strong binding to UDG's catalytic site. UGI competes with DNA for UDG binding to prevent further chemistry. Resulting abasic sites from UDG activity are enzymatically converted to strand breaks with the addition of APE1 to generate the unique fragments corresponding to both single- and double-cleavage events. The samples are then prepared for separation by PAGE, and quantified to determine P_{proc}.

The determination of P_{proc} alone explains the likelihood that the glycosylase will make it to the second lesion in a single binding event; it does not explain *how* the glycosylase got to the second lesion. P_{proc} is the sum of the probabilities of how the

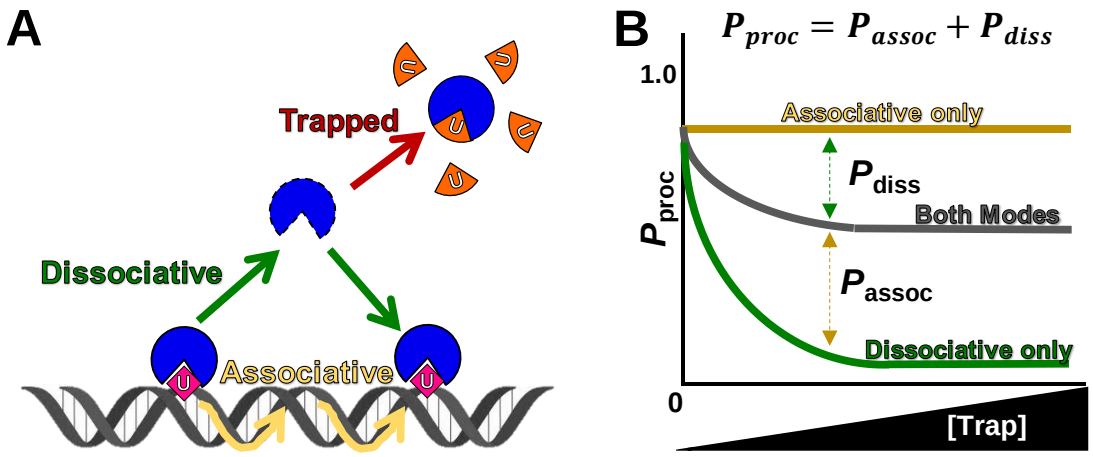

Figure 4.3. Processivity is the sum of contributions from associative and dissociative transfer. (A) Associative and dissociative transfer can be experimentally differentiated with the use of a trap that binds to the glycosylase active site to prevent double-cleavage of the DNA substrate. Only processivity due to associative transfer is visualized under trapping conditions. **(B)** The relative contributions of associative and dissociative transfer to processivity can be revealed with their respective dependencies on the amount of trap present in the experiment.

glycosylase makes it to the second lesion, with contributions from associative and dissociative transfer: $P_{proc} = P_{assoc} + P_{diss}$ (**Figure 4.3.**). Quantifying relative probabilities of each mode of transfer depends on the environmental conditions under which the processivity assay is observed. Under non-limiting low-salt (usually 10-20 mM monovalent ions) conditions, P_{proc} is maximal, and represents both associative and dissociative transfer contributions. Repeating the assay under specific environmental conditions can directly reveal the P_{assoc} contribution ($P_{proc} = P_{assoc}$) by preventing dissociative transfer. For instance, in the case of UDG, the addition of high concentrations of free uracil in the same low ion conditions will "trap" any dissociative UDG and prevent further chemistry on a second site (**Figure 4.3.A**).[18] Alternatively, the use of relatively higher ion concentrations (e.g. 100 mM) also reveals the associative population, since this mode has been shown to be more resistant to ion concentration compared with dissociative transfer.[4,8,18] P_{diss} is therefore the difference observed under non-limiting vs. limiting conditions (**Figure 4.3.B**).

Interestingly, the addition of molecular crowding agents, such as various lengths of polyethylene glycol (PEG) chains, have also been used to mimic the crowded nuclear environment to study processivity.[8,10] The presence of PEG has been shown to rescue UDG's ability for associative transfer in higher salt conditions by acting like a "macromolecular cage" surrounding the DNA and enzymes to promote associative transfer.

4.4.2. Designing and characterizing two-site DNA substrates for UDG processivity assays

Substrates employed in this study to examine UDG processivity in NCPs were designed using the synthetic 145 mer Widom 601 positioning sequence[42] as a template (**Schemes S.4.1.**, **S.4.2.**). This positioning sequence binds to the histone octamer core in a single, predictable manner to ensure the observation of processivity on a homogeneous NCP population, as seen as a single NCP species on a native PAGE (**Figure 4.4.**).[43] The 601 NCP also has a crystal structure available for reference.[44]

Two U lesions were placed either within the same strand of duplex, separated by 9 bp (UUsame; **Figure 4.5.A**,**B**) or on opposite strands with 4 bp in between (UUopp; **Figure 4.5.C**,**D**). U lesions were base paired with G to mimic spontaneous deamination of C. When the duplex are assembled into NCPs, the U lesions are located in the dyad region facing outward toward solution (**Figure 4.5.B,D**). High-solution accessibilities of

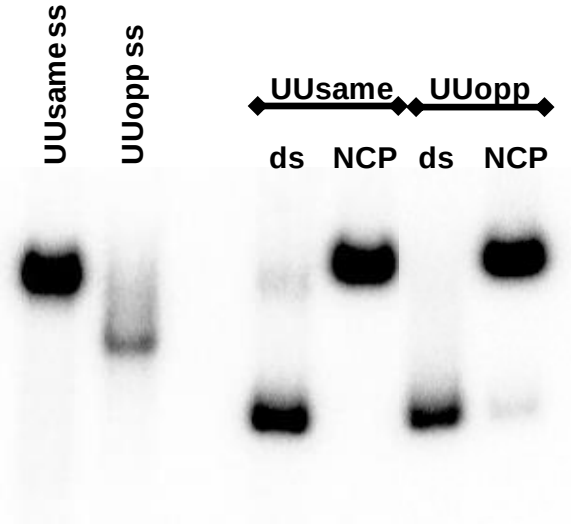

Figure 4.4. Representative native PAGE showing migration of 601 DNA substrates to study processivity. All duplex (ds) preparations used in studies contained <5% single-stranded (ss) DNA; NCP preparations used in studies contained ≤5% duplex.

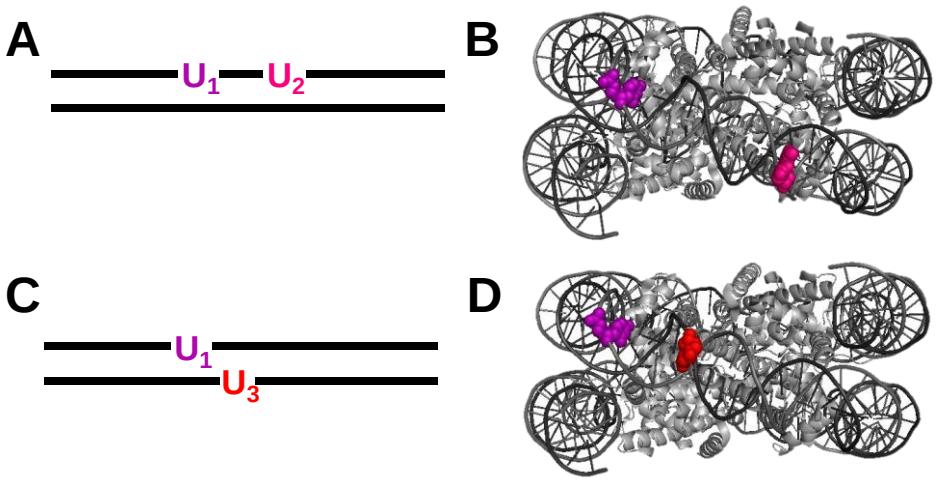

Figure 4.5. Experimental substrates to study processivity in 601 NCPs. Two U lesions located on the same strand to form UUsame **(A)** duplex and **(B)** NCPs. Two U lesions located on opposing strands to form UUopp **(C)** duplex and **(D)** NCPs. NCP images are straight-on views of the dyad region with the outward-facing lesions highlighted as bubble structures. NCP views created with PyMol (PDB 3lz0).

positioned lesions were confirmed by HRF (data not shown). The relatively close spacing of the lesions was chosen to increase the probability of seeing potential associative transfer in the system.[17,18] Such close spacing of U in DNA is observed *in vivo* during replication, with the misincorporation of U opposite A,[45] as well as during adaptive immunity, with activation-induced cytosine deaminase (AID)[46] or class switch recombination (CSH)[47] generating U/G base pairing.

UUsame DNA substrates are designed in such a way that an internal radiolabel is present between the two U lesions to directly visualize each single- and double-cleavage product of the processivity assay (**Figure 4.6.A**). Single-cleavage events in UUsame DNA substrates result in the visualization of either an 80 mer fragment when removal occurs at U_1, or a 74 mer fragment when removal occurs at U_2. Processive events result in the visualization of a 9mer fragment, due to the cleavage at both U_1 and U_2. Assembly of UUsame duplex and treatment with UDG and APE1 show expected product sizes and are

resolved on denaturing PAGE (**Figure 4.6.B**). P_{proc} is determined by taking the ratio of the amount of 9 mer product relative to all cleavage products.

Each strand of the UUopp DNA substrates is 5'-radiolabeled for visualization of single- and double-cleavage products of the processivity assay (**Figure 4.7.A**). In contrast to UUsame analysis, denaturing PAGE cannot differentiate between single- and double-cleavage products of UUopp. Single-cleavage events in UUopp DNA substrates result in the visualization of either a 64 mer fragment (removal at U_1), or a 75 mer fragment (removal at U_3). However, within a single UUopp duplex, cleavage at both sites result in the visualization of both the 64 mer and 75 mer products (**Figure 4.7.B**). Since there is a population of individual DNA substrates observed during the processivity assay, cleavage at site U_1 in one substrate and cleavage at site U_2 in another substrate will appear as if a processive, double-cleavage event has occurred in a single substrate by denaturing PAGE alone. Because a processive, double-cleavage event results in a double-strand break, we may visualize the two halves of the duplex ("L" and "R") on native PAGE (**Figure 4.7.C**). Using native PAGE, "L" and "R" are

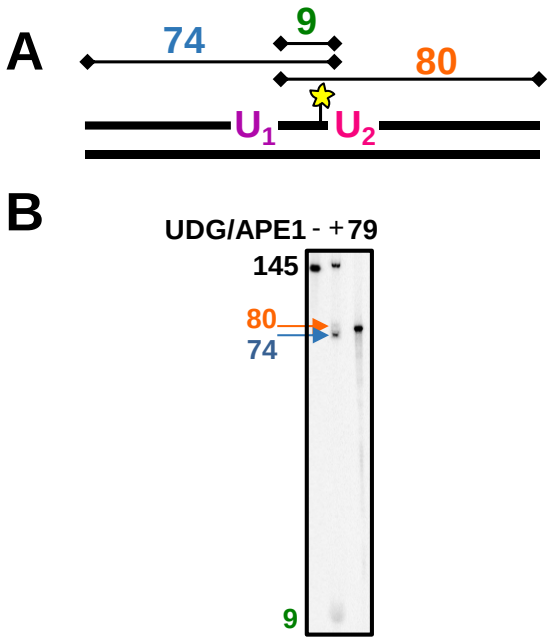

Figure 4.6. 601 UUsame substrate design for unique cleavage product distinctions. (A) Schematic design of duplex containing an internal radiolabel (star) for visualization of potential cleavage products between U_1 and U_2. Single cleavage at U_1 results in the visualization of an 80 mer product; single cleavage at U_2 results in the visualization of a 74 mer product; double-cleavage results in the visualization of a 9 mer product. **(B)** The different cleavage products of the UUsame duplex are resolved on a 10% denaturing PAGE and migrate as expected (+ lane). The 79 lane shows the migration of a 79 mer ssDNA control.

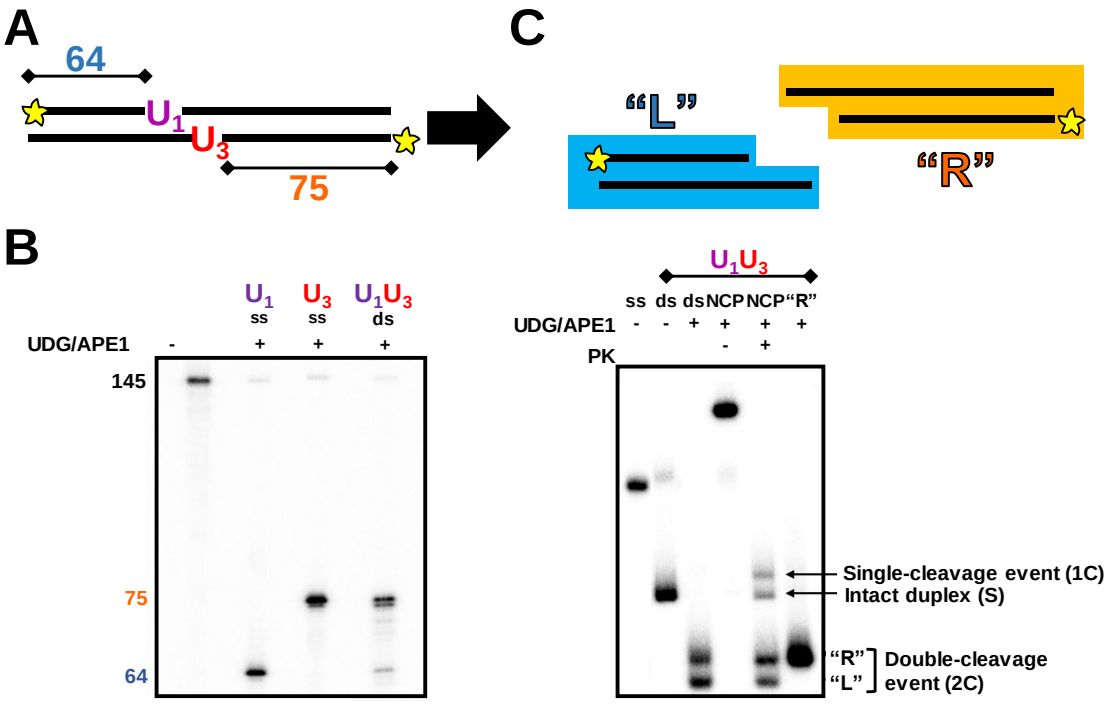

Figure 4.7. 601 UUopp substrate design for unique cleavage product distinctions. (A) Schematic design of duplex containing 5'-radiolabels on each strand (stars) for visualization of potential cleavage products between U_1 and U_3. Single cleavage at U_1 results in the visualization of a 64 mer product; single cleavage at U_3 results in the visualization of a 74 mer product; double-cleavage results in the visualization of both the 64 mer and the 74 mer products. **(B)** The different cleavage products of the UUsame duplex are resolved on a 10% denaturing PAGE and migrate as expected (U_1U_3 ds + lane). **(C)** Double-cleavage within the UUopp DNA substrate is observed when a double-strand break occurs, separating the duplex into two halves, "L" and "R", which may be resolved on native PAGE. Different species were resolved on native PAGE to distinguish between single- and double-cleavage products in UUopp DNA substrates. PK represents the presence of fresh proteinase K for degradation of histone proteins present in the NCP samples observed. "R" migration was confirmed by radiolabeling only the U_3-containing 145mer before duplex formation and UDG/APE1 treatment.

differentiated from single-cleavage products and unreacted substrate. In UUopp substrates, P_{proc} is determined by taking the ratio of the amount of one of the double-cleavage products ("R" *or* "L", since they accumulate in the same manner) relative to all cleavage products.

We tested the reactivities of the U lesions in the NCP context to determine if they were equally competent for chemistry. We added a 30-fold excess of UDG to intentionally saturate the two-site NCP substrates (i.e. two UDG simultaneously bind to the same NCP for chemistry) to determine the relative rates of U removal at each site separately. Any observed difference between rates of the appearance of the single-cleavage products would reveal differences in UDG cleavage due to local sequence or histone context, and may result in a preference for removing one lesion over another. Additionally, this characterization must show that each lesion can be completely converted to product. Any observation of inactivity at a site in the processivity assays will not be attributed to UDG's inability to bind and perform chemistry, but rather to its lack of processivity in the NCP substrate. Indeed, a 30-fold excess of total UDG over NCP substrates after 60 min incubation showed that both the UUsame NCPs (**Figure 4.8.A**) and UUopp NCPs (**Figure 4.8.B**) were ~95% converted from substrate to their respective double-cleavage products. Therefore, ~5% of the U lesions in NCPs are refractory to UDG activity under these conditions. In the UUopp NCP, the appearance of each single-cleavage product had similar rates, namely 0.75 min^{-1} (75 mer) and 0.60 min^{-1} (64 mer) for one trial (**Figure 4.8.C**), suggesting that the sites are comparable for chemistry. Analogous rate determinations are not available at present because the experiment needs to be repeated with faster timepoints. Qualitatively, the rates of product accumulation for the 80 mer and 74 mer products appear similar (**Figure 4.8.A**).

4.4.3. Qualitative observations of processivity in two-site NCP substrates

Initial studies with NCPs showed very little product overall with the 200-fold excess of substrate over UDG in the course of 1 h, and a delayed appearance of the processive product until later timepoints. This observation was unlike previous studies in duplex,

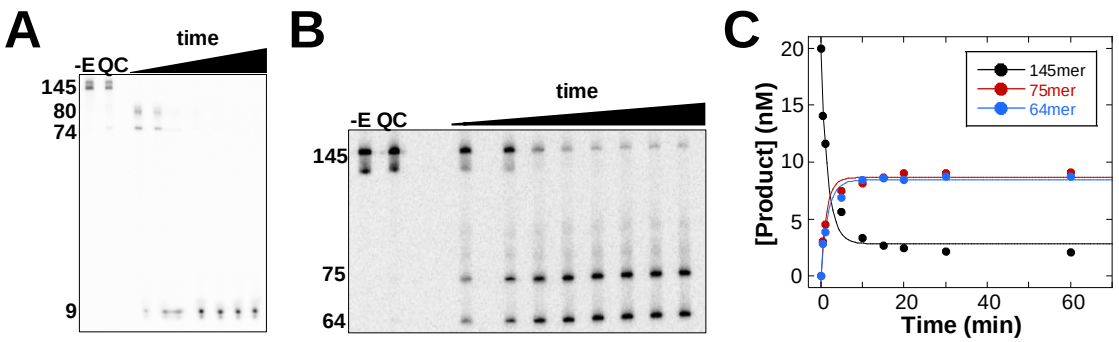

Figure 4.8. Processivity 601 NCPs under saturating UDG conditions shows competency for chemistry. Processivity NCPs **(A)** UUsame and **(B)** UUopp were treated with a 30-fold excess of UDG over the course of 1 h. Complete excision at both lesion positions in the UUsame substrate is indicated by the disappearance of the 145 mer substrate and the sole appearance of the 9 mer by the end of the time course. Conversely, complete excision at both lesion sites in the UUopp substrate is indicated by the disappearance of the 145 mer substrate and the accumulation of the 75 mer and 64 mer products. In both cases, ~5% of each substrate (145 mer) was not converted to product. **(C)** Rates of single-product accumulation in UUopp shown in panel B were determined comparable to each other using single exponential models.

where a processive product was formed at a faster rate than either single-cleavage product.[6,40,41] The more complicated NCP substrate presents additional challenges for initial UDG binding[48] that likely compound its influence by slowing the rates of processivity as well. Indeed the observed rate (k_{obs}) for a similar outward-facing site in the dyad, is about 6x slower in the NCP than in the 145 mer duplex.[26] Due to all these complicating factors whereby the NCP environment slows down observed UDG activity, the delayed appearance of the processive product may not necessarily be a result of further cleavage of single-cleavage intermediates, and still indicate processivity. Therefore, instead of choosing an arbitrarily higher cutoff of reaction observation, we simply set out to qualitatively observe the binary presence or non-presence of the processive product over the course of 1 h for these preliminary NCP studies. We ultimately assumed that the combination of a 200-fold excess of NCP over total UDG, and potentially slower binding rates on NCPs, might be sufficient to minimize the appearance of false-positive processive

products. Alternatively, it may not be at all possible to quantitatively measure the amounts of processivity in an NCP substrate under these current conditions, but could be optimized in the future.

4.4.4. Processivity studies in UUsame DNA substrates

We first conducted processivity assays in UUsame duplex to serve as controls for observations seen in NCPs. We explored the maximal amounts of processivity due to both associative and dissociative modes by looking for the appearance of 9 mer processive product under low-salt conditions (**Figure 4.9.A**). Indeed, there was an accumulation of processive product at a relatively fast rate, starting around 1 min. When the uracil trap was added to the transfer assay (**Figure 4.9.B**), the appearance of the processive product was delayed to around 10 min, and therefore did not accumulate as much by 60 min. Under high-salt conditions (**Figure 4.9.C**), the rate and amount of processive product looked like the uracil-trap results. Generally, the appearance of the 80 mer cleavage product (i.e. cleavage at the U_1 lesion shown in **Figure 4.5.A**) appeared first, followed by the 74 mer cleavage product, and ultimately the processive product. Qualitatively, the rate of the accumulation of each single-cleavage product was consistent across environmental conditions observed, with a slight overall decrease in the amounts of the 74 mer product in the uracil-trap condition.

We next assembled UUsame NCPs to observe how the presence of the histone octamer would affect processivity along the same DNA strand. If associative transfer were to take place, the processive product would accumulate in the presence of the uracil trap or high-salt conditions. This observation of associative transfer in the UUsame NCP ensemble might suggest that UDG is able to track along the phosphate backbone by switching between the phosphate backbones of the two strands to avoid the steric clash

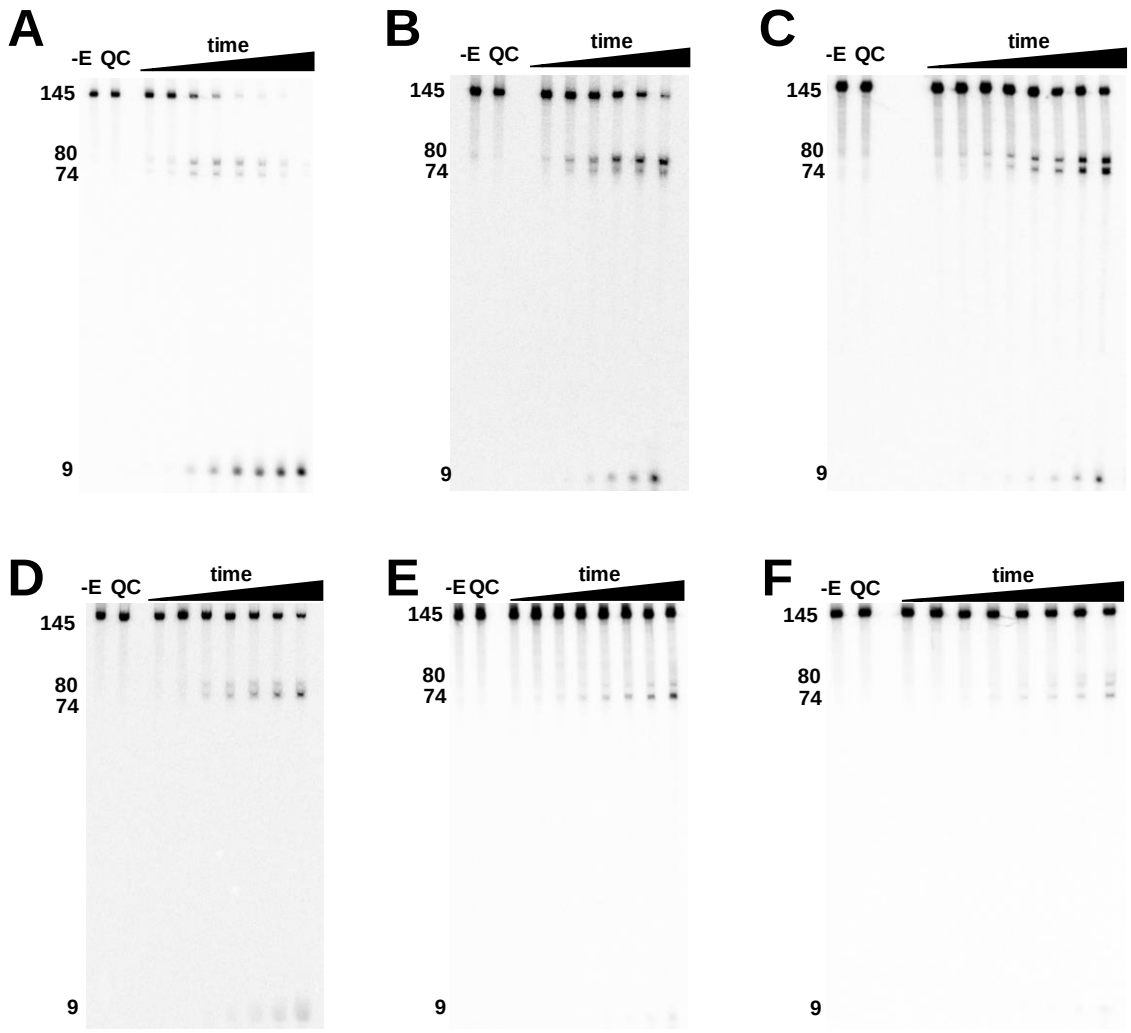

Figure 4.9. Qualitative observations of processivity in 601 UUsame DNA substrates. Denaturing PAGE showing processivity assays conducted under varying environmental conditions in 601 UUsame **(A, B, C)** duplex and **(D, E, F)** NCPs. Single-cleavage products are indicated by the 80 mer and 74 mer, and the processive product is indicated by the 9 mer. DNA substrate was in 200-fold excess over UDG and the reaction was observed over 1 h. **(A, D)** Low-salt conditions were used to show total amounts of processivity possible. The addition of **(B, E)** uracil or **(C, F)** high-salt conditions directly show contributions to processivity by associative transfer.

of the histone octamer. The transfer assay was first conducted under low-salt conditions to establish the maximal potential of the accumulation of processive product in the NCP (**Figure 4.9.D**). Compared with duplex in the same conditions (**Figure 4.9.A**), there was less processive product and a delay in its accumulation appearing around 10 min. The

addition of the uracil trap essentially prevented the formation of the processive product (**Figure 4.9.E**). A similar effect was seen in the high-salt conditions, as well as an additional observation of fewer single-cleavage products (**Figure 4.9.F**). Besides the minimal amounts of processive product overall in each NCP transfer assay observed, the pattern of the single-cleavage products changed when the DNA was incorporated into NCPs. In contrast to duplex, the overall intensity and rate of accumulation of the 80 mer cleavage product was much lower in each environmental condition tested (compare **Figures 4.9.D-F** with **Figures 4.9.A-C**).

4.4.5. Processivity studies in UUopp substrates

Next, we performed processivity assays on UUopp DNA substrates. We first focused on UUopp duplex and established the maximal amount of total processive product possible from both modes of transfer in low-salt conditions (**Figure 4.10.A**). The appearance of the processive product occurred around 5 min and made up about 45% of the products by 1 h. With the addition of the uracil trap, there were minimal amounts of processive product seen in the UUopp duplex (**Figure 4.10.B**). Similarly, the high-salt conditions did not show appreciable amounts of processive product (**Figure 4.10.C**). Comparing the different environmental conditions across the UUopp duplex, the addition of the uracil and increased salt also resulted in less accumulation of the single-cleavage products compared with the low-salt conditions.

Then, we assembled UUopp NCPs in order to study the effects of the histone octamer on UDG processivity when U lesions are located on opposite DNA strands. Processive product accumulation in the UUopp NCP would indicate that UDG is able to make micro-dissociations which could track along the phosphate backbone of one strand, switch strands, and then reorient before cleavage takes place at the second U without

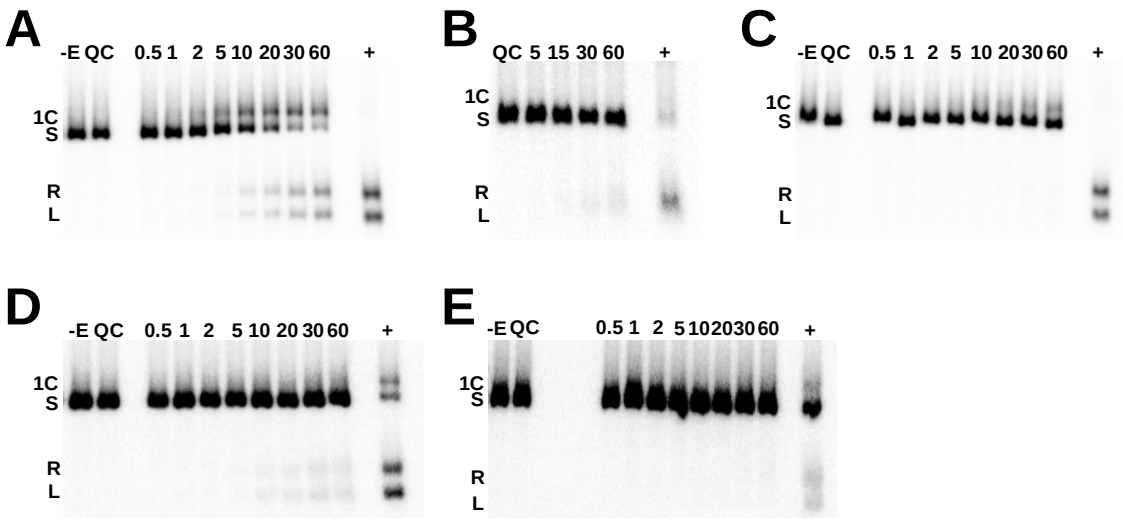

Figure 4.10. Qualitative observations of processivity in 601 UUopp DNA substrates. Native PAGE showing processivity assays conducted under varying environmental conditions in 601 UUopp duplex **(A, B, C)** and NCPs **(D, E)**. Single-cleavage products are indicated by the 1C product migration, and the processive product is indicated by the accumulation of the R and L products. DNA substrate was in 200-fold excess over UDG and the reaction was observed over 1 h. **(A, D)** Low-salt conditions were used to show total amounts of processivity possible. The addition of **(B, E)** uracil or **(C)** high-salt conditions directly show contributions to processivity by associative transfer.

being trapped by free uracil or high salt. We performed the transfer assay under low-salt conditions to observe the maximal processivity in the UUopp NCP ensemble (**Figure 4.10.D**). Compared with the UUopp duplex (**Figure 4.10.A**), there was a decrease in overall processive product appearing at around the same point during the time course. However, when the uracil trap was added to the assay, there was no appearance of processive product during 1 h experimental duration (**Figure 4.10.E**).

4.5. Discussion

4.5.1. Two-site duplex substrates implement both associative and dissociative transfers

As seen in previous processivity assays using UDG and duplex,[18,20] the 145 mer duplex substrates here showed processivity by both associative and dissociative transfer.

The addition of either free uracil or high salt conditions to the assay still allowed for processive product formation, indicating associative transfer. The difference in the amount of processive product seen in the low-salt conditions and the inhibitive conditions is P_{diss}. Qualitatively, P_{assoc} and P_{diss} may be more equal to P_{proc} in UUsame duplex (compare **Figures 4.9.A** and **4.9.B**), while P_{diss} comprises the majority in UUopp duplex (compare **Figures 4.10.A** and **4.10.B**). This observation of UUsame duplex qualitatively showing more associative transfer than the UUopp duplex is consistent with previous studies (directly compare **Figures 4.9.B** with **4.10.B**).[17,18]

An interesting discrepancy between the two duplex designs was the relative amounts of processive product observed in the associative transfer population. For the UUsame duplex, in both the free uracil and high-salt conditions, there were comparable amounts and rates of the processive product (compare **Figures 4.9.B** and **4.9.C**). In contrast, the UUopp duplex had different amounts of processive product: very little (but still observable) processive product in the free uracil assay, and absolutely no processive product generated in the high-salt conditions (compare **Figures 4.10.B** and **4.10.C**). This may suggest that UDG initially binding to the UUopp duplex was influenced negatively by the high-salt conditions.

4.5.2. NCP structure prevents associative transfer of UDG

Overall, the two-site NCP substrates allowed for minimal processivity compared with analogous duplex substrates (**Table 4.1.**). The decreased amounts of processive product from duplex to NCP substrates were likely due to the presence of the histone octamer's affecting UDG processivity. However, the biggest impact of the DNA packaging into NCPs was observed when the assays were conducted in the presence of the uracil trap or high-salt concentrations. Favoring associative transfer under these conditions,

	UUsame		UUopp	
	Free duplex	NCP	Free duplex	NCP
Low salt	✓✓✓	✓	✓✓	✓
Low salt + U trap	✓	0	0	0
High salt	✓✓	0	0	n/a

Table 4.1. Qualitative summary of amounts of processivity seen in 601 DNA substrates. The amount of processivity in each DNA substrate is indicated by the number of check marks (✓), with ✓ indicating some, ✓✓✓ and indicating the most. DNA substrates that did not have any processive product accumulation are indicated with a zero (0). Data that was not collected is indicated with n/a.

there were minimal amounts of processive product seen in both UUsame and UUopp NCPs. A lack of associative transfer indicates that dissociative transfer is the main mode of processivity in these two-site NCPs when observed under low-salt conditions. This result is not entirely surprising since the packaging of DNA into the NCP presents more steric and electrostatic obstacles for UDG's searching and binding. Alternatively, seeing associative transfer in NCPs would have suggested that the organization of the packaged DNA allowed for a more favorable conformation for similar or better processivity compared with the less-structured duplex.

Changes in the processivity due to the incorporation of duplex into NCPs were also manifested in the overall lower accumulation of the 80 mer single-cleavage product observed in the UUsame NCP time course (compare **Figure 4.9.A** with **4.9.D**). This decrease in the 80 mer product may be due to the proximity of the U_1 site to the start of the second superhelix, i.e. near the terminal DNA wrapping. As a result, UDG is favoring directionality to generate the processive product by binding and cleaving at U_2 before transfer to U_1 for cleavage.

4.5.3. Putting processivity assay observations in a biological context

As discussed, we saw a decrease in UDG processivity on two different two-site NCP substrates compared with duplex analogs. These observations from this controlled *in vitro* system of packaged DNA suggest that UDG's dominant transfer mode *in vivo* is purely dissociative. Alternatively, these results may suggest the need for additional events to take place *in vivo* for efficient one-dimensional searching for BER initiation. The observation of a purely dissociative mode of processivity in NCPs is counterintuitive to the hypothesis arguing for a combination of both modes for most efficient searching in the genome. However, the observation of both processivity modes in duplex assays may suggest that UDG associative transfer is exclusively utilized during times of open, fully accessible chromatin, while dissociative transfer is constant throughout the cell cycle. This hypothesis would support UDG's important role during S-phase, of quickly removing mis-incorporated U across A.[24,45] Alternatively, the lack of UDG processivity in NCPs could suggest another potential method for quickly removing U lesions in packaged DNA by relying on high copy numbers of the glycosylase and therefore multiple UDG binding within the same NCP.

These *in vitro* experiments are important for understanding all aspects of the initiation of BER, since the first step of BER takes place before any chemistry can be accomplished. Indeed, damage cannot be repaired unless it is first found. Due to the complexities of the nuclear and DNA packaging environments, there is a possibility that the real limiting factor of BER in a chromatin environment may be the search for lesions in a sea of undamaged DNA. In fact, a previous study using AAG knockout cells, which were then complemented with different AAG mutants specific for decreasing processivity, and found that the cells had decreased survival.[49] The study also shows the importance of glycosylase processivity to the initiation of BER and, therefore, cell survival. Once the damage is found by the glycosylase for BER initiation, it is potentially more obvious for

intermediates to be recognized and processed further by the downstream enzymes using coordination and substrate channeling.[50]

4.6. Future Directions

4.6.1. Expand upon processivity observations in the two-site NCP system

More data is necessary to satisfactorily characterize UDG processivity in two-site NCP substrates than the above-described experiments. The current experiments are incomplete and show general, qualitative observations of processivity in packaged DNA substrates. More replicates of each substrate under various conditions are desired for showing consistency in the preliminary observations described. Exploring how additional environmental factors in this NCP system influence processivity, will help inform behavior in the nuclear environment. Specifically of interest is the exploration of the addition of the inert crowding agent of PEG chains. The crowding agent would further mimic nuclear conditions of mass volume in conjunction with the high-salt conditions. Previous studies have shown that the addition of non-specific "bulk" to the experiments have rescued associative transfer in duplex systems under high-salt conditions by acting like a "macromolecular cage,"[10] and may similarly rescue processivity in NCPs.

Besides expanding upon the qualitative observations of processivity in NCP substrates, we would ultimately want to quantify P_{assoc} and P_{diss} in the NCP assays. As mentioned above, this may not be feasible in the complicated binding landscape of the NCP. However, the two-site NCP processivity system could be modified and optimized for quantitation. One potential way to encourage more processivity in the NCP system would be to relieve the MTO conditions; instead of using a 200-fold excess of NCP substrate over enzyme as in previous duplex studies, it may be more practical to have only a 10- to 20-fold excess of NCP substrate. More studies would have to be conducted varying MTO

conditions to determine the possibility and optimization for quantitative determinations of processivity in NCPs.

4.6.2. Observing processivity in NCPs using the natural 5S positioning sequence

Another goal of studying processivity in NCP substrates was to compare the effects of varying DNA-histone dynamics, using different nucleosome positioning sequence templates. Preliminary studies were conducted using a "looser", naturally-occurring positioning sequence known as the 5S rDNA positioning sequence (**Schemes S.4.3.** and **S.4.4.**).[27,51,52] There is no crystal structure for the 5S sequence in NCPs due to its dynamics and its ability to adopt multiple translational positions by multiples of 10 bp.[53,54] With a minimum duplex of 146 bp, the NCPs form two translational species, but incubation of the NCPs at an elevated temperature allows the DNA to "heat-shift" to a single, thermodynamically favorable translational position (**Figure 4.11**).[35] Relative solution accessibility was determined in 5S NCPs using HRF to inform placement of U lesions (**Figure 4.12.A**,**B**). In addition, we characterized the relative solution accessibilities of the two translational positionings of the NCP before (non-heat-shifted, NHS) and after (heat-shifting, HS) incubation, and verified that the relative rotational, or solution accessibilities at each observed site, were consistent between the

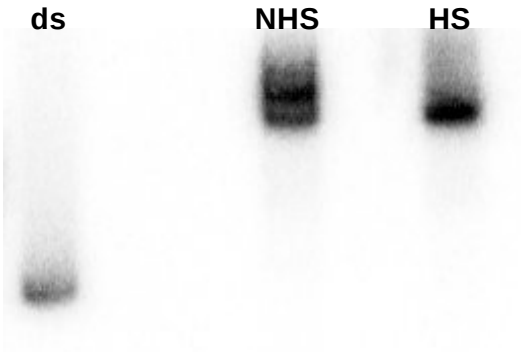

Figure 4.11. Representative native PAGE showing relative migration of 5S duplex and NCP species. The 5S NCPs exist as two translational species, shown as two distinct bands, immediately after reconstitution (non-heat-shifted, NHS lane). Incubation at 40 °C for at least 30 min shifts (heat-shift, HS lane) the NCPs into a single translational species, shown as a single band. All duplex (ds) preparations used in studies contained <5% single-stranded (ss) DNA; NCP preparations used in studies contained ≤5% duplex.

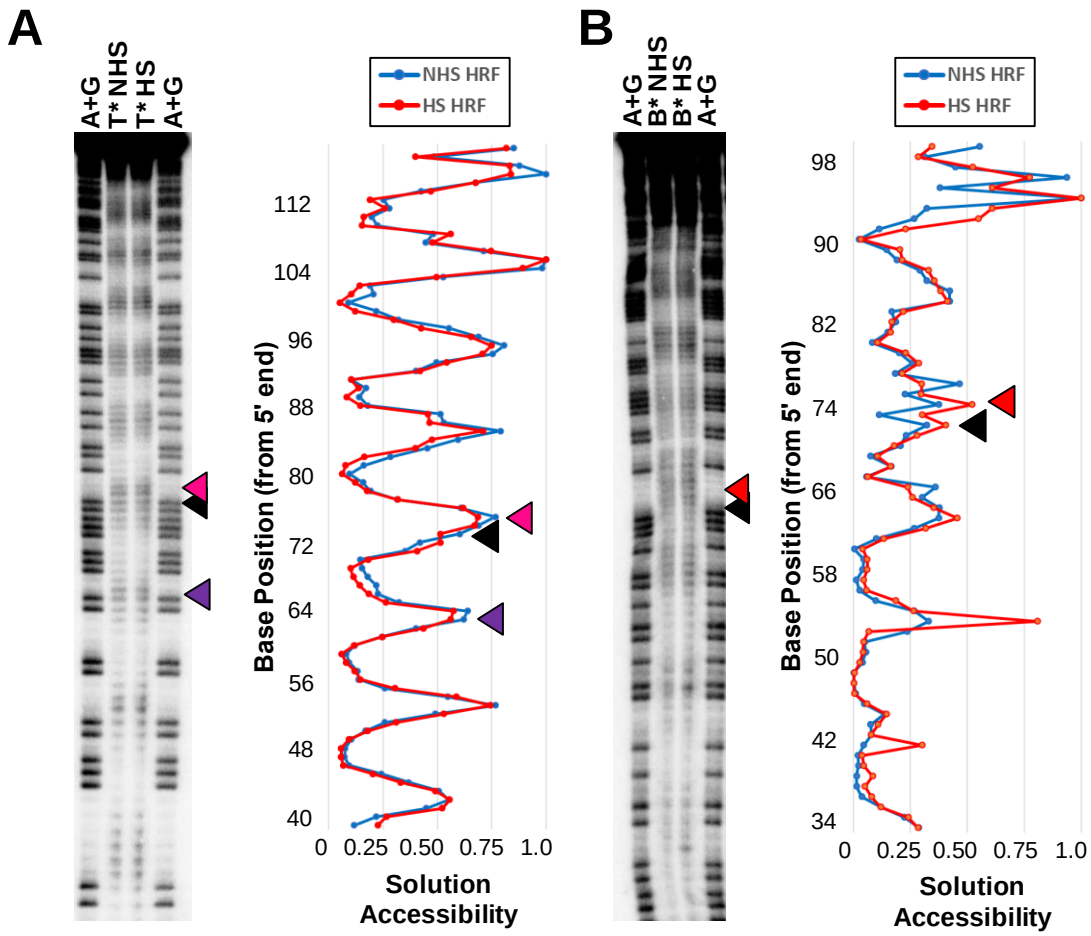

Figure 4.12. Hydroxyl radical characterization of 5S NCPs for designing processivity substrates. Hydroxyl radical footprinting of 5S NCPs with the radiolabel located on the **(A)** T strand and **(B)** B strand characterized relative solution accessibilities of the NCP species. A+G lanes display a ladder of the undamaged 5S DNA sequence created using Maxam Gilbert reactions. HRF reactions performed on non-heat-shifted (NHS) and heat-shifted (HS) NCPs in the lanes indicated. Cleavage patterns were quantified using SAFA to create associated profiles for the NHS (blue lines) and HS (red lines) 5S NCP species. The U1 position is indicated by purple triangles, the U2 position is indicated by pink triangles, the U3 position is indicated by red triangles, and the dyad position is indicated by the black triangle.

two preparations. Once the solution accessibility of the nucleobases in the dyad region of undamaged 5S NCPs was determined by HRF, two U lesions were placed in high solution-accessible sites that were analogous to the 601 NCP substrate designs (**Figure 4.13.A**,**B**). Preliminary studies focused on 5S UUsame duplex and NCPs to observe qualitative levels

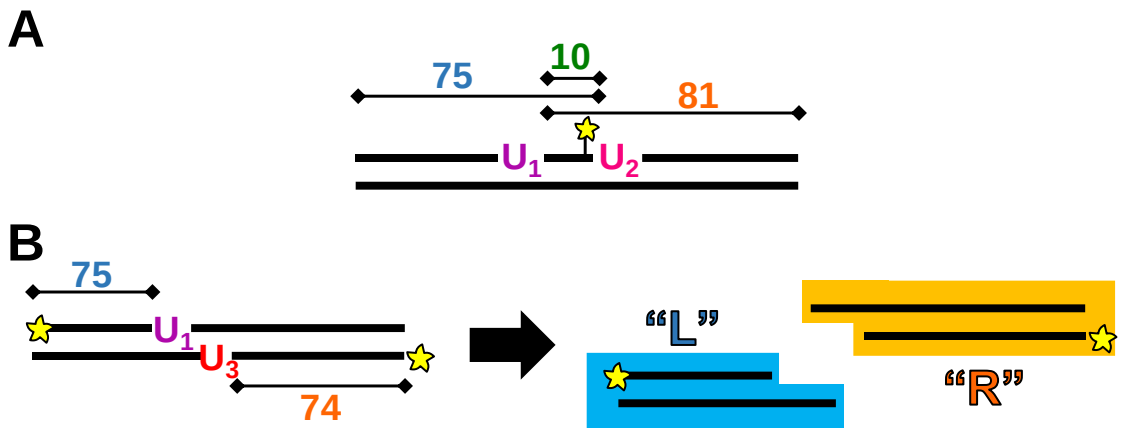

Figure 4.13. 5S processivity substrate design for unique cleavage product distinctions. (A) UUsame and **(B)** UUopp DNA substrates for 5S DNA substrates were similar to the 601 DNA substrate designs.

of processivity in NCPs with more DNA-histone dynamics (**Figure 4.14.**). Before use in transfer assays, all 5S NCPs were heat-shifted to a single translational species to ensure consistency in translational positioning. Similar to the 601 UUsame duplex, the 5S UUsame 10 mer processive product was seen relatively early in the time course, around 10-15 min (**Figure 4.14.A**). However, the addition of the free uracil trap and the high-salt conditions seems to completely inhibit the processive characteristics of UDG in the 5S UUsame duplex (**Figure 4.14.B,C**). This result was unlike that of the 601 UUsame duplex, which had shown some processive product (compare **Figure 4.14.B,C** with **Figure 4.9.B,C**). This may suggest that the 5S UUsame duplex is not as amenable to associative transfer of UDG as is the 601 UUsame duplex. Next, the 5S UUsame duplex was incorporated into NCPs and assayed for transfer under low-salt conditions (**Figure 4.14.D**). The 5S UUsame NCPs amassed a smaller amount of processive product accumulation relative to the duplex, as was seen in the 601 UUsame DNA substrates

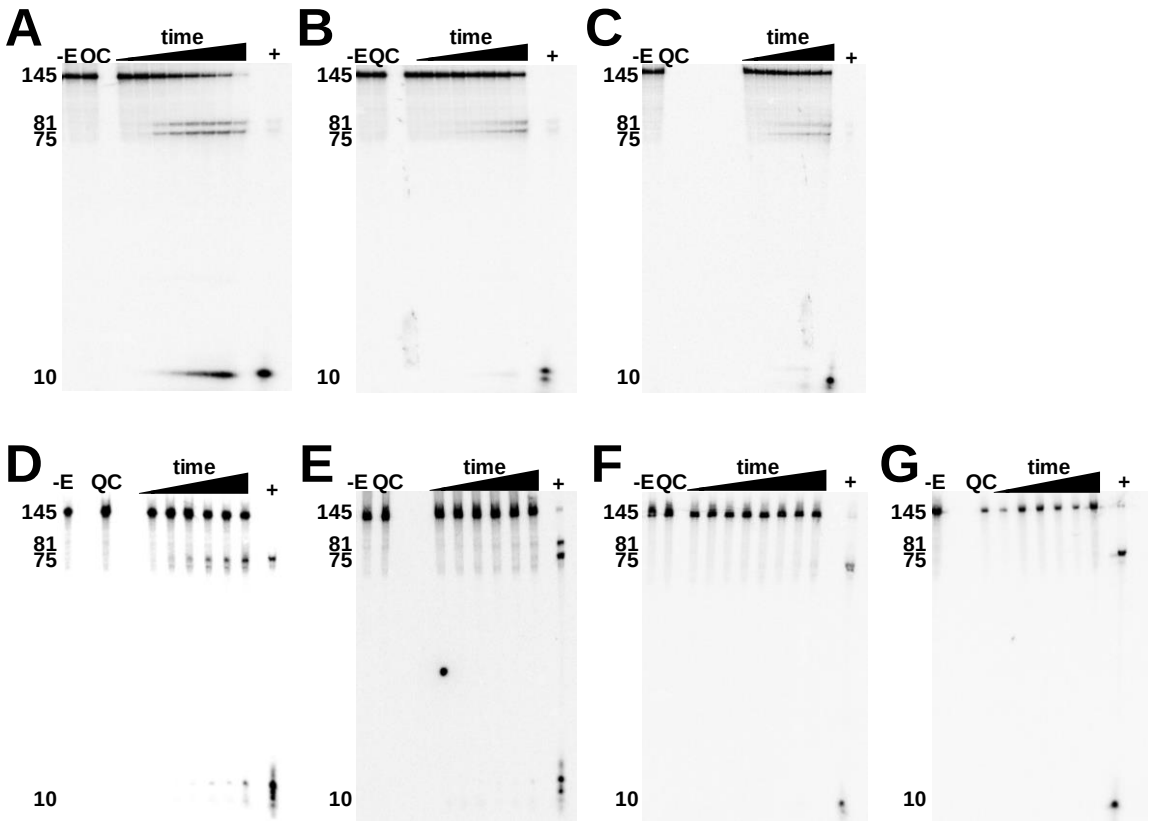

Figure 4.14. Qualitative observations of processivity in 5S UUsame DNA substrates. Denaturing PAGE showing processivity assays conducted under varying environmental conditions in 5S UUsame duplex **(A, B, C)** and NCPs **(D, E, F, G)**. Single-cleavage products are indicated by 81 mer and 75 mer, and the processive product is indicated by the 10 mer. DNA substrate was in 200-fold excess over UDG and the reaction was observed over 1 h. Low-salt conditions **(A, D)** were used to show total amounts of processivity possible. The addition of uracil **(B, E)** or high-salt conditions **(C, F)** directly show contributions to processivity by associative transfer. The addition of 20% PEG6000 to the high-salt conditions was examined to observe possible rescue of associative transfer in NCPs due to the presence of the inert crowding agent.

(**Figure 4.9.A,D**). Additionally, the accumulation of processive product in low-salt conditions for the 5S UUsame NCPs was relatively lower compared with the 601 UUsame NCPs (compare **Figure 4.14.D** with **Figure 4.9.D**). The utilization of the uracil trap and high-salt conditions in the assays with the 5S UUsame NCPs also completely eliminated any processive product accumulation over the time course (**Figure 4.14.E,F**). Further, there were minimal single-cleavage products observed, which may suggest that these

environmental conditions inhibited initial UDG binding to the NCP, completely preventing any chemistry from occurring. We also tested the effects of crowding agents on processivity in the 5S UUsame NCPs, adding 20% (w/v) PEG6000 to the high-salt conditions (**Figure 4.14.G**). Previous studies with duplex substrates showed that the addition of PEG counteracted the dissociative-inducing characteristics of the high-salt to encourage more associative transfer.[8] Here, any rescue of associative behavior of UDG was not observed in this assay, since there was neither processive product nor single-cleavage product.

Indeed, the results from these initial studies using 5S UUsame DNA substrates were somewhat unexpected. Preliminary analysis based on these few transfer experiments suggests that the 5S UUsame NCPs were less conducive to UDG processivity than in the more strongly-bound 601 NCPs. Additional replications of observations would benefit a higher degree of confidence in analysis and conclusions. Performing complementary transfer studies with the 5S UUopp duplex and NCPs will provide a complete dataset to compare how relative levels of DNA-histone interactions can influence the processivity of UDG in NCPs, compared with the strong-binding of the 601 system.

4.6.3. Variation of two-site substrate design on processivity in NCPs

Each individual nucleobase in an NCP has a different microenvironment of DNA-histone interactions that could influence glycosylase binding and chemistry differently compared with another position. In particular, the DNA within the dyad region is known to be less dynamic and somewhat inhibitory to glycosylase activity compared with other regions in the NCP.[55–57] Changing the translational positioning, or the location of the two U lesions from their positions on the dyad, will further elucidate how larger structural features of the DNA wrapping in NCPs can influence glycosylase processivity. Specifically,

placing the lesions outside of the dyad region involves the stacking superhelices' wrapping around the histone core (refer to **Figure 4.5.B,D** for on-dyad views of the NCP). The stacked DNA duplex provides another level of accessibility that is not present in the dyad region, where there is only one duplex wrapping around the histone core. The presence of the additional superhelix may affect how glycosylases approach and navigate the DNA thereby affecting their processivity. Alternatively, the increased dynamics toward the DNA ends[58,59] may facilitate processivity despite the presence of the superhelices.

In addition to moving the two lesions from the dyad region, the position of the lesions may be changed by varying the helical orientation of the nucleobases relative to the histone core. Despite the regional locations of the lesions, UDG overall shows less activity when lesions are facing inward toward the histone octamer core.[24,26,31,60] Although it would be possible to utilize this two-site NCP transfer system with inward-facing lesions, it may not be as informative since the preliminary studies shown above using highly solution-accessible lesions show minimal processive product; less-accessible sites will cause a further decrease in activity.

4.6.4. Observing processivity of other glycosylases in NCPs

Besides looking at UDG processivity in the two-site NCP substrates, a preliminary processivity assay was performed in NCPs using another human glycosylase that removes U lesions: the single-strand-selective monofunctional uracil-DNA glycosylase 1 (SMUG1). SMUG1 was of interest for processivity studies in NCPs because unlike UDG, which is upregulated during S-phase, SMUG1 is not cell cycle-regulated and is constantly present at low levels.[45,61] Therefore, we hypothesized SMUG1 to be more amenable to repair in an NCP due to its role as the "backup" U-seeking glycosylase. We performed a processivity assay in NCPs under low-salt conditions and saw neither single-cleavage nor processive products during the time course (data not shown). The addition of APE1, which

has been shown to stimulate glycosylase activity,[62–65] was supplemented in the assay to test if processivity would be enhanced. However, it did not show improvement throughout the time course (data not shown). These preliminary transfer assays, as well as a recent study in NCPs,[66] suggest that SMUG1 may not be a competent glycosylase for initiating repair in the NCP.

As mentioned, previous transfer studies have explored the processivity of other glycosylases such as AAG and hOGG1 in two-site duplex substrates. Of particular interest for study in NCPs is AAG because it has a stronger overall proclivity for dissociative transfer due to its ability to navigate both difficult DNA structures (i.e. bubbles, gaps, bent structures)[16] and protein roadblocks.[14] These processivity characteristics of AAG seen in modified duplex systems may translate to more successful searching in an NCP context. Building upon duplex processivity studies with the two-site NCPs using different glycosylases will allow for a more complete understanding of which lesions are more likely to be repaired in the context of the chromatin environment. Comparisons of the structural features representative of different glycosylase families[67] and their relative abilities for processivity in NCPs, might help to better understand the structure-function relationships between glycosylases and genomic DNA.

4.6.5. Processivity of glycosylases with the addition of other protein factors

The above studies utilize the *E. coli* UDG and not the human uracil DNA glycosylase nuclear isoform (hUNG2). We used *E. coli* UDG in our studies above because the catalytic domain is 57% identical to the human version, is commercially available, and is generally accepted for use as a replacement in the literature.[24] However, future studies would benefit by instead using the full-length hUNG2 for better biological significances of *in vitro* observations. Previous work with duplex processivity studies has shown that the retention of the unstructured N-terminal tails of hUNG2 and AAG has increased overall

processivity.[6,19,20] It is hypothesized that the N-terminal tails assist in processivity by tethering to the DNA and increasing the probability for the catalytic domain of the glycosylase to rebind and perform chemistry at the second site.

The initiation of BER on DNA in the nuclear environment is not just the interaction of the glycosylases with the DNA. In reality, the nucleus is a complicated and crowded environment with a huge excess of undamaged DNA and other protein "bulk".[68] Within this nuclear context, there is also the specific coordination and interactions of the downstream BER enzymes and factors to facilitate efficient repair.[50] The addition of high-salt conditions and PEG aids in observing nuclear environmental factors affecting processivity, but there is currently no previous literature on how other BER-interacting factors may stimulate glycosylase processivity. For instance, the addition of APE1 to glycosylase reactions has been shown to stimulate glycosidic bond cleavage chemistry by promoting turnover,[62–65] and its addition may also translate to more processive behavior for more efficient searching. Another potential candidate to add to the glycosylase processivity studies would be proliferating cell nuclear antigen (PCNA), which has been shown to interact and coordinate the activities of many BER enzymes, including UDG, and may assist with a sliding clamp mechanism in the search for lesions.[69,70]

4.7. Conclusions

In summary, we observed both associative and dissociative transfer of UDG in duplex containing U lesions located on the same strand and opposite strands. When these duplex were used in the reconstitution of strongly-positioned NCPs, we observe a majority dissociative transfer mode. Preliminary comparisons with a looser positioning sequence show a similar proclivity for the dissociative transfer. These studies show that the presence of the histone octamer core greatly shifts the mode of processivity to that of dissociative transfer. Studying processivity in the two-site NCP system helps us to better understand

how lesions, like needles, are found in the haystack of genomic DNA for the initiation of BER and other repair pathways.

4.8. References

(1) Lindahl, T. (1993) Instability and decay of the primary structure of DNA. *Nature 362*, 709–715.

(2) Segal, E., Fondufe-Mittendorf, Y., Chen, L., Thåström, A., Field, Y., Moore, I. K., Wang, J.-P. Z., and Widom, J. (2006) A genomic code for nucleosome positioning. *Nature 442*, 772–8.

(3) Rodriguez, Y., Hinz, J. M., and Smerdon, M. J. (2015) Accessing DNA damage in chromatin: Preparing the chromatin landscape for base excision repair. *DNA Repair (Amst). 32*, 113–119.

(4) Esadze, A., and Stivers, J. T. (2018) Facilitated Diffusion Mechanisms in DNA Base Excision Repair and Transcriptional Activation. *Chem. Rev.* acs.chemrev.8b00513.

(5) Schonhoft, J. D., Kosowicz, J. G., and Stivers, J. T. (2013) DNA translocation by human uracil DNA glycosylase: role of DNA phosphate charge. *Biochemistry 52*, 2526–35.

(6) Hedglin, M., and O'Brien, P. J. (2008) Human alkyladenine DNA glycosylase employs a processive search for DNA damage. *Biochemistry 47*, 11434–11445.

(7) Cravens, S. L., Hobson, M., and Stivers, J. T. (2014) Electrostatic properties of complexes along a DNA glycosylase damage search pathway. *Biochemistry 53*, 7680–92.

(8) Cravens, S. L., and Stivers, J. T. (2016) Comparative Effects of Ions, Molecular Crowding, and Bulk DNA on the Damage Search Mechanisms of hOGG1 and hUNG. *Biochemistry*.

(9) Blainey, P. C., van Oijen, A. M., Banerjee, A., Verdine, G. L., and Xie, X. S. (2006) A base-excision DNA-repair protein finds intrahelical lesion bases by fast sliding in contact with DNA. *Proc. Natl. Acad. Sci. U. S. A. 103*, 5752–7.

(10) Cravens, S. L., Schonhoft, J. D., Rowland, M. M., Rodriguez, A. A., Anderson, B. G., and Stivers, J. T. (2015) Molecular crowding enhances facilitated diffusion of two human

DNA glycosylases. *Nucleic Acids Res. 43*, 4087–4097.

(11) Rowland, M. M., Schonhoft, J. D., McKibbin, P. L., David, S. S., and Stivers, J. T. (2014) Microscopic mechanism of DNA damage searching by hOGG1. *Nucleic Acids Res. 42*, 9295–9303.

(12) Sidorenko, V. S., and Zharkov, D. O. (2008) Correlated cleavage of damaged DNA by bacterial and human 8-oxoguanine-DNA glycosylases. *Biochemistry 47*, 8970–8976.

(13) Chen, L., Haushalter, K. A., Lieber, C. M., and Verdine, G. L. (2002) Direct visualization of a DNA glycosylase searching for damage. *Chem. Biol. 9*, 345–50.

(14) Hedglin, M., and O'Brien, P. J. (2010) Hopping Enables a DNA Repair Glycosylase To Search Both Strands and Bypass a Bound Protein. *ACS Chem. Biol. 5*, 427–436.

(15) Hedglin, M., Zhang, Y., and O'Brien, P. J. (2013) Isolating Contributions from Intersegmental Transfer to DNA Searching by Alkyladenine DNA Glycosylase. *J. Biol. Chem. 288*, 24550–24559.

(16) Hedglin, M., Zhang, Y., and O'Brien, P. J. (2015) Probing the DNA structural requirements for facilitated diffusion. *Biochemistry 54*, 557–66.

(17) Porecha, R. H., and Stivers, J. T. (2008) Uracil DNA glycosylase uses DNA hopping and short-range sliding to trap extrahelical uracils. *Proc. Natl. Acad. Sci. U. S. A. 105*, 10791–6.

(18) Schonhoft, J. D., and Stivers, J. T. (2012) Timing facilitated site transfer of an enzyme on DNA. *Nat. Chem. Biol. 8*, 205–10.

(19) Rodriguez, G., Esadze, A., Weiser, B. P., Schonhoft, J. D., Cole, P. A., and Stivers, J. T. (2017) Disordered N-Terminal Domain of Human Uracil DNA Glycosylase (hUNG2) Enhances DNA Translocation. *ACS Chem. Biol. 12*, 2260–2263.

(20) Esadze, A., Rodriguez, G., Weiser, B. P., Cole, P. A., and Stivers, J. T. (2017) Measurement of nanoscale DNA translocation by uracil DNA glycosylase in human cells. *Nucleic Acids Res.*

(21) Parker, J. B., Bianchet, M. A., Krosky, D. J., Friedman, J. I., Amzel, L. M., and Stivers, J. T. (2007) Enzymatic capture of an extrahelical thymine in the search for uracil in DNA. *Nature 449*, 433–7.

(22) Friedman, J. I., and Stivers, J. T. (2010) Detection of damaged DNA bases by DNA glycosylase enzymes. *Biochemistry 49*, 4957–67.

(23) Stivers, J. T. (2008) Extrahelical damaged base recognition by DNA glycosylase enzymes. *Chemistry 14*, 786–93.

(24) Xiao, G., Tordova, M., Jagadeesh, J., Drohat, A. C., Stivers, J. T., and Gilliland, G. L. (1999) Crystal structure of Escherichia coli uracil DNA glycosylase and its complexes with uracil and glycerol: structure and glycosylase mechanism revisited. *Proteins 35*, 13–24.

(25) Stivers, J. T., Pankiewicz, K. W., and Watanabe, K. A. (1999) Kinetic mechanism of damage site recognition and uracil flipping by Escherichia coli uracil DNA glycosylase. *Biochemistry 38*, 952–63.

(26) Olmon, E. D., and Delaney, S. (2017) Differential Ability of Five DNA Glycosylases to Recognize and Repair Damage on Nucleosomal DNA. *ACS Chem. Biol. 12*, 692–701.

(27) Prasad, A., Wallace, S. S., and Pederson, D. S. (2007) Initiation of base excision repair of oxidative lesions in nucleosomes by the human, bifunctional DNA glycosylase NTH1. *Mol. Cell. Biol. 27*, 8442–53.

(28) Cole, H. A., Tabor-Godwin, J. M., and Hayes, J. J. (2010) Uracil DNA glycosylase activity on nucleosomal DNA depends on rotational orientation of targets. *J. Biol. Chem. 285*, 2876–2885.

(29) Nilsen, H., Lindahl, T., and Verreault, A. (2002) DNA base excision repair of uracil residues in reconstituted nucleosome core particles. *EMBO J. 21*, 5943–52.

(30) Ye, Y., Stahley, M. R., Xu, J., Friedman, J. I., Sun, Y., McKnight, J. N., Gray, J. J., Bowman, G. D., and Stivers, J. T. (2012) Enzymatic excision of uracil residues in nucleosomes depends on the local DNA structure and dynamics. *Biochemistry 51*, 6028–

6038.

(31) Bilotti, K., Kennedy, E. E., Li, C., and Delaney, S. (2017) Human OGG1 activity in nucleosomes is facilitated by transient unwrapping of DNA and is influenced by the local histone environment. *DNA Repair (Amst). 59*, 1–8.

(32) Schermerhorn, K. M., and Delaney, S. (2013) Transient-State Kinetics of Apurinic/Apyrimidinic (AP) Endonuclease 1 Acting on an Authentic AP Site and Commonly Used Substrate Analogs: The Effect of Diverse Metal Ions and Base Mismatches. *Biochemistry 52*, 7669–7677.

(33) Luger, K., Rechsteiner, T. J., and Richmond, T. J. (1999) Expression and purification of recombinant histones and nucleosome reconstitution. *Methods Mol. Biol. 119*, 1–16.

(34) Dyer, P. N., Edayathumangalam, R. S., White, C. L., Bao, Y., Chakravarthy, S., Muthurajan, U. M., and Luger, K. (2003) Reconstitution of Nucleosome Core Particles from Recombinant Histones and DNA. *Methods Enzymol. 375*, 23–44.

(35) Flaus, A., Luger, K., Tan, S., and Richmond, T. J. (1996) Mapping nucleosome position at single base-pair resolution by using site-directed hydroxyl radicals. *Proc. Natl. Acad. Sci. U. S. A. 93*, 1370–5.

(36) Jain, S. S., and Tullius, T. D. (2008) Footprinting protein–DNA complexes using the hydroxyl radical. *Nat. Protoc. 3*, 1092–1100.

(37) Das, R., Laederach, A., Pearlman, S. M., Herschlag, D., and Altman, R. B. (2005) SAFA: semi-automated footprinting analysis software for high-throughput quantification of nucleic acid footprinting experiments. *RNA 11*, 344–54.

(38) Haushalter, K. A., Todd Stukenberg, P., Kirschner, M. W., and Verdine, G. L. (1999) Identification of a new uracil-DNA glycosylase family by expression cloning using synthetic inhibitors. *Curr. Biol. 9*, 174–185.

(39) Sidorenko, V. S., Mechetin, G. V, Nevinsky, G. A., and Zharkov, D. O. (2008) Correlated cleavage of single- and double-stranded substrates by uracil-DNA glycosylase.

FEBS Lett. 582, 410–4.

(40) Stanford, N. P., Szczelkun, M. D., Marko, J. F., and Halford, S. E. (2000) One- and three-dimensional pathways for proteins to reach specific DNA sites. *EMBO J. 19*, 6546–57.

(41) Schonhoft, J. D., and Stivers, J. T. (2013) DNA translocation by human uracil DNA glycosylase: the case of single-stranded DNA and clustered uracils. *Biochemistry 52*, 2536–44.

(42) Lowary, P. T., and Widom, J. (1998) New DNA sequence rules for high affinity binding to histone octamer and sequence-directed nucleosome positioning. *J. Mol. Biol. 276*, 19–42.

(43) Lowary, P. T., and Widom, J. (1997) Nucleosome packaging and nucleosome positioning of genomic DNA. *Proc. Natl. Acad. Sci. U. S. A. 94*, 1183–8.

(44) Vasudevan, D., Chua, E. Y. D., and Davey, C. A. (2010) Crystal Structures of Nucleosome Core Particles Containing the “601” Strong Positioning Sequence. *J. Mol. Biol. 403*, 1–10.

(45) Kavli, B., Sundheim, O., Akbari, M., Otterlei, M., Nilsen, H., Skorpen, F., Aas, P. A., Hagen, L., Krokan, H. E., and Slupphaug, G. (2002) hUNG2 is the major repair enzyme for removal of uracil from U:A matches, U:G mismatches, and U in single-stranded DNA, with hSMUG1 as a broad specificity backup. *J. Biol. Chem. 277*, 39926–36.

(46) Di Noia, J. M., and Neuberger, M. S. (2007) Molecular Mechanisms of Antibody Somatic Hypermutation. *Annu. Rev. Biochem. 76*, 1–22.

(47) Stavnezer, J., Guikema, J. E. J., and Schrader, C. E. (2008) Mechanism and regulation of class switch recombination. *Annu. Rev. Immunol. 26*, 261–92.

(48) Odell, I. D., Wallace, S. S., and Pederson, D. S. (2013) Rules of engagement for base excision repair in chromatin. *J. Cell. Physiol. 228*, 258–66.

(49) Zhang, Y., and O’Brien, P. J. (2015) Repair of Alkylation Damage in Eukaryotic

Chromatin Depends on Searching Ability of Alkyladenine DNA Glycosylase. *ACS Chem. Biol. 10*, 2606–15.

(50) Prasad, R., Shock, D. D., Beard, W. A., and Wilson, S. H. (2010) Substrate channeling in mammalian base excision repair pathways: passing the baton. *J. Biol. Chem. 285*, 40479–88.

(51) Simpson, R. T., and Stafford, D. W. (1983) Structural features of a phased nucleosome core particle. *Proc. Natl. Acad. Sci. U. S. A. 80*, 51–5.

(52) Anderson, J. D., and Widom, J. (2000) Sequence and position-dependence of the equilibrium accessibility of nucleosomal DNA target sites. *J. Mol. Biol. 296*, 979–987.

(53) Dong, F., Hansen, J. C., and van Holde, K. E. (1990) DNA and protein determinants of nucleosome positioning on sea urchin 5S rRNA gene sequences in vitro. *Proc. Natl. Acad. Sci. U. S. A. 87*, 5724–8.

(54) Ura, K., Hayes, J. J., and Wolffe, A. P. (1995) A positive role for nucleosome mobility in the transcriptional activity of chromatin templates: restriction by linker histones. *EMBO J. 14*, 3752–65.

(55) Kim, J., Wei, S., Lee, J., Yue, H., and Lee, T. H. (2016) Single-Molecule Observation Reveals Spontaneous Protein Dynamics in the Nucleosome. *J. Phys. Chem. B 120*, 8925–8931.

(56) Bilotti, K., Tarantino, M. E., and Delaney, S. (2018) Human Oxoguanine Glycosylase 1 Removes Solution Accessible 8-Oxo-7,8-dihydroguanine Lesions from Globally Substituted Nucleosomes Except in the Dyad Region. *Biochemistry 57*, 1436–1439.

(57) Kennedy, E. E., Caffrey, P. J., and Delaney, S. (2018) Initiating base excision repair in chromatin. *DNA Repair (Amst). 71*, 87–92.

(58) Polach, K. J., and Widom, J. (1995) Mechanism of protein access to specific DNA sequences in chromatin: a dynamic equilibrium model for gene regulation. *J. Mol. Biol. 254*, 130–49.

(59) Wei, S., Falk, S. J., Black, B. E., and Lee, T. H. (2015) A novel hybrid single molecule approach reveals spontaneous DNA motion in the nucleosome. *Nucleic Acids Res. 43*, e111–e111.

(60) Beard, B. C., Wilson, S. H., and Smerdon, M. J. (2003) Suppressed catalytic activity of base excision repair enzymes on rotationally positioned uracil in nucleosomes. *Proc. Natl. Acad. Sci. U. S. A. 100*, 7465–70.

(61) Visnes, T., Doseth, B., Pettersen, H. S., Hagen, L., Sousa, M. M. L., Akbari, M., Otterlei, M., Kavli, B., Slupphaug, G., and Krokan, H. E. (2009) Uracil in DNA and its processing by different DNA glycosylases. *Philos. Trans. R. Soc. Lond. B. Biol. Sci. 364*, 563–8.

(62) Vidal, A. E., Hickson, I. D., Boiteux, S., and Radicella, J. P. (2001) Mechanism of stimulation of the DNA glycosylase activity of hOGG1 by the major human AP endonuclease: bypass of the AP lyase activity step. *Nucleic Acids Res. 29*, 1285–92.

(63) Baldwin, M. R., and O'Brien, P. J. (2009) Human AP endonuclease 1 stimulates multiple-turnover base excision by alkyladenine DNA glycosylase. *Biochemistry 48*, 6022–33.

(64) Fitzgerald, M. E., and Drohat, A. C. (2008) Coordinating the initial steps of base excision repair. Apurinic/apyrimidinic endonuclease 1 actively stimulates thymine DNA glycosylase by disrupting the product complex. *J. Biol. Chem. 283*, 32680–90.

(65) Hill, J. W., Hazra, T. K., Izumi, T., and Mitra, S. (2001) Stimulation of human 8-oxoguanine-DNA glycosylase by AP-endonuclease: potential coordination of the initial steps in base excision repair. *Nucleic Acids Res. 29*, 430–8.

(66) Tarantino, M. E., Dow, B. J., Drohat, A. C., and Delaney, S. (2018) Nucleosomes and the three glycosylases: High, medium, and low levels of excision by the uracil DNA glycosylase superfamily. *DNA Repair (Amst). 72*, 56–63.

(67) Brooks, S. C., Adhikary, S., Rubinson, E. H., and Eichman, B. F. (2013) Recent

advances in the structural mechanisms of DNA glycosylases. *Biochim. Biophys. Acta - Proteins Proteomics 1834*, 247–271.

(68) Minton, A. P. (2001) The influence of macromolecular crowding and macromolecular confinement on biochemical reactions in physiological media. *J. Biol. Chem. 276*, 10577–80.

(69) Moldovan, G.-L., Pfander, B., and Jentsch, S. (2007) PCNA, the Maestro of the Replication Fork. *Cell 129*, 665–679.

(70) Hagen, L., Kavli, B., Sousa, M. M. L., Torseth, K., Liabakk, N. B., Sundheim, O., Peňa-Diaz, J., Otterlei, M., Hørning, O., Jensen, O. N., Krokan, H. E., and Slupphaug, G. (2008) Cell cycle-specific UNG2 phosphorylations regulate protein turnover, activity and association with RPA. *EMBO J. 27*, 51–61.

4.9. Appendix: Supplementary Information

Scheme S.4.1: Ligation strategy for 601 145 mer processivity oligonucleotides. Ligation schemes for processivity DNA substrates for **(A)** UUsame and **(B)** UUopp. Each I strand 145 mer was assembled by the ligation of two component oligonucleotides; the J strand 145 mers was assembled by the ligation of three component oligonucleotides. **(A)** For the I strand 145 mer containing U_1 and U_2, i.2 was 5'-phosphorylated and combined with equal amounts of i.1 and scaffold i.s12 for annealing. Annealed strands were subsequently ligated to create the full-length strand. For the associated J 145 mer not containing damage, j.2 and j.3 were 5'-phosphorylated and combined with equal amounts of j.1 and scaffolds j.s12 and j.s23. **(B)** For the I strand 145 mer containing U_1 only, i.3 was 5'-phosphorylated and combined with equal amounts of i.1 and scaffold i.s12 for annealing. Annealed strands were subsequently ligated to create the full-length strand. For the associated J 145 mer containing U_3, j.4 and j.3 were 5'-phosphorylated and combined with equal amounts of j.1 and scaffolds j.s12 and j.s23.

I and J strand designations based on the crystal structure of Vasudevan *et al*. of the Widom 601 NCP.[44]

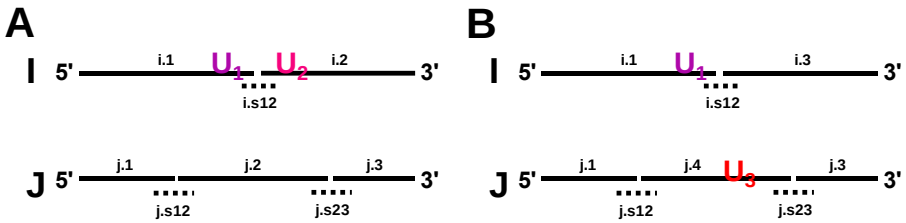

601

Component	Length	Sequence (5' to 3')
i.1	66mer	ATCAGAATCCCGGTGCCGAGGCCGCTCAATTGGTCGTAGACAGCTCTAGCACCGCTTAAACGCAUG
i.2	79mer	GTACGCGCTUTCCCCCGCGTTTTAACCGCCAAGGGGATTACTCCCTAGTCTCCAGGCACGTGTCAGATATATACATCGAT
i.3	79mer	TACGCGCTCTCCCCCGCGTTTTAACCGCCAAGGGGATTACTCCCTAGTCTCCAGGCACGTGTCAGATATATACATCGAT
i.s12	30mer	GGGGGAGAGCGCGTACGTGCGTTTAAGCGG
j.1	45mer	ATCGATGTATATATCTGACACGTGCCTGGAGACTAGGGAGTAATCCCCTTGGCGGT
j.2	40mer	TAAAACGCGGGGGAGAGCGCGTACGTGCGTTTAAGCGGTG
j.3	49mer	CTAGAGCTGTCTACGACCAATTGAGCGGCCTCGGCACCGGGATTCTGAT
j.4	40mer	TAAAACGCGGGGGAGAGCGUGTACGTGCGTTTAAGCGGTG
j.s12	30mer	CGTAGACAGCTCTAGCACCGCTTAAACGCA
j.s23	30mer	CTCCCCCGCGTTTTAACCGCCAAGGGGATT

Scheme S.4.2. Widom 601 sequences for processivity DNA substrates.

I strand containing U_1 and U_2 (for UUsame):

5′- ATC AGA ATC CCG GTG CCG AGG CCG CTC AAT TGG TCG TAG ACA GCT CTA GCA CCG CTT AAA CGC AUG* TAC GCG CTU TCC CCC GCG TTT TAA CCG CCA AGG GGA TTA CTC CCT AGT CTC CAG GCA CGT GTC AGA TAT ATA CAT CGA T

***** = position of internal radiolabel

J strand complement for UUsame duplex formation:

5′- ATC GAT GTA TAT ATC TGA CAC GTG CCT GGA GAC TAG GGA GTA ATC CCC TTG GCG GTT AAA ACG CGG GGG AGA GCG CGT ACG TGC GTT TAA GCG GTG CTA GAG CTG TCT ACG ACC AAT TGA GCG GCC TCG GCA CCG GGA TTC TGA T

I strand containing U_1 only (for UUopp):

5′- ATC AGA ATC CCG GTG CCG AGG CCG CTC AAT TGG TCG TAG ACA GCT CTA GCA CCG CTT AAA CGC AUG TAC GCG CTC TCC CCC GCG TTT TAA CCG CCA AGG GGA TTA CTC CCT AGT CTC CAG GCA CGT GTC AGA TAT ATA CAT CGA T

J strand containing U_3 (UUopp):

5′- ATC GAT GTA TAT ATC TGA CAC GTG CCT GGA GAC TAG GGA GTA ATC CCC TTG GCG GTT AAA ACG CGG GGG AGA GCG UGT ACG TGC GTT TAA GCG GTG CTA GAG CTG TCT ACG ACC AAT TGA GCG GCC TCG GCA CCG GGA TTC TGA T

Scheme S.4.3. Ligation strategy for 5S 146 mer processivity oligonucleotides. Ligation schemes for 5S processivity DNA substrates for **(A)** UUsame and **(B)** UUopp. Each 146mer strand was assembled by the ligation of two component oligonucleotides. **(A)** For the T strand 146 mer containing U_1 and U_2, T.2 was 5'-phosphorylated and combined with equal amounts of T.1 and scaffold T.s for annealing. Annealed strands were subsequently ligated to create the full-length strand. For the associated B 146 mer not containing damage, B.2 was 5'-phosphorylated and combined with equal amounts of B.1 and scaffolds B.s. **(B)** For the T strand 146 mer containing U_1 only, T.3 was 5'-phosphorylated and combined with equal amounts of T.1 and scaffold T.s for annealing. Annealed strands were subsequently ligated to create the full-length strand. For the associated B 146 mer containing U_3, T.3 was 5'-phosphorylated and combined with equal amounts of B.1 and scaffold B.s.

Top (T) and Bottom (B) strand designations were arbitrarily made based on how the 5S rDNA sequence was presented in Prasad *et al.*[27] In the referenced study, strand T was their lesion-containing strand.

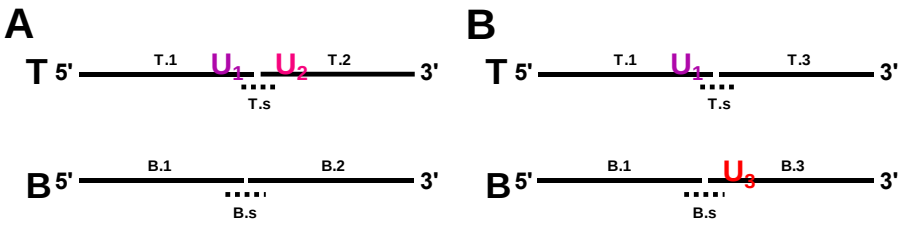

5S

Component	Length	Sequence (5' to 3')
T.1	68mer	ATCCAGGGATTTATAAGCTGATGACGTCATAACATCCCTGACCCTTTAAATAGCTTAACTTTGAUCAA
T.2	78mer	GCAGGAGUCTACGACCATACCATGCTGAATATACCGGTTCTCGTCCGATCACCGAAGTCAAGCAGCATAGGGCTCGAT
T.3	78mer	GCAGGAGCCTACGACCATACCATGCTGAATATACCGGTTCTCGTCCGATCACCGAAGTCAAGCAGCATAGGGCTCGAT
T.s	30mer	GTCGTAGGCTCCTGCTTGATCAAAGTTAAG
B.1	71mer	ATCGAGCCCTATGCTGCTTGACTTCGGTGATCGGACGAGAACCGGTATATTCAGCATGGTATGGTCGTAGG
B.2	75mer	CTCCTGCTTGGTCAAAGTTAAGCTATTTAAAGGGTCAGGGATGTTATGACGTCATCAGCTTATAAATCCCTGGAT
B.3	75mer	CTCUTGCTTGAGCAAAGTTAAGCTATTTAAAGGGTCAGGGATGTTATGACGTCATCAGCTTATAAATCCCTGGAT
B.s	30mer	TTGACCAAGCAGGAGCCTACGACCATACCA

Scheme S.4.4. 5S sequences for processivity DNA substrates.

T strand containing U1 and U2 (for 5S UUsame):

5′- ATC CAG GGA TTT ATA AGC TGA TGA CGT CAT AAC ATC CCT GAC CCT TTA AAT
AGC TTA ACT TTG AUC AA*G CAG GAG UCT ACG ACC ATA CCA TGC TGA ATA TAC CGG
TTC TCG TCC GAT CAC CGA AGT CAA GCA GCA TAG GGC TCG AT

* = position of internal radiolabel

B strand complement for 5S UUsame duplex formation:

5′- ATC GAG CCC TAT GCT GCT TGA CTT CGG TGA TCG GAC GAG AAC CGG TAT ATT
CAG CAT GGT ATG GTC GTA GGC TCC TGC TTG GTC AAA GTT AAG CTA TTT AAA GGG
TCA GGG ATG TTA TGA CGT CAT CAG CTT ATA AAT CCC TGG AT

T strand containing U1 only (for 5S UUopp):

5′- ATC CAG GGA TTT ATA AGC TGA TGA CGT CAT AAC ATC CCT GAC CCT TTA AAT
AGC TTA ACT TTG AUC AAG CAG GAG CCT ACG ACC ATA CCA TGC TGA ATA TAC CGG
TTC TCG TCC GAT CAC CGA AGT CAA GCA GCA TAG GGC TCG AT

B strand containing U3 (for 5S UUopp):

5′- ATC GAG CCC TAT GCT GCT TGA CTT CGG TGA TCG GAC GAG AAC CGG TAT ATT
CAG CAT GGT ATG GTC GTA GGC TCU TGC TTG AGC AAA GTT AAG CTA TTT AAA GGG
TCA GGG ATG TTA TGA CGT CAT CAG CTT ATA AAT CCC TGG AT

Chapter 5. Conclusions and Perspectives

5.1. Conclusions

In the preceding work, we have created nucleosome core particle (NCP) substrates as a model for studying how the initiation of base excision repair (BER) with glycosylase enzymes is influenced by DNA packaging. In these experiments, we have created homogeneous NCP populations utilizing the Widom 601 nucleosome positioning sequence[1,2] as our DNA templates, with the four highly-conserved canonical histone proteins purified from *X. laevis*.[3,4] This controlled model system has helped us to create a foundation for investigating the effects of well-positioned nucleosomes found in the eukaryotic genome on glycosylase activity. We were able to create three different NCP substrate set-ups to study the recognition and removal of lesions from NCPs by glycosylases. Using these NCP substrates, we have gained insight into the activities of three different glycosylases in the packaged DNA environment: human oxoguanine DNA glycosylase (hOGG1), uracil DNA glycosylase (UDG), and human alkyladenine adenine DNA glycosylase (AAG). These three glycosylases belong to three different structural superfamilies,[5] which allow for some general comparisons to be made about the glycosylase structure-activity relationship on NCPs. Further, the lesions studied for each glycosylase, 8-oxo-7,8-dihydroguanine (8-oxoG) for hOGG1, uracil (U) for UDG, and ethenoadenine (εA) for AAG, are representative lesions of damage that occur from oxidation, deamination, and alkylation events.[6]

First, we assembled site-specific NCPs containing a lesion in one of three rotational positions (OUT, MID, IN), located ~20 bp from the end of the NCP substrate. Our goal was to expand upon previous work done on the dyad of the NCPs,[7] to see if a lesion position off-dyad would improve glycosylase activity, specifically comparing hOGG1 and UDG activities. We performed single-turnover kinetics to measure the observed rate of the nucleobase lesions over time from the off-dyad NCPs. Unlike what was observed on the dyad,[7] the kinetics of each off-dyad NCP rotational location was best explained by

a double exponential model for both enzymes, consisting of a fast phase and a slow phase of activity. The first phase was comparable to rates on duplex, which we attributed to a sub-population of the NCPs being in an amenable configuration for immediate repair. The second, slower phase was attributed to the need for transient unwrapping to allow access to the remaining lesion population in NCPs. This was consistent with another study using human UDG to examine kinetics in multiple site-specific off-dyad positions that described multiphasic kinetic behaviors.[8] Although we did see an increase in glycosylase activity at all rotational off-dyad positions relative to those on the dyad,[7] we were surprised to observe a break in the correlation between solution accessibility of the lesion positions and glycosylase activity. As seen on the dyad, we hypothesized that the off-dyad OUT position would be conducive for the best glycosylase activity. In the case of hOGG1, the lowest amount of product accumulation was observed at the OUT position. Conversely, while UDG had quantitative product accumulation at both the OUT and MID positions, the U in the OUT position was removed 10-fold more slowly in comparison. Upon consultation with a merged crystal structure representation of an NCP containing the Widom 601 sequence and histone tails,[2,9] we noticed an H2B tail protruding from the histone core near our lesion positions, specifically closest to the OUT position. We repeated our kinetic evaluations of hOGG1 and UDG using NCPs lacking H2B tails and found that while UDG demonstrated no difference, hOGG1 activity improved, suggesting that the tail was specifically suppressing the activity of hOGG1. Indeed, other studies have shown that the histone tails have varying effects on the activity of other BER enzymes.[10,11] Ultimately, these site-specific NCP studies highlighted the complex environment the NCP creates for glycosylase activity, from influences of transient unwrapping as a result of translational positioning, to unexpected correlations of activity with respect to rotational positioning, and to the potential for histone tails to suppress glycosylase activity that prevent efficient repair in NCPs.

Most of the previous literature examining glycosylase activity in NCPs used site-specific lesion-containing NCPs like our initial experiments outlined above. However, as described, we quickly appreciated that every nucleobase in an NCP inherently has a unique microenvironment, and therefore no one lesion location could be representative of repair in the context of packaged DNA. Instead of obtaining information about each potential lesion position in the NCP by creating 290 different site-specific NCPs (145 nucleobases/strand x 2 strands) for just one lesion and/or glycosylase of interest, we[12] set out to design a global lesion-containing NCP system for a more high-throughput approach. With a global population of NCPs, one can simultaneously study multiple lesion positions and a variety of NCP microenvironments to explore the nuanced relationships between glycosylase repair and NCP environment.[8,12] In the current work, we created a global system that substituted εA lesions for A in either strand of the nucleosomal duplex such that 95% of each NCP contained 0 or 1 lesion; specifically, our εA-containing population made up ~25% of the total population. We used this global εA NCP system to determine the kinetic parameters of removal of εA at 49 distinct geometric positions by AAG. From these studies, we observed monophasic characteristics of εA excision at all positions observed across the NCP landscape, which was contrary to the works in off-dyad experiments described above.[8,13] We attributed the lack of multiple kinetic phases to AAG's slower activity[7,14–16] in comparison with hOGG1 and UDG, thus making AAG unable to capture the faster phases that reflect dynamic conformational changes in the NCP. Despite AAG's monophasic behavior across the NCP, we captured interesting relationships between amounts of εA excision and NCP architecture. Overall, there was a strong correlation between solution accessibility of the lesion position and the amount of repair observed. However, there were exceptions to this correlation that further revealed interesting architectural nuances of the NCP landscape. We observed potentially inhibitory interactions due to nearby tails, as others had observed previously,[10,11,13,17] or local

stretching from DNA's wrapping around the histone core.[2,9,18] In addition, we also identified increased repair toward the DNA end that is known to asymmetrically unwrap,[19–21] providing increased access to repair. These global experiments have allowed us to appreciate a more complete picture of the subtle relationships between NCP architecture and DNA repair in cells which might contribute to mutagenesis.

Not only are we interested in the amounts and rates of lesion removal in NCPs, but we are also interested in *how* glycosylases find the lesions to initiate BER in the context of packaged DNA. To explore this concept of glycosylase searching, we have made preliminary progress in studying the processivity of glycosylases in NCPs. Glycosylase processivity, or its movement between two lesions during a single DNA binding event, has only ever been characterized in duplex substrates. The previous literature in duplex establishes two modes of processivity: associative transfer ("sliding") and dissociative transfer ("hopping"). In our studies, we used a two-site lesion-containing NCP system to qualitatively determine how the presence of the histone octamer core influenced the processivity behaviors of UDG between U lesions. We created two different such NCP substrates: UUsame, where the two lesions were located on the same DNA strand, and UUopp, where the two lesions were located on opposite DNA strands. We first established that UDG had varying amounts of associative and dissociative contributions depending on where the second lesion was located relative to the first, as observed in previous processivity work in duplex.[22,23] When the duplex was assembled into NCPs, there was a strong shift in UDG's processivity to a fully dissociative transfer mode. Additionally, we created analogous NCPs using the natural 5S nucleosome positioning sequence, and observed this same shift, despite a more dynamic template sequence. These data together suggest that the presence of the histone octamer core greatly shifts the mode of processivity to favor dissociative transfer for efficient repair in NCPs. This observation was not entirely surprising, since the presence of the histone octamer has been described to

physically impede glycosylase activity in this thesis work, as well as in many previous studies.[24,25] Building upon processivity studies in duplex, we hypothesize that glycosylases utilize the two modes of processivity depending on the DNA packaging context for the most efficient searching and repair in the nuclear environment: a focus on more associative transfer in times/regions where the DNA is more open and accessible, and a focus on dissociative transfer throughout the cell cycle and among regions of packaged DNA. Indeed, an *in vivo* study has shown that there is decreased cell survival when glycosylase searching is impaired.[26] Expansion of processivity studies in NCP substrates will help us better understand how DNA damage is found to initiate BER efficiently in the dynamic genomic environment, and potentially how it can be improved to combat mutagenesis.

5.2. Ongoing and future work

Studies using the above-described NCP systems have not only provided us with valuable insight about glycosylase activity on NCPs, but they also provide us with a controlled means to study a multitude of different interactions and hypotheses about repair in packaged, eukaryotic DNA. However, there is still so much to explore. *In vitro* experiments using the NCP systems allow us to bridge the gap between what we know about how repair enzymes function on duplex and how they function in the context of the cell *in vivo*. Inspired by *in vivo* observations, we can create NCP models to better understand the molecular mechanisms of the delicate balance between DNA damage, repair, and human disease.

5.2.1. Studying other human glycosylases on NCP substrates

The ability to create global lesion-containing NCPs allows for a wide variety of rotational and translational positions for initial observations of less-studied glycosylases in

the packaged DNA environment. Screening for glycosylase activity across an NCP can open possibilities for further specific characterizations of a particularly interesting NCP microenvironment, with the use of a site-specific lesion NCP system. At the time of writing this thesis, there were three glycosylases that have never been characterized in an NCP substrate: NEIL2, NEIL3, and MUTYH, all of which are involved in preventing mutations from oxidized nucleobase damage. NEIL2 and NEIL3 are implicated in the removal of oxidized nucleobases during S-phase based on their preference for removing lesions from ssDNA substrates, and their interactions with replication proteins.[27,28] Interestingly, UDG has similar characteristics: a high affinity for ssDNA substrates[29,30] and an important role in repair during S-phase due to increased expression,[31] as well as relatively robust activity in the NCP.[7,8,13,32,33] It has been suggested previously[7] that UDG's ability to remove lesions from ssDNA may be a contributing factor for its proficiency in removing lesions from an NCP context; it would be interesting if this hypothesis were tested with NEIL2 and NEIL3 in the NCP context. Conversely, MUTYH is responsible for the removal of A in A:8-oxoG mispairs and does not work on ssDNA.[34] Studying the global NCP repair profile of MUTYH and comparing it with that of hOGG1[12] would be fascinating to see if they might be complementary in their repair abilities.

In addition to the aforementioned glycosylases having never been studied in the context of packaged DNA, there have only been cursory site-specific NCP studies on other glycosylases such as SMUG1,[35,36] TDG,[36] MBD4,[37] and NEIL1/NTH1.[38–41] By gaining global repair profiles of more glycosylases within the NCP environment, we can create bigger correlations between types of damage being removed, glycosylase structure, and NCP architecture. These data might inform on NCP characteristics that are conducive to different mutagenic hotspots due to inefficient repair of lesions by the various glycosylases.

5.2.2. Histone octamer composition on glycosylase activity

We can better understand how structure influences the initiation of BER not only by studying glycosylases from different structural families, but also by changing the composition of the histone octamer. Current work in our lab is exploring how architectural features of the histone proteins might influence glycosylase activity. Of particular interest are the histone tails, which were directly observed to influence hOGG1 activity in the off-dyad work,[13] and also were implicated in the global εA/AAG work presented in Chapter 3 of this thesis. The tails are known to be targets for different types of post-translational modifications (PTMs) including acetylation, methylation, ubiquitination, and sumoylation.[42] Specifically, we[13] have briefly explored the varied effects of the acetylation of histone proteins and glycosylase repair. Generally, acetylation is associated with open chromatin structure because it neutralizes the positive charge of the basic lysines found in the histone tails.[43] The acetylation of histone proteins has previously been shown to increase DNA-histone dynamics[44,45] thus increasing accessibility to damaged lesions by repair enzymes.[25] Indeed, other BER enzymes have had varying outcomes on repair due to acetylation of the histone proteins.[37,46] We are interested in exploring how acetylation of the histone tails influences glycosylase activity.

To understand the full effects of the histone tails and glycosylases during repair in NCPs, a more dramatic change would be to remove them completely. Interestingly, an upcoming field of research is focused on histone clipping and the endopeptidases that are responsible. Histone clipping has been observed to be involved in biological processes such as development, transcription, and replication.[42] Unlike the PTMs described above, removal of the histone tails is irreversible, and is hypothesized to potentially promote histone turnover, remove all existing PTMs on histone tails to prevent signaling, or to destabilize the histone octamer for access.[47,48] Early *in vitro* work found that the removal of the histone tails did not influence UDG activity in the NCP.[10] However, many NCP

studies have shown that UDG works relatively well in packaged DNA,[7,8,13,32,33] so there may not be much improvement gained by removing the tails. However, glycosylases such as hOGG1 and AAG, which may have suppressed activity as a consequence of the presence of the tails, may benefit and result in improved repair in the NCP.

In addition to making modifications to the histone tails, we are also interested in how the replacement of canonical histones with their variant counterparts will influence NCP architecture and glycosylase initiation. Histone variants are nonallelic isoforms of the four canonical histone proteins, and their diversity allows for the regulation of a variety of DNA access-related processes including transcription, gene silencing, replication, recombination, and repair.[49] We are particularly interested in histones that are known to be involved in other repair pathways, to observe if they have any influence on BER as well. For instance, the phosphorylation of H2A.X (indicated as γ-H2A.X) is a proposed signal for the recruitment of double-strand break repair machinery.[50] Additionally, previous work studying hOGG1 activity in NCPs incorporated the histone variant H2A.Bbd and observed an increase in hOGG1 activity relative to canonical H2A incorporation.[51] This result suggests that the change in DNA-histone contacts with variant histone deposition during the described cellular processes may also facilitate BER-related repair in NCPs.

5.2.3. Additional protein factors to facilitate glycosylase activity in NCPs

It is important to note that the interactions between glycosylases and packaged DNA do not occur in isolation *in vivo*. In fact, the nucleus is a crowded environment with many enzymes and proteins and undamaged DNA present all at once. It is likely that BER initiation *in vivo* is facilitated by other proteins and/or factors present to support glycosylases. Previous studies have looked at the role of ATP-dependent chromatin remodelers and their abilities generally to increase BER activity in NCPs.[25,52] However, it is possible that single NCP systems are essentially stripped of the duplex during, and

therefore not providing a good representation, of the remodeling event's influence. Therefore, it is important to consider less aggressive protein factors that might facilitate BER initiation in NCPs. For example, the intimate relationships among the BER enzyme cascade has been well-characterized as a "passing of the baton"[53] to ensure coordination for efficient repair of the damage. Specifically, APE1 is known to coordinate with glycosylases to stimulate glycosidic bond cleavage chemistry by promoting turnover.[54–57] As of now, there have only been studies combining BER enzymes in the NCPs in the form of UDG and APE1.[10,32,33,58] We need more variety in combinatorial BER experiments to get a better picture of the coordination of BER in NCPs. In addition to downstream BER enzymes, a recently discovered "factor" that is not ATP-dependent, has emerged to have a potential role in facilitating glycosylase activity in NCPs.[41]

5.3. Biological Perspectives

Continuing to study the initiation of BER and its downstream players in the NCP system will allow us to bridge the gap between *in vitro* biochemical studies in duplex and *in vivo* observations in chromatin to better understand how deficiencies of BER in NCPs contribute to mutagenesis and human disease. Indeed, recent mutagenic mapping in eukaryotic genomes of yeast[59] and human cancers[60] have underlined the connection between BER and DNA packaging in NCPs. Both studies show that there is decreased BER activity when the helical turns of the DNA duplex are facing closest to the histone octamer cores and along the dyad region. Specifically, the lack of BER activity at these less accessible regions contributes to mutational signatures that lead to a subset of human cancers, rather than due to an increase in damage occurence.[60] This might suggest that increased repair at these inaccessible regions might resolve these particular mutagenic signatures.

It may also be argued that the suppression of initiating BER within a packaged DNA environment can be protective and advantageous for a cell.[61] Preventing the formation of an abasic site by suppressing glycosylase can decrease incidences of single- or double-strand breaks, DNA-DNA interstrand crosslinks, DNA-protein crosslinks from reaction with histone tails, and other protein adducts, which may be more deleterious to the cell.[61,62,63] Indeed, *E. coli* with deletions of all three glycosylases dealing with removing oxidative lesions were more resistant to ionizing damage compared with wild-type cells due to reduced double-strand breaks caused by the initiation of BER on cluster damage.[64] Additionally, the suppression of BER initiation also shown a protective effect in the context of non-replicating neuronal cells in preventing trinucleotide repeat expansions. Specifically, in a mouse model of Huntington's disease, the deletion of the OGG1 gene prevented the trinucleotide repeat expansion mutation, suggesting a BER-dependent mechanism of disease.[65]

The delicate balance of repair – either too little, or too much – leading to genetic instability and disease phenotypes necessitates a better understanding of repair on the molecular level. Fortunately, *in vivo* observations including the mutagenic mapping in eukaryotic genomes of yeast[59] and human cancers[60] reveal similar patterns of repair as the *in vitro* work of BER activity in NCPs. The work done *in vitro* using NCP systems can provide a molecular-level understanding of such biological observations, and can be expanded upon to include chromatin remodelers and other protein-protein interactions with glycosylases to develop a more comprehensive understanding of DNA damage, repair, and disease. These connections between BER activity-profiling in NCPs and the incidence of human cancers emphasize the power of the NCP model not only to predict, but also potentially to inform ways to prevent the disease-inducing mutagenesis.

5.4. References

(1) Lowary, P. T., and Widom, J. (1998) New DNA sequence rules for high affinity binding to histone octamer and sequence-directed nucleosome positioning. *J. Mol. Biol. 276*, 19–42.

(2) Vasudevan, D., Chua, E. Y. D., and Davey, C. A. (2010) Crystal Structures of Nucleosome Core Particles Containing the “601” Strong Positioning Sequence. *J. Mol. Biol. 403*, 1–10.

(3) Luger, K., Rechsteiner, T. J., and Richmond, T. J. (1999) Expression and purification of recombinant histones and nucleosome reconstitution. *Methods Mol. Biol. 119*, 1–16.

(4) Sullivan, S. A., Aravind, L., Makalowska, I., Baxevanis, A. D., and Landsman, D. (2000) The Histone Database: a comprehensive WWW resource for histones and histone fold-containing proteins. *Nucleic Acids Res. 28*, 320–322.

(5) Brooks, S. C., Adhikary, S., Rubinson, E. H., and Eichman, B. F. (2013) Recent advances in the structural mechanisms of DNA glycosylases. *Biochim. Biophys. Acta - Proteins Proteomics 1834*, 247–271.

(6) Schermerhorn, K. M., and Delaney, S. (2014) A chemical and kinetic perspective on base excision repair of DNA. *Acc. Chem. Res. 47*, 1238–1246.

(7) Olmon, E. D., and Delaney, S. (2017) Differential Ability of Five DNA Glycosylases to Recognize and Repair Damage on Nucleosomal DNA. *ACS Chem. Biol. 12*, 692–701.

(8) Ye, Y., Stahley, M. R., Xu, J., Friedman, J. I., Sun, Y., McKnight, J. N., Gray, J. J., Bowman, G. D., and Stivers, J. T. (2012) Enzymatic excision of uracil residues in nucleosomes depends on the local DNA structure and dynamics. *Biochemistry 51*, 6028–6038.

(9) Davey, C. A., Sargent, D. F., Luger, K., Maeder, A. W., and Richmond, T. J. (2002) Solvent Mediated Interactions in the Structure of the Nucleosome Core Particle at 1.9Å Resolution. *J. Mol. Biol. 319*, 1097–1113.

(10) Beard, B. C., Stevenson, J. J., Wilson, S. H., and Smerdon, M. J. (2005) Base excision repair in nucleosomes lacking histone tails. *DNA Repair (Amst). 4*, 203–209.

(11) Chafin, D. R., Vitolo, J. M., Henricksen, L. A., Bambara, R. A., and Hayes, J. J. (2000) Human DNA ligase I efficiently seals nicks in nucleosomes. *EMBO J. 19*, 5492–5501.

(12) Bilotti, K., Tarantino, M. E., and Delaney, S. (2018) Human Oxoguanine Glycosylase 1 Removes Solution Accessible 8-Oxo-7,8-dihydroguanine Lesions from Globally Substituted Nucleosomes Except in the Dyad Region. *Biochemistry 57*, 1436–1439.

(13) Bilotti, K., Kennedy, E. E., Li, C., and Delaney, S. (2017) Human OGG1 activity in nucleosomes is facilitated by transient unwrapping of DNA and is influenced by the local histone environment. *DNA Repair (Amst). 59*, 1–8.

(14) Lee, C.-Y. I., Delaney, J. C., Kartalou, M., Lingaraju, G. M., Maor-Shoshani, A., Essigmann, J. M., and Samson, L. D. (2009) Recognition and processing of a new repertoire of DNA substrates by human 3-methyladenine DNA glycosylase (AAG). *Biochemistry 48*, 1850–61.

(15) O'Brien, P. J., and Ellenberger, T. (2004) Dissecting the Broad Substrate Specificity of Human 3-Methyladenine-DNA Glycosylase. *J. Biol. Chem. 279*, 9750–9757.

(16) Hedglin, M., and O'Brien, P. J. (2008) Human alkyladenine DNA glycosylase employs a processive search for DNA damage. *Biochemistry 47*, 11434–11445.

(17) Meas, R., Smerdon, M. J., and Wyrick, J. J. (2015) The amino-terminal tails of histones H2A and H3 coordinate efficient base excision repair, DNA damage signaling and postreplication repair in Saccharomyces cerevisiae. *Nucleic Acids Res. 43*, 4990–5001.

(18) Chua, E. Y. D., Vasudevan, D., Davey, G. E., Wu, B., and Davey, C. A. (2012) The mechanics behind DNA sequence-dependent properties of the nucleosome. *Nucleic Acids Res. 40*, 6338–6352.

(19) Ngo, T. T. M., Zhang, Q., Zhou, R., Yodh, J. G., and Ha, T. (2015) Asymmetric

unwrapping of nucleosomes under tension directed by DNA local flexibility. *Cell 160*, 1135–1144.

(20) Gansen, A., Felekyan, S., Kühnemuth, R., Lehmann, K., Tóth, K., Seidel, C. A. M., and Langowski, J. (2018) High precision FRET studies reveal reversible transitions in nucleosomes between microseconds and minutes. *Nat. Commun. 9*, 4628.

(21) Chen, Y., Tokuda, J. M., Topping, T., Sutton, J. L., Meisburger, S. P., Pabit, S. A., Gloss, L. M., and Pollack, L. (2014) Revealing transient structures of nucleosomes as DNA unwinds. *Nucleic Acids Res. 42*, 8767–76.

(22) Schonhoft, J. D., and Stivers, J. T. (2012) Timing facilitated site transfer of an enzyme on DNA. *Nat. Chem. Biol. 8*, 205–10.

(23) Esadze, A., Rodriguez, G., Weiser, B. P., Cole, P. A., and Stivers, J. T. (2017) Measurement of nanoscale DNA translocation by uracil DNA glycosylase in human cells. *Nucleic Acids Res.*

(24) Kennedy, E. E., Caffrey, P. J., and Delaney, S. (2018) Initiating base excision repair in chromatin. *DNA Repair (Amst). 71*, 87–92.

(25) Rodriguez, Y., Hinz, J. M., and Smerdon, M. J. (2015) Accessing DNA damage in chromatin: Preparing the chromatin landscape for base excision repair. *DNA Repair (Amst). 32*, 113–119.

(26) Zhang, Y., and O'Brien, P. J. (2015) Repair of Alkylation Damage in Eukaryotic Chromatin Depends on Searching Ability of Alkyladenine DNA Glycosylase. *ACS Chem. Biol. 10*, 2606–15.

(27) Hazra, T. K., Kow, Y. W., Hatahet, Z., Imhoff, B., Boldogh, I., Mokkapati, S. K., Mitra, S., and Izumi, T. (2002) Identification and characterization of a novel human DNA glycosylase for repair of cytosine-derived lesions. *J. Biol. Chem. 277*, 30417–20.

(28) Dou, H., Mitra, S., and Hazra, T. K. (2003) Repair of Oxidized Bases in DNA Bubble Structures by Human DNA. *Biochemistry 278*, 49679–49684.

(29) Slupphaug, G., Eftedal, I., Kavli, B., Bharati, S., Helle, N. M., Haug, T., Levine, D. W., and Krokan, H. E. (1995) Properties of a recombinant human uracil-DNA glycosylase from the UNG gene and evidence that UNG encodes the major uracil-DNA glycosylase. *Biochemistry 34*, 128–38.

(30) Kavli, B., Sundheim, O., Akbari, M., Otterlei, M., Nilsen, H., Skorpen, F., Aas, P. A., Hagen, L., Krokan, H. E., and Slupphaug, G. (2002) hUNG2 is the major repair enzyme for removal of uracil from U:A matches, U:G mismatches, and U in single-stranded DNA, with hSMUG1 as a broad specificity backup. *J. Biol. Chem. 277*, 39926–36.

(31) Slupphaug, G., Olsen, L. C., Helland, D., Aasland, R., and Krokan, H. E. (1991) Cell cycle regulation and in vitro hybrid arrest analysis of the major human uracil-DNA glycosylase. *Nucleic Acids Res. 19*, 5131–7.

(32) Hinz, J. M., Rodriguez, Y., and Smerdon, M. J. (2010) Rotational dynamics of DNA on the nucleosome surface markedly impact accessibility to a DNA repair enzyme. *Proc. Natl. Acad. Sci. U. S. A. 107*, 4646–51.

(33) Rodriguez, Y., and Smerdon, M. J. (2013) The Structural Location of DNA Lesions in Nucleosome Core Particles Differentially Influence Accessibility of Base Excision Repair Enzymes. *J. Biol. Chem. 19*, 13863–13875.

(34) Au, K. G., Clark, S., Miller, J. H., and Modrich, P. (1989) Escherichia coli mutY gene encodes an adenine glycosylase active on G-A mispairs. *Proc. Natl. Acad. Sci. U. S. A. 86*, 8877–81.

(35) Nilsen, H., Lindahl, T., and Verreault, A. (2002) DNA base excision repair of uracil residues in reconstituted nucleosome core particles. *EMBO J. 21*, 5943–52.

(36) Tarantino, M. E., Dow, B. J., Drohat, A. C., and Delaney, S. (2018) Nucleosomes and the three glycosylases: High, medium, and low levels of excision by the uracil DNA glycosylase superfamily. *DNA Repair (Amst). 72*, 56–63.

(37) Ishibashi, T., So, K., Cupples, C. G., and Ausió, J. (2008) MBD4-mediated

glycosylase activity on a chromatin template is enhanced by acetylation. *Mol. Cell. Biol. 28*, 4734–44.

(38) Prasad, A., Wallace, S. S., and Pederson, D. S. (2007) Initiation of base excision repair of oxidative lesions in nucleosomes by the human, bifunctional DNA glycosylase NTH1. *Mol. Cell. Biol. 27*, 8442–53.

(39) Odell, I. D., Newick, K., Heintz, N. H., Wallace, S. S., and Pederson, D. S. (2010) Non-specific DNA binding interferes with the efficient excision of oxidative lesions from chromatin by the human DNA glycosylase, NEIL1. *DNA Repair (Amst). 9*, 134–43.

(40) Maher, R. L., Prasad, A., Rizvanova, O., Wallace, S. S., and Pederson, D. S. (2013) Contribution of DNA unwrapping from histone octamers to the repair of oxidatively damaged DNA in nucleosomes. *DNA Repair (Amst). 12*, 964–71.

(41) Pederson, D. S., Sweasy, J. B., Wallace, S. S., Averill, A. M., Marsden, C. G., and Maher, R. L. (2017) Human cells contain a factor that facilitates the DNA glycosylase-mediated excision of oxidized bases from occluded sites in nucleosomes. *DNA Repair (Amst). 57*, 91–97.

(42) Azad, G. K., Swagatika, S., Kumawat, M., Kumawat, R., and Tomar, R. S. (2018) Modifying Chromatin by Histone Tail Clipping. *J. Mol. Biol. 430*, 3051–3067.

(43) Turner, B. M., and O'Neill, L. P. (1995) Histone acetylation in chromatin and chromosomes. *Semin. Cell Biol. 6*, 229–36.

(44) Piersen, C. E., Prasad, R., Wilson, S. H., and Lloyd, R. S. (1996) Evidence for an Imino Intermediate in the DNA Polymerase Deoxyribose Phosphate Excision Reaction. *J. Biol. Chem. 271*, 17811–17815.

(45) Kim, J., Wei, S., Lee, J., Yue, H., and Lee, T. H. (2016) Single-Molecule Observation Reveals Spontaneous Protein Dynamics in the Nucleosome. *J. Phys. Chem. B 120*, 8925–8931.

(46) Rodriguez, Y., Hinz, J. M., Laughery, M. F., Wyrick, J. J., and Smerdon, M. J. (2016)

Site-specific Acetylation of Histone H3 Decreases Polymerase β Activity on Nucleosome Core Particles in Vitro. *J. Biol. Chem. 291*, 11434–45.

(47) Dhaenens, M., Glibert, P., Meert, P., Vossaert, L., and Deforce, D. (2015) Histone proteolysis: A proposal for categorization into 'clipping' and 'degradation.' *BioEssays 37*, 70–79.

(48) Azad, G. K., and Tomar, R. S. (2014) Proteolytic clipping of histone tails: the emerging role of histone proteases in regulation of various biological processes. *Mol. Biol. Rep. 41*, 2717–2730.

(49) Pusarla, R.-H., and Bhargava, P. (2005) Histones in functional diversification. Core histone variants. *FEBS J. 272*, 5149–68.

(50) Paull, T. T., Rogakou, E. P., Yamazaki, V., Kirchgessner, C. U., Gellert, M., and Bonner, W. M. (2000) A critical role for histone H2AX in recruitment of repair factors to nuclear foci after DNA damage. *Curr. Biol. 10*, 886–895.

(51) Menoni, H., Gasparutto, D., Hamiche, A., Cadet, J., Dimitrov, S., Bouvet, P., and Angelov, D. (2007) ATP-dependent chromatin remodeling is required for base excision repair in conventional but not in variant H2A.Bbd nucleosomes. *Mol. Cell. Biol. 27*, 5949–56.

(52) Menoni, H., Di Mascio, P., Cadet, J., Dimitrov, S., and Angelov, D. (2017) Chromatin associated mechanisms in base excision repair - nucleosome remodeling and DNA transcription, two key players. *Free Radic. Biol. Med. 107*, 159–169.

(53) Prasad, R., Shock, D. D., Beard, W. A., and Wilson, S. H. (2010) Substrate channeling in mammalian base excision repair pathways: passing the baton. *J. Biol. Chem. 285*, 40479–88.

(54) Vidal, A. E., Hickson, I. D., Boiteux, S., and Radicella, J. P. (2001) Mechanism of stimulation of the DNA glycosylase activity of hOGG1 by the major human AP endonuclease: bypass of the AP lyase activity step. *Nucleic Acids Res. 29*, 1285–92.

(55) Baldwin, M. R., and O'Brien, P. J. (2009) Human AP endonuclease 1 stimulates multiple-turnover base excision by alkyladenine DNA glycosylase. *Biochemistry 48*, 6022–33.

(56) Fitzgerald, M. E., and Drohat, A. C. (2008) Coordinating the initial steps of base excision repair. Apurinic/apyrimidinic endonuclease 1 actively stimulates thymine DNA glycosylase by disrupting the product complex. *J. Biol. Chem. 283*, 32680–90.

(57) Hill, J. W., Hazra, T. K., Izumi, T., and Mitra, S. (2001) Stimulation of human 8-oxoguanine-DNA glycosylase by AP-endonuclease: potential coordination of the initial steps in base excision repair. *Nucleic Acids Res. 29*, 430–8.

(58) Beard, B. C., Wilson, S. H., and Smerdon, M. J. (2003) Suppressed catalytic activity of base excision repair enzymes on rotationally positioned uracil in nucleosomes. *Proc. Natl. Acad. Sci. U. S. A. 100*, 7465–70.

(59) Mao, P., Brown, A. J., Malc, E. P., Mieczkowski, P. A., Smerdon, M. J., Roberts, S. A., and Wyrick, J. J. (2017) Genome-wide maps of alkylation damage, repair, and mutagenesis in yeast reveal mechanisms of mutational heterogeneity. *Genome Res. 27*, 1674–1684.

(60) Pich, O., Muiños, F., Sabarinathan, R., Reyes-Salazar, I., Gonzalez-Perez, A., and Lopez-Bigas, N. (2018) Somatic and Germline Mutation Periodicity Follow the Orientation of the DNA Minor Groove around Nucleosomes. *Cell 175*, 1074–1087.e18.

(61) Cannan, W. J., Tsang, B. P., Wallace, S. S., and Pederson, D. S. (2014) Nucleosomes Suppress the Formation of Double-strand DNA Breaks during Attempted Base Excision Repair of Clustered Oxidative Damages. *J. Biol. Chem. 289*, 19881–19893.

(62) Greenberg, M. M. (2014) Abasic and oxidized abasic site reactivity in DNA: Enzyme inhibition, cross-linking, and nucleosome catalyzed reactions. Acc. Chem. Res. 47, 646−655.

(63) Zhou, C., Sczepanski, J. T., and Greenberg, M. M. (2012) Mechanistic studies on

histone catalyzed cleavage of apyrimidinic/ apurinic sites in nucleosome core particles. J. Am. Chem. Soc. 134, 16734−16741.

(64) Blaisdell, J. O., and Wallace, S. S. (2001) Abortive base-excision repair of radiation-induced clustered DNA lesions in Escherichia coli. Proc. Natl. Acad. Sci. U. S. A. 98, 7426−7430.

(65) Kovtun, I. V, Liu, Y., Bjoras, M., Klungland, A., Wilson, S. H., and McMurray, C. T. (2007) OGG1 initiates age-dependent CAG trinucleotide expansion in somatic cells. *Nature 447*, 447–52.